

**ASSESSMENT OF COOLING
PERFORMANCE OF HIGH TEMPERATURE
QUENCHANTS FOR INDUSTRIAL HEAT
TREATMENT**

Thesis

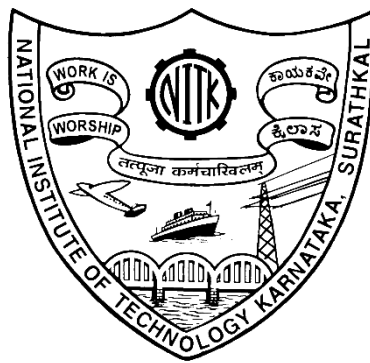
Submitted in partial fulfilment of the requirements for the degree

of

DOCTOR OF PHILOSOPHY

by

Pranesh Rao K M



**DEPARTMENT OF METALLURGICAL AND MATERIALS
ENGINEERING**

NATIONAL INSTITUTE OF TECHNOLOGY KARNATAKA,

SURATHKAL, MANGALORE 575025

OCTOBER 2019

DECLARATION

By the Ph.D. Research Scholar

I hereby declare that the Research Synopsis titled “**ASSESSMENT OF COOLING PERFORMANCE OF HIGH TEMPERATURE QUENCHANTS FOR INDUSTRIAL HEAT TREATMENT**” which is being submitted to the National Institute of Technology Karnataka, Surathkal in partial fulfillment of the requirements for the award of the Degree of Doctor of Philosophy in **Metallurgical and Materials Engineering** is a bonafide report of the research work carried out by me. The material contained in this Research Thesis has not been submitted to any University or Institution for the award of any degree.

145085MT14F05, **PRANESH RAO K M**

Department of Metallurgical and Materials Engineering

Place : **Mangalore**

Date :

C E R T I F I C A T E

This is to certify that the Research Synopsis titled “**ASSESSMENT OF COOLING PERFORMANCE OF HIGH TEMPERATURE QUENCHANTS FOR INDUSTRIAL HEAT TREATMENT**” submitted by **Mr. PRANESH RAO K M (Register Number: 145085MT14F05)** as the record of the research work carried out by him, is accepted as the Research Thesis submission in partial fulfillment of the requirements for the award of degree of **Doctor of Philosophy**.

Dr. K. Narayan Prabhu

Research Guide

(Signature with Date and Seal)

Chairman-DRPC

(Signature with Date and Seal)

ACKNOWLEDGEMENTS

Firstly, I want to thank Dr. K Narayan Prabhu. It has been my privilege to pursue Ph.D. under his guidance. His immense knowledge and experience in this field has been the sole motivation for me to pursue my research in quench hardening. Apart from the enormous technical inputs, I am grateful to him for the painstaking effort put forth by him to eliminate the obstacles in the course of my work.

I would also like to thank ex-head of the department Prof Jagannath Nayak, and Prof Udaya Bhat K., and present head of the department Prof Anandhan Srinivasan, Department of Metallurgical and Materials Engineering, NITK, Surathkal for their support and help.

I would like to extend my gratitude to my RPAC members: Prof K Rajendra Udupa, Dr. Ravishankar K S, Assistant Professor, and Prof. Shrikantha S Rao, for their critical evaluation of my research work.

I thank Dr. Gangadharan K V, Professor, Department of Mechanical Engineering and Mr. Praveen Shenoy of the SOLVE lab, NITK, Surathkal for providing the data logger.

I thank all faculty members of the Department who have educated and helped me in the course of my work.

I thank Mrs. Sharmila, Mr. Sundar, Mrs. Vinaya, and all non-teaching staff for facilitating and supporting me during my research. I also thank lab technicians of Department of Metallurgical and Materials Engineering namely Mr. Dinesh, Mr. Satish, Mr Yashwanth, Mr Ismail and Mr Prajwal for their warm and gracious support.

I thank our research group members Dr. Ramesh, Dr. Vijeesh, Dr. Mrunali, Dr.Sudheer, Dr Vignesh, Mr. Sanjay , Ms Swati and Mr Augustine for their cooperation during the research work.

I would like to express my deepest gratitude to my Mother and sisters who have been supporting me throughout my research work. Lastly, I thank my late father Murari Rao K who remains an everlasting inspiration.

Finally, I thank all those who directly and indirectly helped me to complete the research work.

Pranesh Rao K M

ABSTRACT

The present work provides a significant insight into cooling performance of molten salt mixtures and hot oils used for austempering/martempering of steel parts.

The analysis is based on the assessment of spatially dependent transient heat flux at the metal-quenchant interface using an inverse heat transfer method. The results were used for quantification of the cooling performance as well as cooling uniformity of quench baths maintained at different bath temperatures. Cooling performance of hot oil and molten NaNO_2 eutectic mixture at bath temperature of 150°C was studied. The heat extraction mechanism was completely different, and the study revealed that the molten salt offered higher cooling rate and more uniform cooling as compared to hot oil quench media. For molten KNO_3 - NaNO_3 eutectic mixture, a linear regression model to predict critical average heat flux parameters during cooling of standard Inconel probe at a given bath temperature was developed. In the case of molten NaNO_3 - KNO_3 mixtures, a contour map was drawn to predict average peak heat flux, heat flux at the start of convective cooling stage and corresponding average surface temperatures with varying quench bath composition and temperature. The bath composition significantly affected their cooling performance and uniformity of cooling. The increase in NaNO_3 content of the salt bath enhanced its cooling performance and cooling uniformity. A mechanism of boiling heat transfer based on endothermic thermochemical decomposition of the salt is proposed.

A low melting KNO_3 - LiNO_3 - NaNO_3 eutectic salt mixture and neem oil were investigated to assess their suitability as high temperature quench media. Inconel probe experiments involving this salt mixture suggested lower hardness. However, the wettability study on steel indicated an extended boiling stage yielding hardness comparable to that obtained with conventional molten salt mixtures. The cooling performance and uniformity of neem oil was higher compared to hot oils. A simulation study to model the effect of diameter, heat transfer coefficient, bath temperature and residence time on hardness distribution during martempering of AISI 4140 steel cylinders was conducted. An artificial neural network model to predict hardness distribution in AISI 4140 cylinder was proposed.

Keywords: Quench media, Inverse method, heat flux, uniformity, molten salt, hot oil

CONTENTS

LIST OF FIGURES	i
LIST OF TABLES	x
Chapter 1 INTRODUCTION	1
1.1 Organization of the thesis	1
Chapter 2 LITERATURE REVIEW	2
2.1 Heat treatment of steels	2
2.2 Physical phenomena occurring during quenching	3
2.3 Types of quenching	4
2.3.1 Conventional quench hardening	5
2.3.2 Time quenching	5
2.3.3 Isothermal quenching	7
2.4 Heat extraction mechanism in liquid quench media.	10
2.4.1 Vapour blanket stage	10
2.4.2 Wetting Kinematics	11
2.4.3 Nucleate boiling stage	11
2.4.4 Convective cooling stage	12
2.5 Factors affecting heat extraction process during quench hardening process	12
2.5.1 Quench part	12
2.5.2 Quenching system	14
2.5.3 Quenching medium	15
2.6 Low temperature quench media	15
2.6.1 Water	16
2.6.2 Brine	16
2.6.3 Aqueous polymer solutions	17
2.6.4 Mineral Oil	18

2.6.5 Alternative low temperature quench media	19
2.7 High temperature quench media	22
2.7.1 Molten metals and alloys	22
2.7.2 Molten salt bath	22
2.7.3 Hot quenching oils	28
2.7.4 Fluidized-bed	29
2.7.5 Alternative high temperature quench media	30
2.8 Evaluating cooling performance of a quench media	32
2.9 Estimation of metal quenchant interfacial heat flux	33
2.10 Summary	33
Chapter 3 SCOPE	36
Chapter 4 OBJECTIVES	37
Chapter 5 MATERIALS METHODS AND EXPERIMENTAL DESCRIPTION	38
5.1 Quench media	38
5.2 Inconel probe dimensions	38
5.3 Quenching experiments	39
5.4 Quenching of steel probe	40
5.5 Inverse heat transfer model for estimating heat flux	41
5.6 Micrographs	45
5.7 Hardness measurement	45
5.8 Contact angle measurement	45
5.9 Oxidation study and viscosity measurement	45
5.10 FEM based phase transformation model	46

5.11 Numerical experiment to simulate the effect heat transfer coefficient, bath temperature, section thickness and residence time on hardness during martempering:	49
Chapter 6 RESULTS	52
6.1 Spatially dependent transient heat flux	52
6.2 Validation of calculated quench heat flux	53
6.3 Assessment of spatially dependent transient heat flux	54
6.3.1 Average heat flux	55
6.3.2 Uniformity of quench cooling	55
6.4 Simulation of effect of heat transfer coefficient, bath temperature and section thickness on phase evolution during martempering	56
Chapter 7 DISCUSSION	58
7.1 Comparison of cooling performance of hot oil and molten salt media	58
7.1.1 Heat extraction mechanism	58
7.1.2 Uniformity of heat extraction along the surface of Inconel probe	60
7.1.3 Distribution of characteristic cooling time (t_{85}) in the Inconel probe	62
7.2 Effect of bath temperature on the cooling performance of eutectic KNO ₃ - NaNO ₃ mixture.	63
7.2.1 Regression models to predict critical points at a given bath temperature	63
7.2.2 Characteristic cooling time in the Inconel probe	65
7.3 Effect of bath temperature on the cooling performance of NaNO ₃ -KNO ₃ mixtures.	66
7.3.1 Average surface heat flux	66
7.3.2 Variation of critical points with composition and bath temperature	67
7.3.3 Steel probe quenching	69
7.3.4 Uniformity of quench cooling of Inconel probe	70

7.3.5 Thermo chemical decomposition of salt and boiling heat transfer	71
7.4 Cooling performance of molten KNO_3 - LiNO_3 - NaNO_3 eutectic mixture.	73
7.4.1 Quench heat flux parameters	73
7.4.2 Uniformity of cooling	75
7.4.3 Hardness of steel probes	76
7.4.4 Centre cooling data for Inconel and steel probes	76
7.4.5 Equilibrium contact angle	78
7.5 Hot Neem Oil as alternative to Hot Mineral Oils for Martempering.	80
7.5.1 Heat extraction mechanism	80
7.5.2 Uniformity of heat extraction	80
7.5.3 Quench heat flux parameters	81
7.5.4 Quenching of steel probes	82
7.5.5 Oxidation of oils	86
7.6 Effect of Section thickness, heat transfer coefficient, bath temperature and residence time on hardness of AISI 4140 steel cylinders during martempering	88
7.6.1 Variation of maximum residence time	88
7.6.2 Artificial neural network model for predicting hardness distribution in AISI 4140 steel cylinder	89
7.6.3 Relative importance of input variables	93
Chapter 8 CONCLUSIONS	95
REFERENCES	98
APPENDIX A: TIME TEMPERATURE CURVES MEASURED DURING QUENCHING OF INCONEL PROBE	105
APPENDIX B: SPATIALLY DEPENDENT TRANSIENT QUENCH HEAT FLUX CALCULATED USING INVERSE METHOD FOR INCONEL PROBE	112

APPENDIX C: EFFECT OF SECTION THICKNESS, HEAT TRANSFER COEFFICIENT, BATH TEMPERATURE AND RESIDENCE TIME ON HARDNESS OF AISI 4140 STEEL CYLINDER DURING MARTEMPERING	121
APPENDIX D: WEIGHTS AND BIAS FOR ARTIFICIAL NEURAL NETWORK MODEL	131
LIST OF PUBLICATIONS	132
BIO-DATA	133

LIST OF FIGURES

Figure No	Caption	Page
2.1	Classification of heat treatment processes based on cooling rate	2
2.2	Physical fields and interactions involved in the quenching process	3
2.3	Classification of quenching techniques	4
2.4	Cooling curve super imposed on TTT diagram for (a) conventional quench hardening (b) Martempering (c) Modified martempering (ASM, 1999)	6
2.5	Cooling curves during Austempering superimposed on TTT diagram	8
2.6	Three stages of liquid quenching	10
2.7	Factors affecting quench hardening process	12
2.8	Classification of liquid quench media based on operating temperature	15
2.9	Quench severity of industrial quench media	16
2.10	Alternative low temperature quench media	19
2.11	Isothermal sections of the liquidus surface of nitrate-nitrite system (Lisicic et al. 2010).	24
2.12	Bonds between water and molten salt at high temperature	25
5.1	Dimensions of Inconel probe used for quenching experiments	39
5.2	Schematic diagram for quenching experiment	40
5.3	Dimensions of steel probe used for quenching experiments	41
5.4	Axisymmetric model of the probe	41
5.5	Flow chart for Inverse solution algorithm	43

	Temperature dependent variation of a) Density b) Thermal conductivity c) Specific heat d) enthalpy of transformations for different phases.	47
5.6		
5.7	TTT diagram of AISI 4140 steel probe obtained from JMatPro	48
5.8	Flow chart of numerical experiment	50
5.9	Hardness as a function of yield strength	51
	Transient variation of a) Measured temperature b) Cubic equation parameters calculated using Inverse method c) Spatially dependent quench heat flux for inconel probe quenched in NaNO ₃ probe maintained at bath temperature of 350°C	52
6.1		
6.2	Error calculated at various thermocouple locations for Inconel probe quenched in NaNO ₂ eutectic mixture maintained at quench bath temperature of 150°C	53
	a) q_{Avg} as a function of T_{Avg} b) Spatial variation of heat energy extracted per unit area obtained for 55N salt mixture maintained at 250°C	55
6.3		
6.4	a) Transient variation of temperature at geometric center and surface of the cylinder and b) Volume fraction of various phases at geometric center of the cylinder obtained for numerical experiment with $D=60\text{mm}$, $h=1000\text{W/m}^2\text{K}$, $T_b=M_s$ (323.6°C) and $f=1$	56
	a) Phase fractions and b) Predicted hardness as a function of radial distance obtained for numerical experiment with $D=60\text{mm}$, $h=1000\text{W/m}^2\text{K}$, $T_b=M_s$ (323.6°C) and $f=1$	57
6.5		
7.1	Heat extraction mechanism illustrated using q_{avg} plotted as a function of T_{avg} for Inconel probe quenched in a) Hot oil b) NaNO ₂ maintained at 150°C	59

7.2	Spatial distribution of a)Energy extracted per unit area b) Peak heat flux during quenching of inconel probe in hot oil and NaNO ₂ eutectic mixture maintained at 150°C	60
7.3	Variation of T _{Range} with T _{Avg} at the metal/quenchant interface for an inconel probe quenched in NaNO ₂ and hot oil quench media maintained at 150°C	61
7.4	Distribution of t ₈₅ values in the Inconel probe quenched in a)molten eutectic NaNO ₂ mixture b) Hot oil quench media maintenance at 150°C	62
7.5	Variation of q _{Avg} with T _{Avg} calculate for inconel probe quenched in 55N salt mixture maintained at different quench bath temperatures.	63
7.6	Linear regression models for variation of a) T _{max} b) q _{max} c) T _{Conv} and d) q _{Conv} as a function of quench bath temperature for Inconel probe quenched in 55N salt mixture	64
7.7	Linear regression model to predict the maximum t ₈₅ value for the Inconel probe quenched in 55N salt mixture as a function of bath temperature.	65
7.8	Normalized t ₈₅ distribution in axisymmetric hot Inconel probe quenched in eutectic NaNO ₃ -KNO ₃ quench medium maintained at a) 250°C b)300°C c)350°C d)400°C e)450°C	66
7.9	Variation of average surface temperature with average surface heat flux for Inconel probe quenched in molten NaNO ₃ -KNO ₃ mixtures at a) 250°C, b) 300°C c) 350°C C) d)400°C e)450°C f) 500°C	67
7.10	Contour plots presenting variation of average heat flux curve parameters, a)q _{max} , b)T _{max} , c)q _{conv} and d)T _{conv} with respect to the composition and quench bath temperature in molten NaNO ₃ -KNO ₃ mixtures	68

7.11	Average hardness of AISI 4140 steel probe quenched in molten NaNO ₃ -KNO ₃ mixtures with varying KNO ₃ composition maintained at 300°C and 350°C	69
7.12	Spatial variation of normalized heat energy along the surface for Inconel probe quenched in molten NaNO ₃ -KNO ₃ mixtures maintained at a) 250°C, b) 300°C c) 350°C C) d)400°C e)450°C f) 500°C	70
7.13	Contour plots presenting variation of uniformity with respect to the composition and quench bath temperature in molten NaNO ₃ -KNO ₃ mixtures	71
7.14	a) Change in standard enthalpy and standard Gibbs free energy b) Equilibrium constant for nitrate-nitrite decomposition of NaNO ₃ and KNO ₃	72
7.15	Variation of q_{Avg} with T_{Avg} for Inconel probe quenched in molten a)NaNO ₂ b) LiNO ₃ eutectic mixtures maintained at different quench bath temperatures	73
7.16	Variation of heat energy removed per unit area along the surface of the Inconel probe quenched in a) NaNO ₂ b) LiNO ₃ eutectic mixtures maintained at different quench bath temperatures	75
7.17	Average hardness measured in steel probes quenched in molten NaNO ₂ and LiNO ₃ eutectic mixtures maintained at varying bath temperatures	76
7.18	Time temperature and cooling rate curves measured at geometric centre during quenching of Inconel and steel probes quenched in molten NaNO ₂ eutectic mixture maintained at a)150°C b)200°C c) 250°C d)300°C	77
7.19	Time temperature and cooling rate curves measured at geometric centre during quenching of Inconel and steel probes quenched in	77

	molten LiNO_3 eutectic mixture maintained at a)150°C b)200°C c) 250°C d)300°C	
7.20	Contact angle for spreading of LiNO_3 and NaNO_2 eutectic mixtures maintained at different temperatures on Inconel and AISI-4140 steel surfaces	78
7.21	Variation of equilibrium contact angle with ambient temperature for spreading of LiNO_3 and NaNO_2 eutectic mixtures on Inconel and AISI-4140 steel surfaces	78
7.22	Mean heat flux v/s mean surface temperature in inconel probe cooling in hot oil and neem oil maintained at a) 100°C b) 150°C c) 200°C	80
7.23	Spatial variation of heat energy for inconel probe quenched in a) hot oil b)neem oil maintained at different bath temperatures	81
7.24	Cooling and rate curves obtained at the geometric centre of Inconel and AISI-52100 quenched in hot oil maintained at a) 100°C b) 150°C c) 200°C and neem oil maintained at d) 100°C e) 150°C f) 200°C	83
7.25	a) TTT diagram for AISI-52100 steel and b) variation of average measured in steel probe quenched in hot oil and neem oil	83
7.26	Micrographs of AISI-52100 probe quenched in hot oil at a)center b) near surface and neem oil at a)center b) near surface for bath temperature of 100°C	84
7.27	Micrographs of AISI-52100 probe quenched in hot oil at a)center b) near surface and neem oil at a)center b) near surface for bath temperature of 150°C	84
7.28	Micrographs of AISI-52100 probe quenched in hot oil at a)center b) near surface and neem oil at a)center b) near surface for bath temperature of 200°C	85

7.29	Photographs of a) hot oil and b) neem oil oxidized in hot air oven	86
7.30	Effect of oxidation on dynamic viscosity of a) hot oil and b) neem oil	86
7.31	Cooling rate v/s measured temperature curve at the geometric centre of an Inconel probe quenched in oxidized and non-oxidized neem oil quench media maintained at 150°C.	87
7.32	Variation of maximum residence time with a) diameter of steel cylinder b) heat transfer coefficient c) bath temperature	89
7.33	Architecture of artificial neural network model used to predict hardness distribution in martempered AISI 4140 steel cylinders	90
7.34	a) Variation of standard error with number of neurons in the hidden layer b) Error plot for $N_{HL}=30$	92
7.35	Distribution of hardness predicted by simulation experiment and ANN model in AISI 4140 cylinder of a) 80mm diameter and $h=1000W/m^2K$ $T_b=373.6^\circ C$ and $f=0.99$ b) 100mm diameter and $h=3000W/m^2K$ $T_b=273.6^\circ C$ and $f=0.5$	93
7.36	Pie chart showing percentage of relative importance input variables	94
A.1	Time temperature curves measured at different locations in Inconel probe quenched in 0N salt maintained at a)350°C b)400°C c)450°C d)500°C	105
A.2	Time temperature curves measured at different locations in Inconel probe quenched in 25N salt maintained at a)300°C b)350°C c)400°C d)450°C e)500°C	106
A.3	Time temperature curves measured at different locations in Inconel probe quenched in 45N salt maintained at a)250°C b)300°C c)350°C d)400°C e)450°C	107

	Time temperature curves measured at different locations in	
A.4	Inconel probe quenched in 75N salt maintained at a)300°C b)350°C c)400°C d)450°C e)500°C	108
	Time temperature curves measured at different locations in	
A.5	Inconel probe quenched in 100N salt maintained at a)350°C b)400°C c)450°C d)500°C	109
	Time temperature curves measured at different locations in	
A.6	Inconel probe quenched in NaNO ₂ eutectic salt mixture maintained at a)150°C b)200°C c)250°C d)300°C	109
	Time temperature curves measured at different locations in	
A.7	Inconel probe quenched in LiNO ₃ eutectic salt mixture maintained at a)150°C b)200°C c)250°C	110
	Time temperature curves measured at different locations in	
A.8	Inconel probe quenched in hot oil maintained at a)100°C b)150°C c)200°C	110
	Time temperature curves measured at different locations in	
A.9	Inconel probe quenched in hot oil maintained at a)100°C b)150°C c)200°C	111
	Spatially dependent transient heat flux for inconel probe	
B.1	quenched in 100N salt mixture maintained at a)350°C b) 400°C c) 450°C d)500°C	112
	Spatially dependent transient heat flux for inconel probe	
B.2	quenched in 75N salt mixture maintained at a)300°C b) 350°C c) 400°C d)450°C e) 500°C	113
	Spatially dependent transient heat flux for inconel probe	
B.3	quenched in 55N salt mixture maintained at a)250°C b) 300°C c) 350°C d)400°C e)500°C	114

	Spatially dependent transient heat flux for inconel probe	
B.4	quenched in 25N salt mixture maintained at a)300°C b) 350°C c) 400°C d)450°C e)500°C	115
	Spatially dependent transient heat flux for inconel probe	
B.5	quenched in 0N salt mixture maintained at a)350°C b) 400°C c) 450°C d)500°C	116
	Spatially dependent transient heat flux for inconel probe	
B.6	quenched in Hot oil maintained at a)100°C b) 150°C c) 200°C	117
	Spatially dependent transient heat flux for inconel probe	
B.7	quenched in Neem oil maintained at a)100°C b) 150°C c) 200°C	118
	Spatially dependent transient heat flux for inconel probe	
B.8	quenched in molten NaNO ₂ eutectic salt mixture maintained at a)150°C b) 200°C c) 250°C d)300°C	119
	Spatially dependent transient heat flux for inconel probe	
B.9	quenched in molten LiNO ₃ eutectic salt mixture maintained at a)150°C b) 200°C c) 250°C d)300°C	120
	Effect of heat transfer coefficient and bath temperature on the average hardness in AISI 4140 cylinder of 2mm diameter for residence time fraction of	
C.1	a) 1 b) 0.99 c) 0.95 d)0.9 e) 0.75 f) 0.5	121
	Effect of heat transfer coefficient and bath temperature on the average hardness in AISI 4140 cylinder of 5mm diameter for residence time fraction of	
C.2	a) 1 b) 0.99 c) 0.95 d)0.9 e) 0.75 f) 0.5	122
	Effect of heat transfer coefficient and bath temperature on the average hardness in AISI 4140 cylinder of 10mm diameter for residence time fraction of	
C.3	a) 1 b) 0.99 c) 0.95 d)0.9 e) 0.75 f) 0.5	123
	Effect of heat transfer coefficient and bath temperature on the average hardness in AISI 4140 cylinder of 15mm diameter for residence time fraction of	
C.4	a) 1 b) 0.99 c) 0.95 d)0.9 e) 0.75 f) 0.5	124

C.5	Effect of heat transfer coefficient and bath temperature on the average hardness in AISI 4140 cylinder of 20mm diameter for residence time fraction of a) 1 b) 0.99 c) 0.95 d)0.9 e) 0.75 f) 0.5	125
C.6	Effect of heat transfer coefficient and bath temperature on the average hardness in AISI 4140 cylinder of 30mm diameter for residence time fraction of a) 1 b) 0.99 c) 0.95 d)0.9 e) 0.75 f) 0.5	126
C.7	Effect of heat transfer coefficient and bath temperature on the average hardness in AISI 4140 cylinder of 40mm diameter for residence time fraction of a) 1 b) 0.99 c) 0.95 d)0.9 e) 0.75 f) 0.5	127
C.8	Effect of heat transfer coefficient and bath temperature on the average hardness in AISI 4140 cylinder of 60mm diameter for residence time fraction of a) 1 b) 0.99 c) 0.95 d)0.9 e) 0.75 f) 0.5	128
C.9	Effect of heat transfer coefficient and bath temperature on the average hardness in AISI 4140 cylinder of 80mm diameter for residence time fraction of a) 1 b) 0.99 c) 0.95 d)0.9 e) 0.75 f) 0.5	129
C.10	Effect of heat transfer coefficient and bath temperature on the average hardness in AISI 4140 cylinder of 100mm diameter for residence time fraction of a) 1 b) 0.99 c) 0.95 d)0.9 e) 0.75 f) 0.5	130

LIST OF TABLES

Table No	Caption	Page No
5.1	Quenching experiment matrix	38
5.2	Composition of grade AISI 4140 and AISI 52100	40
5.3	Boundary conditions for heat transfer model of the probe.	42
5.4	Temperature dependent thermal properties of Inconel 600 alloy	42
5.5	Yield strength of different phases	51
6.1	Maximum %error calculated for inconel probe quenched in different quench media maintained at various bath temperatures	53
6.2	Mean %error calculated for inconel probe quenched in quench media maintained at various bath temperatures	54
7.1	Quench heat flux parameters for Inconel probe quenched in molten NaNO ₂ and LiNO ₃ eutectic mixtures quench media maintained at different bath temperatures	75
7.2	Quench heat flux parameters calculated for Inconel probe quenched in hot oil and neem oil quench media maintained at different bath temperatures	81
7.3	Parameters used to normalize inputs and outputs of ANN model	91
7.4	Relative importance parameter calculated for input variables of neural network model.	93

Chapter 1 INTRODUCTION

Quench hardening heat treatment is often used to augment hardness and toughness of the steel parts. Conventional quench hardening involves, rapid cooling of austenitized steel part in a quench media maintained at room temperature. Rapid cooling of steel part to room temperature ensures the transformation of austenite to martensite by avoiding high temperature diffusion-based transformation of austenite to ferrite, cementite or pearlite.

Rapid cooling results in establishment of large thermal gradients in the steel part. Transformation stress develops in the steel part due to volumetric expansion associated with transformation of austenite to martensite. Thermal and transformational stresses combine and appear in form of distortion, residual stress and cracks in quench hardened steel parts (Narazaki et al. 2002). Distortion, residual stress and cracking are the defects observed in the steel parts subjected to conventional quench hardening heat treatment.

Austempering and martempering heat treatment are industrial quench hardening processes which are widely used to harden steel parts with minimum distortion, residual stress and cracking. Austempering and martempering require high temperature quench media which can operate in the temperature range of 160°C to 600°C. These high temperature quench media are expected to cool the steel part from austenitizing temperature to quench bath temperature rapidly enough to avoid transformation of austenite to ferrite, cementite and pearlite (Bates et al. 1991). This study focusses on characterizing cooling performance of these high temperature quench media.

1.1 Organization of the thesis

The thesis is divided into eight chapters. Chapter 1 presents introduction. Chapter 2 provides a detailed discussion on the available research in the field of quench hardening and high temperature quench media. Detailed description of the experimental methodology and materials used for assessing quench heat transfer has been provided in chapter 3. Chapter 4 describes the scope and Chapter 5 lists the objectives of the present work. The results of the experiments have been provided in chapter 6. Detailed analysis of the results and their interpretation has been provided in Chapter 7. The important findings of the present work have been provided in Chapter 8.

Chapter 2 LITERATURE REVIEW

2.1 Heat treatment of steels

Chapter 1 Most of industrial steel parts are subjected to heat treatment process before being put into service. The essential parts of heat treatment process are the heating cycle (holding time and temperature) and cooling cycle.

Heating cycle involves heating the steel part to austenitizing temperature to obtain homogeneous austenite phase in the steel part. Austenite grain growth and carbide dissolution into austenite grain are the desired microstructural transformations at the austenitizing temperature. These are diffusion-based transformations. The holding time at austenitizing temperature should thus be long enough for completion of desired microstructural transformations.

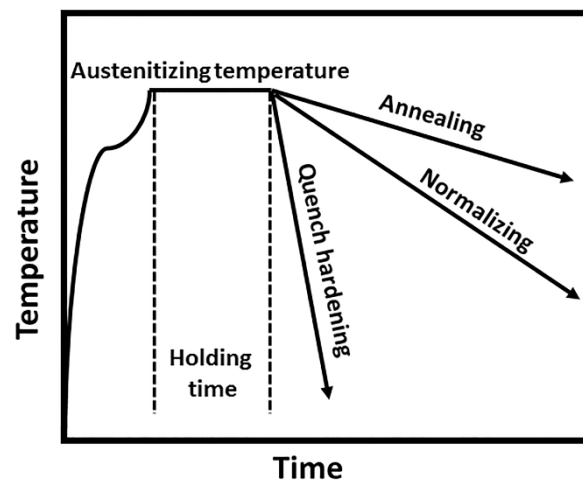


Figure 2.1: Classification of heat treatment processes based on cooling rate

Based on the cooling cycle employed, the heat treatment process can be broadly classified into three types annealing, normalizing and quench hardening. Depending on the composition of steel, Ferrite, Pearlite and Cementite phases are obtained in the steel parts subjected to annealing and normalizing heat treatments. The transformation of austenite to Ferrite, Pearlite and Cementite are diffusion-based transformations which require low cooling rates. The austenitized steel part is generally subjected to furnace cooling and air cooling during annealing and normalizing heat treatment processes.

Quench hardening heat treatment commonly known as quenching involves rapid cooling of austenitized steel part in a suitable cooling medium (quenchant) to obtain

martensite, bainite or a mixture of these two phases. The rapid cooling ensures that austenite does not transform to equilibrium phases. Ferrite, Pearlite and Cementite are the equilibrium phases which possess inferior mechanical properties as compared to Martensite and Bainite which are. Martensite phase is obtained by cooling the steel part rapidly below martensite start temperature, whereas bainite is obtained by rapidly cooling the part to bainitic transformation temperature and holding at that temperature until the bainitic transformation is completed. (Totten et al. 1993).

2.2 Physical phenomena occurring during quenching

Quench hardening is a multi-physics process involving complicated pattern of couplings between different physical events such as heat transfer, phase transformations and stress evolution.

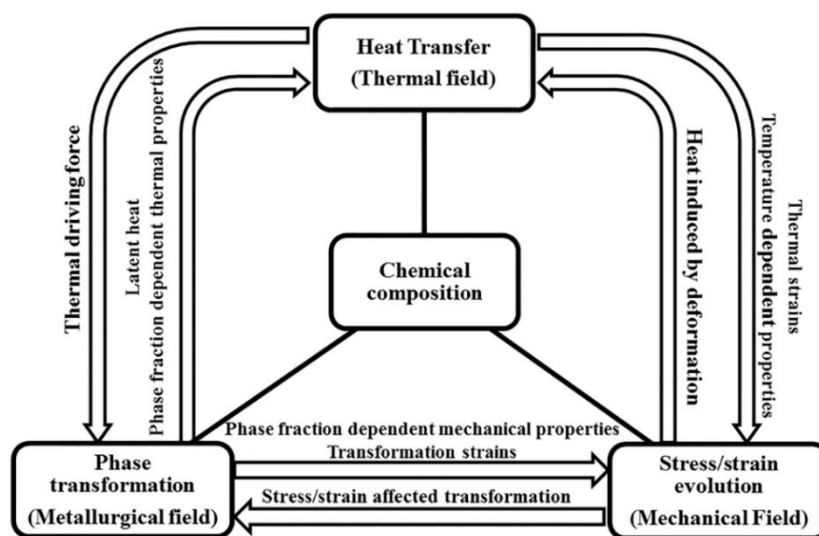


Figure 2.2: Physical fields and interactions involved in the quenching process

Heat transfer to the quenching medium is the driving physical event as it triggers other processes. Austenite is thermodynamically unstable at lower temperatures. The rate at which the steel part is cooled from austenitizing temperature to quenchant temperature defines the microstructure of heat-treated steel part. Austenite may transform to ferrite, pearlite, carbides, bainite or martensite depending on the cooling rate (Şimşir and Gür 2008a; b).

Conduction of heat from core of the part to its surface is affected by phase transformation. Phase transformation results in variation of thermo-physical properties

of steel part namely density, thermal conductivity and specific heat. Latent heat evolution associated with the exothermic phase transformation of austenite alters the thermal field in the quenched part.

The heat transfer at the metal-quenchant is a function of both time and space. This spatial and transient variation of heat flux is one of the major reasons for thermal and transformational stresses. Distortion, cracking and residual stresses are the adverse effects of combination of thermal and transformational stresses. A continuously fluctuating thermal stress field is induced in the component due to the variation of thermal contractions/expansions and thermomechanical properties as a function of temperature and time. Heat evolved due to plastic deformation is generally neglected during modelling of quenching.

Decomposition of austenite into product phases results in increase of volume in the course of transformation. Apart from the volumetric change, mechanical properties of the steel part are affected by the metallurgical transformation of austenite. On the other hand, thermodynamics and kinetics of transformation are affected by the internal stress fields. In some cases, it is observed that phase transformations are accelerated by stress field in the quenched part. The interaction of stress fields and microscopic plasticity due to transformation induces irreversible strains in the quenched part, this phenomenon is called transformation induced plasticity.

2.3 Types of quenching

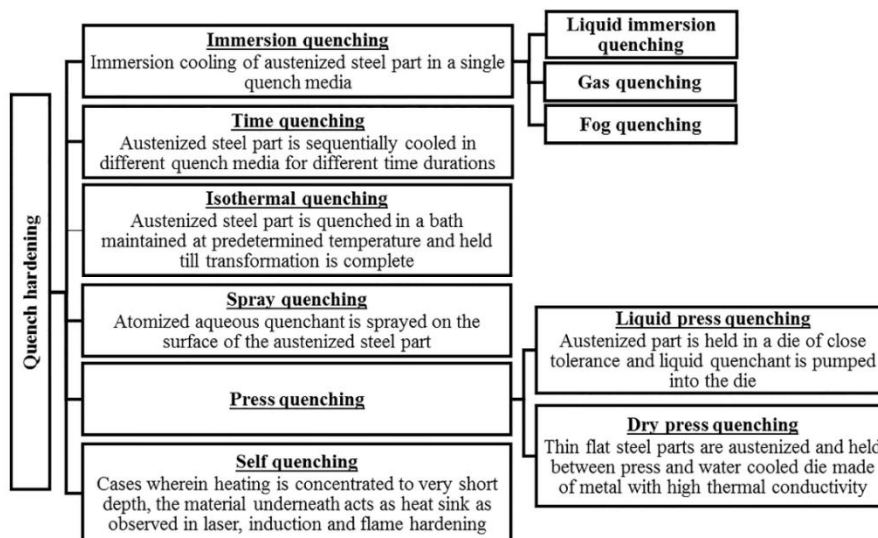


Figure 2.3: Classification of quenching techniques

The technique used to quench the part can alter the heat extraction process and thus help in achieving the optimum cooling rate. Figure 2.3 shows the graphical representation of classification of quenching technique. This classification is based on work of Lisicic (Lisicic et al. 2010). Most of the steel parts are hardened using Immersion quenching, time quenching and isothermal quench hardening techniques.

2.3.1 Conventional quench hardening

Immersion of a steel part in a single quenchant which may be gas or liquid and it is cooling it near to room temperature is the most widely used method to quench harden steel parts.

Gas quenching provides lower cooling rates and better control over the heat extraction process. Gas quenching offer cooling rates higher than still air and lesser than liquid quenching. Fog quenching which is a variation of gas quenching, offers cooling rates intermediate to cooling rates of gas and liquid immersion quenching. Gas and fog quenching techniques substitute liquid immersion quenching in order to reduce distortion and stresses. Gases have a fundamental disadvantage in comparison to fluids, which is poor heat transfer characteristics under normal condition (Liščić and Singer 2014).

Conventional quench hardening (liquid immersion quench hardening) process involves direct immersion of austenitized steel part in a vaporizable quenchant is the most commonly used technique to quench hardenable steels and other metal. The cooling rate can be significantly controlled by changing liquid quenchant type, temperature of quenchant and agitation rate. Water, brine, oil and water soluble polymer are widely used media for conventional hardening of steel parts (Ramesh and Prabhu 2014a).

2.3.2 Time quenching

Time quenching technique involves use of two or more quenching media on a timed basis. Partial quench in water, followed by quenching in oil in molten salt followed by air cooling are some of examples for time quenching process. Interrupted quenching, martempering and rinse quenching are the commercial examples for this type of quenching practice. The quench part is cooled in a medium at a high cooling rate till the martensitic start temperature and then cooled in another medium at moderate

cooling rate to room temperature. The practice is to avoid quench defects in the heat-treated part.

2.3.2.1 Marquenching

Figure 2.4a shows clearly the difference between conventional quench hardening, martempering and modified martempering. In conventional quench hardening, large temperature exists between surface and core of the part through the cooling. During martempering, the austenitized steel part is quenched in a quenchant maintained just above M_s , the part is held in the quenchant until temperature is equalized throughout its cross section. The part is then remove from high temperature quench bath and cooled in air to room temperature allowing austenite to transform to martensite. Temperature gradient between the surface and the core, observed in the parts quenched in high temperature quenchant is much less as compared to that observed in conventional quenchants (water, mineral oil, aqueous polymer, etc.). This reduces both thermal and transformational stresses, which aids to minimize distortion and susceptibility to cracking in the quenched part.

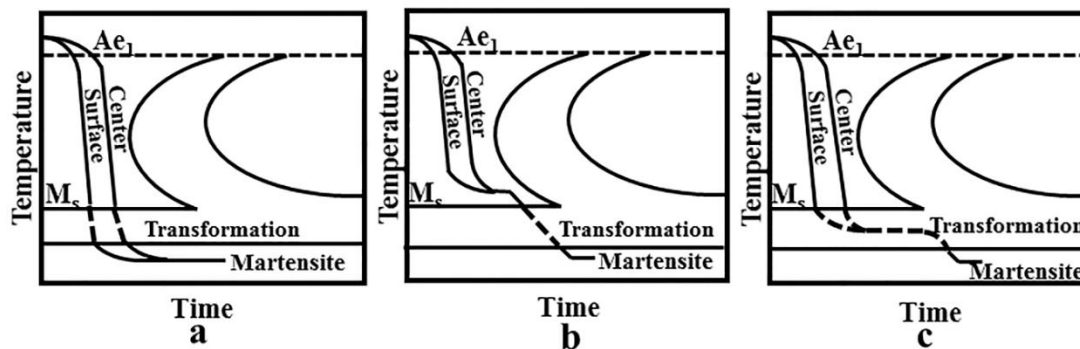


Figure 2.4: Cooling curve super imposed on TTT diagram for (a) conventional quench hardening (b) Martempering (c) Modified martempering [ASM, 1999]

The marquenched parts are subsequently subjected to tempering. Carbon steels, low alloy steels and grey cast iron parts can be subjected to martempering. There are many variants of martempering which are discussed below.

Figure 2.4-c shows one of the variations of martempering process. Low hardenability steel parts are subjected to this process. In this process, the part is quenched in quenchant maintained at temperature just below M_s . The low temperature of the

quenchant i.e. 150-175°C increases the severity of the quenchant. Higher cooling rates thus offered by the quenchants help in evading high temperature pearlitic transformation in the quenched part.

Another variant of martempering process is used to heat treat steel parts with large cross sectional area. In this process, the part is first quenched in water or brine for very short time and subsequently transferred to martempering bath. This process increases the depth of hardening as compared to the conventional martempering process.

Some parts require reforming or straightening operations after heat treatment this is not feasible in conventional quenching and hardening. Straightening or forming operations can be accomplished upon removal from the marquenching bath. It is to be noted that while straightening the part has largely austenite microstructure. The distortion is significantly reduced in this method as the part will hold its shape during subsequent stage of air cooling where in austenite transforms to martensite.

Carbomartempering is another variation of martempering which is used for heat treating low carbon steels. Low carbon steel are often carburized or carbo-nitride to enhance the surface toughness of the part. Carbomartempering process combines the benefits of carburizing and martempering. Carbomartempered parts are thus observed to have higher toughness and reduced distortion compared to conventionally carburized and hardened parts. The Carbomartempering temperature is chosen between the M_s of the core and the surface. Quench bath temperature is generally maintained between 175°C to 260°C the part is held for few minutes for temperature equalization.

2.3.3 Isothermal quenching

The quench part is cooled into a medium maintained at specific predetermined temperature and is held at that temperature till transformation is completed in the case of isothermal quenching technique. Austempering is a commercial example for this process. Here the steel high temperature quench part is held medium at incubation temperature until bainitic transformation is completed.

2.3.3.1 Austempering

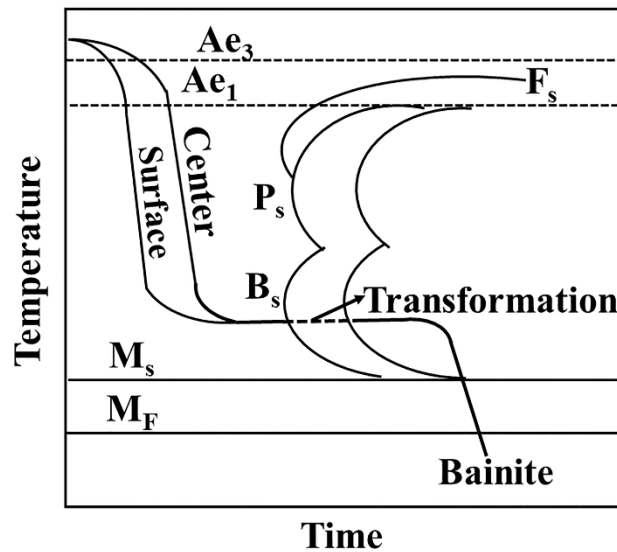


Figure 2.5: Cooling curves during Austempering superimposed on TTT diagram

Figure 2.5 describes typical Austempering process. The steel part is austenitized and the quenched into a medium maintained at a temperature above M_s . Rate of cooling of the part is fast enough to avoid pearlitic nose of the TTT diagram. The temperature throughout the part is equalized with the bath temperature and held for a duration long enough to facilitate isothermal Bainitic transformation throughout the part (Totten 2007). Following this, the part air cooled to room temperature. The operating temperature and holding time varies from few minutes to couple of hours depending on the section thickness and grade of steel. Carbon steels with 1% Manganese, low alloy steels, ductile iron and grey irons can be subjected to austempering.

Wire patenting is a modified austempering process wherein the part is cooled at cooling rate lower than that required to avoid pearlitic nose of TTT diagram. The part thus has a microstructure which is a mixture of pearlite and bainite. Operating temperature for modified austempering is 510°C - 540°C . The objective of this heat treatment is to improve ductility and strength of the part. As a consequence, hardness of the part is reduced.

Another variation of austempering combines the benefits of martempering and austempering processes. In this process, the part is first quenched in austempering bath and held for relatively less time so that bainitic transformation is incomplete.

Subsequently the part is air cooled to facilitate martensitic transformation of untransformed austenite. Unique combination of hardness and toughness is realized as martensite and bainite both the phases are present in the part. The time temperature cycles can be tailored to provide a fine balance between hardness and toughness which would not be possible by either process alone.

Low hardenability steels can be austempered using 2 quenching baths. The first bath is maintained at a temperature just below M_s which increases the severity of the quench and thus offers cooling rate higher than the critical cooling rate in TTT diagram. In the next stage, the part is quenched in a quench media maintained at austempering temperature.

Conventionally the part is first formed and later subjected to hardening. The part undergoes distortion during hardening heat treatment. This undesirable effect of heat treatment could be overcome by ausforming process. Ausforming is another variant of austempering process wherein the austenized part is formed in the austempering bath. The forming operation is completed in the austempering bath before the commencement of bainitic transformation. The formed part is held in the bath until the bainitic transformation is complete and later removed from the bath and cooled in air. Thus the part is simultaneously formed and hardened. Distortion control is the main objective of the process. Apart from other benefits, the lubrication provided by the liquid quench during forming is the additional advantage realized through this process (Mehrkam 1967).

Ductile iron is austempered at 230°C-370°C for 0.5-4 hours, depending on steel composition, cross-section and mechanical property requirements. The microstructure produced is ausferrite instead of bainite. ADI components have successfully replaced steel castings, forging, welded fabrications and even aluminium in both structural and wear applications due to their excellent combination of strength, toughness, ductility, and strength to weight ratio.

Steels with low carbon content are often subjected to carburizing followed quench hardening. This process generally associated with high level of distortion and only low depth of hardening. Carbo-austempering involves austempering of carburized steel parts. This produces a high carbon bainitic case and either a martensitic or bainitic core

depending on composition of steel and severity of the quench bath. The uniqueness of this process is that the core hardens first and then hardening progresses towards the surface, this reduces distortion.

2.4 Heat extraction mechanism in liquid quench media.

The most widely used industrial practice is immersing austenitized steel part in a suitable liquid quench media. This is a common for direct quenching, time quenching and isothermal quenching practices.

The Figure 2.6 shows the three stages of heat removal during quenching in vaporizable liquid media.

They are as follows:

- Vapor blanket stage
- Nucleate boiling stage
- Convective or liquid cooling stage

2.4.1 Vapour blanket stage

Also referred to as film boiling stage, this stage occurs when the supply of heat from the surface of the quenched part is more than the amount of heat needed to vaporize liquid quenchant. The rate of heat transfer is low during this stage as the vapour envelope acts as an insulator, and cooling occurs by radiation from part surface and conduction through the vapour film. The vapour film on the part surface breaks when the surface temperature reduces to liebfrost/rewetting temperature.

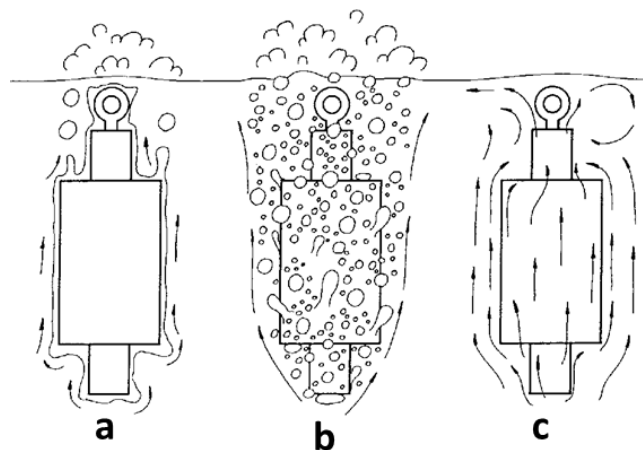


Figure 2.6: Three stages of liquid quenching

2.4.2 Wetting Kinematics

The process of liquid quenchant coming in contact with the surface of the part by rupturing vapour blanket is called wetting kinematics. Variation in wall temperature, resulting from part geometry, surface depositions, oxide layers, immersion, pressure deviations and locally differing immersion periods, lead to locally confined wetting. The local wetting results in simultaneous existence of all the 3 stages of cooling i.e. vapour blanket, nucleate boiling and convection stages on the surface of the part during quenching.

There are 2 types of wetting processes namely Newtonian wetting and non-Newtonian wetting. Newtonian wetting occurs in a short period of time like an explosion. Non-Newtonian wetting occurs over long time period and an ascending wetting front is generally observed in this kind of wetting.

Wetting front is defined as a locus of points separating regions undergoing vapour stage and nucleate boiling stage. The wetting front is observed to advance with a significant velocity (Totten et al. 2003).

Wetting kinematics has a significant effect on the state of residual stresses in the quenched part. Minimum distortion and residual stresses are observed in parts which undergo Newtonian wetting during quenching. On the contrary, non-Newtonian wetting is associated with large temperature differences, resulting in considerable in microstructural variation and distortion.

If heat transfer coefficients during vapour blanket, boiling and convective cooling stages are similar in comparable liquid quenchants, wetting time describes the cooling behaviour at the surface of the steel part. The hardness at locations with same wetting time at the surface of the parts are expected to be same. Therefore, wetting kinematics can be used to predict hardness at a given location on the surface of the part (Stitch and Tensi 1990).

2.4.3 Nucleate boiling stage

This stage begins after rewetting of the quenched part surface. The liquid quench medium in contact with the quenched part surface boils and number of small bubbles are formed on the surface of the part. Evaporation of the fluid and gravity driven upward

movement of the vapour bubble causes extremely strong convection heat transfer. This results in high heat extraction rates.

2.4.4 Convective cooling stage

This stage begins when the temperature of the metal surface is reduced below the boiling point of the quenchant. The quenchant exists in single phase i.e. liquid. Thermomigration of fluid takes place through heat conduction and convection. The heat extraction rate is very low compared to preceding stages.

2.5 Factors affecting heat extraction process during quench hardening process

Conventional liquid immersion quenching, time quenching, and isothermal quenching techniques are fundamentally different in terms of the intended microstructure and the process itself. Nevertheless, they operate on the same principle where in, austenitized steel part is rapidly cooled in a liquid quench medium. The factors that influence the cooling characteristics of quenched part in these three quench hardening techniques are therefore essentially the same.

The three major factors that affect heat extraction characteristics during quench hardening process are given in Figure 2.7

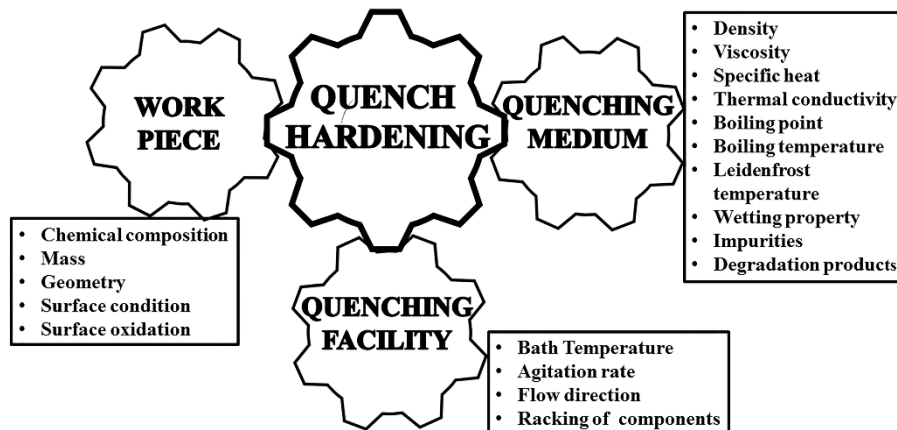


Figure 2.7: Factors affecting quench hardening process

2.5.1 Quench part

Chemical composition, surface oxidation, surface roughness, geometry and mass of a quench part are the attributes of the steel part which greatly influence the heat extraction process at the part/quenchant interface.

2.5.1.1 Chemical composition

Chemical composition of the steel is central to all the multi-physics phenomena occurring during quench hardening process. This means that if 2 steel parts of different grades but same geometry, surface conditions, etc. undergo same quenching process, the microstructure and residual stress distribution in the quenched part will be different.

2.5.1.2 Surface roughness

Heat transfer from the quenched part to the quenchant occurs at the surface of the quenched part. The surface properties of the part have thus an important influence on the quench heat transfer. In case of quenchant with low viscosity like water, the maximum cooling rate increases with increasing surface roughness. Whereas in the case of viscous quenchant like oil, the maximum cooling rate decreases with increasing surface roughness. This is because in the case of low viscous fluids, the vapour film becomes unstable as peaks on the surface tend to puncture the vapour film. This results in early start of nucleate boiling stage, whereas in the case of higher viscous quenchant the vapour film is trapped in surface roughness thus reducing heat transfer in nucleate boiling stage (Prabhu et al. 2009).

2.5.1.3 Surface oxidation

Surface oxidation and scales on the surface of a quenched part are due to the presence of moisture and air in a furnace. The low thermal conductivity of surface oxide layer reduces heat transfer at the surface/quenchant interface. However, in some cases the researchers found that the oxide layer reduced surface crack tendency.

2.5.1.4 Geometry and mass

Geometry of the quenched part is an important variable which influences the conduction heat transfer from core of the quenched part to its surface. Geometry of the surface has significant effect on the stability of different stages during quenching and the magnitude of heat transfer offered by the quenchant during these stages. Parameter module defined as the ratio of volume to surface area is also an important factor in determining the actual cooling. For a given quench media, a large piece will be cooled more slowly than a small piece (Sidney.H. Avner 1997). In case of a large sized part, high thermal gradient results in high thermal stresses.

2.5.2 Quenching system

When a part is immersed into a quench tank various factors like flow of quenchant relative to the part, volume of quenchant, racking procedures of the quenched part and temperature of the quenchant affect the heat extraction process. Out of these factors, agitation and temperature of quenchants have significant effect on the cooling of a part.

2.5.2.1 Agitation and flow direction

Agitation causes a quenchant to flow and thus mechanically disrupts the vapour blanket causing the surface to come into contact with the liquid. Agitation during nucleate boiling stage reduces the size of bubbles and increases their frequency. In a nutshell, agitation increases the peak heat flux in all the quenching media (Fernandes and Prabhu 2007). In convective cooling, agitation circulates cool liquid to replace the heated liquid surrounding the quenched part. Agitation of a quenchant not only increases the heat transfer but also ensures uniform heat removal from the quenched part thereby reducing thermal stresses.

2.5.2.2 Bath temperature

Maintaining higher temperature of quenchant has 2 major motives one being facilitation of agitation by decreased viscosity at elevated temperatures and other being reduction of distortion in a steel part. The distortion is avoided by reduced cooling rate at lower temperatures i.e. below M_s . Though vapour film of the quenchant is more stable at elevated quenchant temperatures, in the presence of agitation the vapour film ruptures easily and causes an increase in cooling rate. Heat exchangers are used to maintain the temperature of quenchant in quench tanks as the temperature of oil increases when the part is quenched in it. For marquenching and austempering, quench bath is held inside furnaces designed to maintain the temperature of the bath at desired temperature.

2.5.2.3 Racking procedure

Proper part racking so as to ensure fluid flow around the part during quenching is necessary for ensuring uniform cooling of the quenched part. It has been experimentally proved that increasing packing fraction increases vapour blanket stage there by decreasing heat transfer. The combined weight of parts and fixture must be limited to

allow for sufficient heat transfer during the quenching to minimize quench bath temperature rise.

Parts should be racked to ensure maximum flow and contact during quenching. Slender parts should be suspended. Symmetric parts should be supported on grid. Thin and flat parts should be supported on slotted rods to ensure necessary inter part separation for fluid flow. Small parts should be loaded into perforated ladle or basket to facilitate quenchant contact (Webster and Liard 1991).

2.5.3 Quenching medium

Of all the factors that affect quench hardening process listed above, only few can be changed at the heat treatment shop. Quenching medium which can produce desired microstructure distribution in the quenched steel part with minimum distortion, residual stress and cracking must be selected.

Based on the operating bath temperature (T_b), the quench media can be categorised as low temperature and high temperature quench media. Critical quench bath temperature of 100°C has been selected to differentiate between low and high temperature quench media. This is based on the fact that mineral oils having operating above 100°C bath temperature are categorized as hot oils.

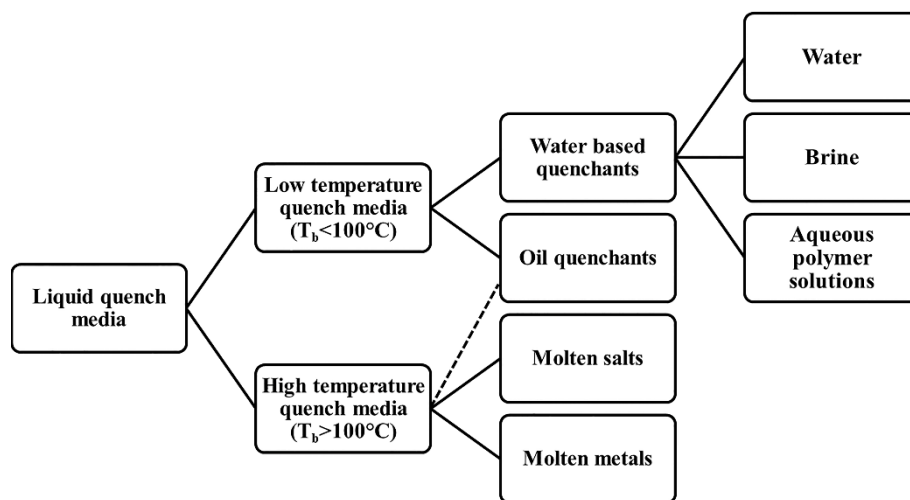


Figure 2.8: Classification of liquid quench media based on operating temperature

2.6 Low temperature quench media

Conventional liquid immersion quenching is used to harden low, medium and high hardenability steel parts of different cross sections. Figure 2.9 shows the wide range of low temperature quench media organized in the order of their quench severity. Among the present industrial quenchants, brine solutions and water have highest quench severity. These are followed by water-based polymer quenchants and oils. For lower severity air or gases can be used as quenching medium.

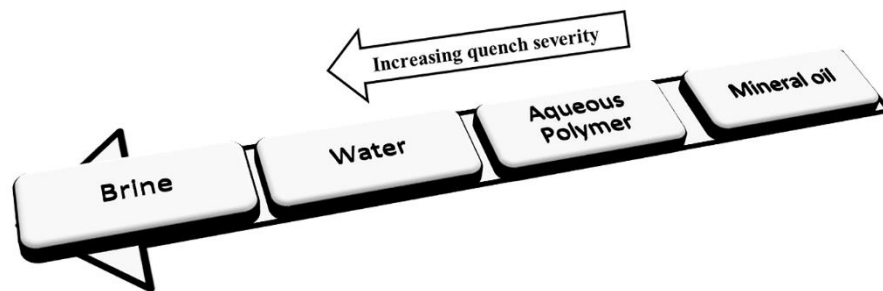


Figure 2.9: Quench severity of industrial quench media

2.6.1 Water

Water is the most common quenching agent used in the heat treatment industry for hardening of steels. The ease of availability and disposal and low cost has facilitated extensive use of water as a quenchant. Water is unable to wet the surface of the part evenly and this results in non-uniform heat extraction from the cooling metal. Austenitized steel parts are quenched in water maintained at 60°C-70°C to aid uniform heat extraction. This reduces distortion and residual stresses, but lower hardness is the consequence of quenching steel part in hot water.

2.6.2 Brine

Brine and other solutions of water and inorganic salts have higher cooling rates in vapour blanket and nucleate boiling stages of cooling. Salts such as NaCl, MgCl₂, LiCl, CaCl₂, MgCl₂, KMnO₄, Na₂CO₃, and NaOH are mixed with water to form brine quench media. Brine quench of 3% sulphuric acid + 97% water helps in removing scale from the cooling hardened carbon steel tools surface. These salts precipitate out of water solution and provide a uniform heat transfer during quenching by upsetting the steam vapor that is formed on the metal surface during the initial quenching stage. The concentration of salt in the brine solution has the most significant effect on cooling performance of the quench medium. The increase in concentration of salt decreases the

duration of vapour blanket stage and at sufficiently high concentration, vapour blanket stage does not occur. Very high concentration of salt, however, decreases the cooling performance of brine quench media. The disadvantages of using brine solutions over water is accelerated corrosion attack of the parts. Quenching small parts of high hardenable steels in brine media increases risk of cracking (Totten et al. 1993) (Boyer and Cary 1988).

2.6.3 Aqueous polymer solutions

The cooling performance of polymer quenchants is intermediate between water and mineral oils. Polymer solutions are non-flammable, nontoxic, harmless to the operating personnel, easily removed from parts after quenching and biodegradable. The use of polymer quenchants enhances the wetting and controls the quenching speed hence proves useful in control of distortion and reduction in residual stress.

Poly alkylene glycol (PAG), poly vinyl pyrrolidone (PVP), poly sodium acrylate (PSA), and poly ethyl oxazoline (PEOX), polyvinyl alcohol, poly acrylamide, cellulosic derivatives, polyethylene oxide and vinyl copolymer etc are some of the important polymer quenchants which are widely used for industrial heat treatment (Prabhu et al. 2016). PAG is the most commonly used polymer for quenchant preparation.

Aqueous PAG solution exhibits inverse solubility phenomena. Inverse solubility results in separation of water and PAG above 60°C-70°C. The separation leads to increased viscosity near the surface of the quenched probe. The inverse solubility phenomenon, triggers a change in the conventional three stage cooling mechanism (Totten et al. 1998). Analogous to film boiling stage, encapsulation stage occurs during quenching in PAG solution. During encapsulating stage phase medium consisting of a combination of water vapor and polymer prevents liquid quenchant from meeting surface of the steel part. PVP, PSA and PEOX do not exhibit inverse solubility and have relatively oil like quenching characteristics. The cooling performances of polymer solution quenchants are dependent on agitation, concentration and temperature of quenchant (Hilder 1988). With increase in concentration of PAG, stability of encapsulating stage increases and cooling performance of the quench media decreases (Pai et al. 2015). Operating bath temperature ranging between room temperature and 70°C has been reported in literature.

2.6.4 Mineral Oil

After water, oil is the most widely used industrial quench media (de Souza et al. 2009). This is because oils help in reducing distortion and residual stresses as the cooling rate during convective stage is low. Mineral oils are petroleum by-products, generally mixtures of chemical structures with a range of molecular weights. Crude based mineral oils are distilled from the C26 to C38 fraction of petroleum and composed of mixture of branched paraffins (C_nH_{2n+2}) and cycloparaffins (C_nH_{2n}) together with a small quantity of aromatics (benzene ring and its derivatives). Crude oils containing primarily branched paraffin hydrocarbons are called paraffinic oils and those containing large percentage of cycloparaffins in are called Naphthenic oils. Paraffinic and Naphthenic oils are the base oils for mineral quench oils (Ramesh and Prabhu 2014a).

The petroleum-based quench oils can be broadly classified into 4 types namely normal speed quench oils, medium speed quench oils, high speed quench oils, marquenching oils or hot oils (MacKenzie 2003).

- a) **Normal speed quench oils** have relatively low rates of heat extraction and are used to harden high alloy steel or tool steel parts.
- b) **Medium speed quench** oils provide intermediate quenching characteristics and are widely used to harden parts of medium and high hardenability steel grades which require dependable and consistent metallurgical properties.
- c) **High speed quench oils** are used for hardening low hardenability alloys, carburized and carbonitrided components, or large cross-sections of medium hardenability steels where high rates of cooling are required to ensure maximum mechanical properties.
- d) **Mar-quenching oils/hot oils** are used for marquenching heat treatment where in the part is quenched into a medium maintained at elevated temperature, typically 100-200°C. The work piece is held in the quenchant until temperature equilibrium is established throughout the section, and then air-cooled to ambient temperature. A detailed discussion on hot oil quench media would be carried out in further section.

Normal, medium and high speed quench oils contain paraffinic and naphthenic fraction. Antioxidants, accelerators and emulsifiers are added to base oil to improve service life

of oil, enhance cooling performance by improving wettability and ease post quench cleaning of steel parts respectively (Salawa et al. n.d.). Mineral oils have better aging stability, thermal stability and oxidation resistance. Through careful formulation and blending and by the addition of wetting agents, accelerators and anti-oxidants a wide range of quenching characteristics can be obtained. The operating temperature for these oils varies between room temperature and 80°C.

2.6.5 Alternative low temperature quench media

New quench media which offer enhanced economic, technological and environmental benefits as compared to traditional low temperature quench media have been developed. The range of severity of these alternative quench media is illustrated in Figure 2.10.

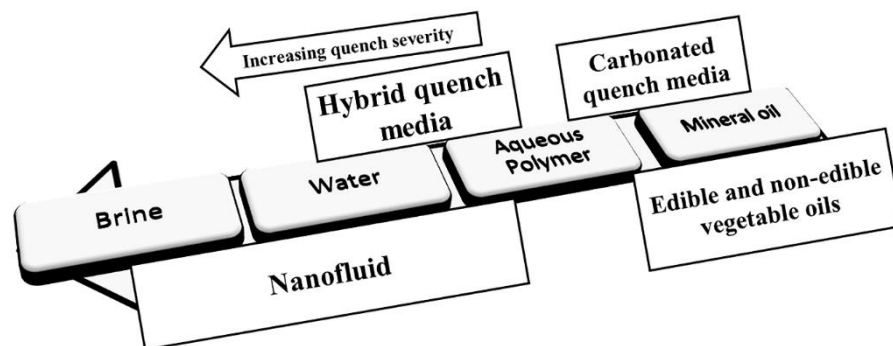


Figure 2.10: Alternative low temperature quench media

2.6.5.1 Nano fluid quench media

Nanofluids are a new class of quench media. These fluids alter the quench performance of base fluid i.e. water. Typically, nanoparticles with average sizes below 100 nm are dispersed in water and used as quench media. Proposed mechanisms for increased thermal conductivity observed in nano fluid are as follows (Ramesh and Prabhu 2011):

- a) Brownian motion of nanoparticles
- b) Ordered layering of liquid molecules at the solid particle surface which acts as thermal bridge between the solid nanoparticles and the base liquid
- c) Change in heat transport mechanism from diffusive to ballistic due to reduction in mean free path

- d) Clustering of nanoparticles due to van der Waals force to form percolating patterns with low thermal resistance paths.

The addition of nanoparticles has a significant effect on the critical cooling parameters of water. The increase in the copper, aluminum and MWCNT nanoparticle concentration resulted in increased cooling rates at critical temperatures for nanofluids with concentrations of up to a critical concentration, further increase in the concentration of nanoparticles resulted in a decrease in the cooling rate. (Nayak and Prabhu 2015; Ramesh and Prabhu 2013a; b). In case of CuO and graphene nano fluids, increase in nanoparticle concentration resulted in decreases cooling rates at critical temperatures. (Nayak and Prabhu 2016a; b)

2.6.5.2 Hybrid quench media

Hybrid quench media is a blend of aqueous polymer brine solution. Ramesh and Prabhu prepared hybrid quench media prepared by adding 10 wt% of NaCl to aqueous 20 vol% PAG solution. The addition of salt shortened the duration of polymer encapsulation stage. At temperatures above 720°C, the hybrid quench media offer cooling rate higher than polymer quench media. The lower cooling rate offered by this medium at lower temperatures reduces distortion and crack propensity of steel parts. This media thus combines the advantages offered by aqueous polymer and brine quench media. (Ramesh and Prabhu 2014b)

2.6.5.3 Carbonated quench media

Nayak et al. prepared carbonated quench media by passing CO₂ at 60PSI through water and aqueous polymer solutions (Nayak et al. 2016). Quenching in carbonated media resulted in slow cooling and the peak cooling rate reduced by over 50% compared to non-carbonated aqueous quench media. High cooling rates are offered by the carbonated media at lower temperatures. This increases the risk of distortion and cracking. The heat extraction mechanism was altered and a very stable layer consisting of mixture of vapour and CO₂ encapsulates the interface during film boiling stage and the rewetting occurred at a very low surface temperature. Carbonated water can be an effective replacement for mineral oil to quench harden medium-carbon steel parts to obtain uniform hardness distribution across the cross section (Mathews et al. 2019).

2.6.5.4 Vegetable oil

Mineral oils are derived from non-renewable sources and they are non-biodegradable and toxic in nature. There has been a continuing effort to identify eco-friendly and safer alternative liquids as quenchants. Vegetable oil-based quench media are perceived to be a suitable replacement for mineral oil-based quench oil. Unlike mineral oils, vegetable oils are biodegradable and non-toxic.

Some of the vegetable oils used for quenching purpose listed in literature are canola, soybean, rapeseed, sunflower, linseed, corn, cottonseed, gingelly, coconut, olive, palm, peanut, groundnut, castor, cashew nut shell, neem, crambe and tea seed (Ramesh and Prabhu 2012). Cooling behaviour of vegetable oils are different from mineral oils in a sense that no stable film boiling stage is present on the surface of the sample for a significant time (de Souza et al. 2009).

Totten et al (Totten et al. 1999) compared performance of commercial mineral quench with crude expelled soya bean oil and partially winterized and hydrogenated soybean oil. The quench cooling characteristics of these vegetable oils were better than that of the mineral oil. Pranesh and Prabhu (Pranesh Rao and Prabhu 2015) studied quench performance of olive oil, rice bran oil and canola oil, and some mineral oil blends. A very short duration of vapour blanket stage was observed in these vegetable oils which resulted in faster heat extraction rate compared to mineral oil. Grossman's H factor for sunflower oil, coconut oil and palm oil is higher than mineral oil, this indicates better quench performance by these vegetable oils. However Ground nut oil and castor oil have lower Grossman's H factor than mineral oil (Dean et al. 2009).

Use of edible vegetable oils for heat treatment purpose will cause a shortfall for food processing industry, non-edible vegetable oils are hence preferable alternative as quenching media. The quench performance of non-edible vegetable oils namely neem (*Azadirachta indica*) oil and karanja (*Pongamia pinnata*) oil was studied by Nayak, Ramesh and Prabhu (Nayak and Prabhu 2018; Ramesh and Prabhu 2014c). They concluded that these non-edible vegetable oils are potential quench media to heat treat steel. Hassan. et al observed that neem oil can be used where cooling severity less than that of water but greater than SAE 40 engine oil is required for hardening of plain carbon steels and ductile cast iron (Hassan et al. 2011).

2.7 High temperature quench media

Distortion and residual stresses are inherent during quench hardening process owing to thermo-mechanical and thermo-metallurgical physics. Growing concerns to improve reliability of the quenched part has forced researches to seek methods to reduce the risk of distortion and residual stress in the quenched part. Austempering and Marquenching for long have successfully proved to fulfil the purpose by providing an optimum combination of hardness and residual stress state in the quenched part. Austempering and martempering require quench media that can operate at temperatures from 150°C-550°C. Hot petroleum oil, molten salts or alkali, low melting point alloys or metals and fluidized beds are some quench media which are suitable for this purpose.

2.7.1 Molten metals and alloys

One of the most common metals used in molten form as a quenchant is lead. For special applications, lead-based alloys with bismuth and tin having lower melting points are used. Lead has a melting point of 327°C and is typically used at 343°C to 927°C. Molten lead is used for austempering, and patenting of steel parts. However, because lead possesses a high thermal conductivity and no film-boiling stage, it provides relatively rapid cooling rates in a high-temperature range not easily achievable with other quenching media (Totten et al. 2002). Due to the toxicity and disposal problems with lead, it is seldom used in the thermal processing of steel.

2.7.2 Molten salt bath

Molten salt baths have been used in the heat treatment industry as quench media for more than 50 years. Molten salts possess properties such as wide operating temperature range, excellent thermal stability and tolerance for contaminants. These properties make salt quenching systems almost maintenance-free and thus they can provide satisfactory performance for many years simply by adding salt to replace dragged out (Dubal 1999).

The cooling in molten salts is observed to be primarily by boiling and convection mechanism. The performance of molten metal and molten salt baths as quenchants do not differ greatly. Thermal diffusivity of molten salts are very low as compared to that of molten metals (Sudheer and Prabhu 2016). The viscosity of molten salt bath is much

lower compared to molten metal bath. The change in viscosity of molten salt quench media over a wide temperature range is miniscule. Lower viscosity eases the motion of the quenchant during agitation and hence increases the cooling performance of the quenchant.

There are two main categories of quenching salts: nitrate/nitrite-based and chloride-based, having working ranges of 150 to 595°C and 425 to 705°C, respectively. Hydroxide- and carbonate-based salts are not recommended for quenching or austenizing, because these materials adversely affect surface corrosion susceptibility (Dubal 1999).

2.7.2.1 Chloride based salt quench media

Molten ternary mixtures of sodium, potassium and barium chlorides are generally used as quench media. Since most grades of steel require lower quench bath temperature, the usage of molten alkali chloride quench media is limited for heat treatment of high-speed tool steels which need to be marquenched in quench media at 450°C-600°C.

Insoluble and soluble metal oxides develop in the molten chloride salt bath. These oxides cause decarburizing of the quenched steel part. The maintenance of the bath thus requires frequent removal of these metal oxides. This is done using silica or methyl chloride rectifiers in conjunction with graphite/carbon rods. Silica and methyl chloride react with the metal oxide and form in-soluble sludge. The sludge settles in the bottom of the quench tank and can be desludged. The carbon atoms in the graphite/carbon rods reduces the metal oxides to metal. The metal atoms stick to the surface of the graphite rod. The rod is then removed from the bath and cleaned by scrapping the metal attached to the surface (Dexter n.d.).

2.7.2.2 Nitrate/Nitrite based salt quench media

Sodium and Potassium nitrate/nitrites also known as salt peter salts are the most commonly used alkali nitrate- nitrite based salts. A salt commonly used for martempering is composed of 50-60% KNO_3 , 37-50% NaNO_2 and 0-10% of KNO_3 . These salts melt at 140°C. Higher melting point salts composed of 0-50% of KNO_3 0-30% NaNO_2 and 20-60% of NaNO_3 are used for higher operating temperatures. These nitrate-nitrite mixture salts are used within the working range of 165-540°C(ASM

Handbook Committee 1998) Figure 2.11 shows the dependence of melting point of the salt mixture on its composition. The sides and the diagonal of this square enable us to find the melting point of the binary system and each point inside the triangle represents composition of the ternary system. Mixtures of salts having melting points ranging between 440°C and 140° can be obtained. It is suggested to choose the composition of the salt mixture such that the operating temperature is at least 55°C greater than the melting point of the mixture (Dubal 1999).

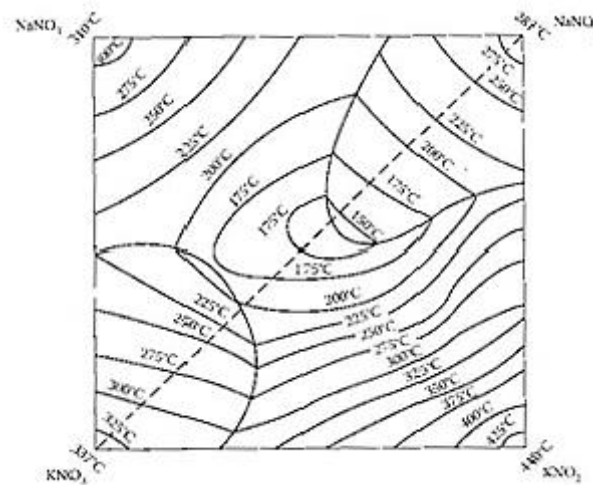


Figure 2.11: Isothermal sections of the liquidus surface of nitrate-nitrite system
(Lisicic et al. 2010).

As in case of other of other quenchants, the severity of the molten saltpetre salt bath systems depends on temperature and agitation of the quench system. As the temperature of this molten bath decreases or intensity of agitation increases, the severity of the quench system increases.

Addition of water: Addition of small amount of water (less than 10%) to the molten salts have been observed to be highly effective in improving the cooling performance of the quenchant. Figure 2.12 demonstrates the nature of bonds that exist when water is introduced into molten NaNO₃ salt. Water molecules form Vander wall bonds with the molten salt ions. Hydrogen bonds are formed between water molecules. Hydrogen and oxygen atoms form Vander-walls bond with anion and cation of the salt respectively (Reid 1996).

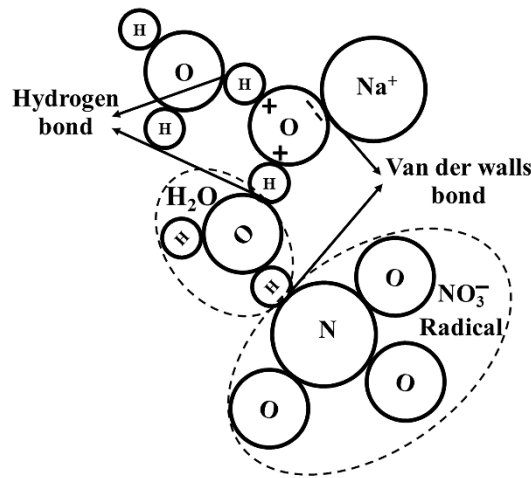


Figure 2.12: Bonds between water and molten salt at high temperature

Significant reduction in melting point of the molten salt bath is observed upon addition of water. The water is sprayed/atomized onto the vortex created during agitation. The water content in the salt bath may decrease as it may evaporate when the quenched part is being cooled or due to the bath temperature thus timely water must be added to the quench bath to maintain the desired level of water content.

The water content is checked either by sampling method or continuous method. In sampling method, samples of quenchant containing water are collected weighed and subsequently dried at 400°C in a furnace. The difference between the weights of hydrated and dried quenchant samples gives the water content in the bath. Continuous method enables continuous monitoring of water content in the quenchant through electric conductivity of the quenchant. Automatic water content maintaining systems controls the water flow into the quenchant based on water content measured by continuous method.

Adding water to these mixtures improves their cooling performance and reduces their melting temperature. NaNO_2 eutectic mixture (53% KNO_3 -40% NaNO_2 - 7% NaNO_3) melts at 140°C while mixture containing 2-3% water melts at about 100°C. An Addition of 0.09% of water increased cooling rate of $\phi 20$ mm sliver ball from $\sim 160^\circ\text{C/s}$ to $\sim 210^\circ\text{C/s}$. A small addition of water to a salt bath produces a significant increase in its quench severity.

Effect of Agitation: Foreman (R.W. Foreman 1993) studied change in average cooling rate between 650°C and 260°C with agitation and water content. For dry salt bath at 175°C, the average cooling rate increased from 40°C/s to ~95°C/s when agitation rate was increased from 0cm/s to 175cm/s. At the same bath temperature and agitation rate of 50cm/s, when the water content was increased to 5% the average cooling rate increased to 135°C/s. Increasing agitation results in a substantial increase in the quench severity. The addition of water also decreases the viscosity of the molten salt. This further enhances the effect of agitation. The synergetic combination of agitation and a water addition increases quench severity three-folds compared with that of a non-agitated dry salt bath.

Risks and limitations:

Salt bath quenchants are non-flammable but there exists a potential risk of explosion when the temperature of the quenchant exceeds 600°C (thermal degradation) or due to reaction of these molten salts with cyanide carried over by the part from carburizing media. These risks can be dealt with by maintaining the temperature of the quenchant below 600°C and treating it with neutral salt baths before treating with nitrate/nitrite salts.

Spattering of molten salt when it comes in contact with moisture is another problem associated with salt bath quenchants. The parts should be thoroughly dried before quenching in the bath and care should be taken while adding water to molten salt bath (*A guide to the safe use of molten salt baths* 1996). Alkali chlorides, alkali carbonates, metallic scale and complexes are some of the insoluble contaminants that settle as sludge and are removed by filtration process.

Advantages: The ease of cleaning the quenched part is one of the important benefits of using molten salt quenchants. The thin layer of salt that adheres to the surface of the quenched specimen can be washed off easily by spraying hot or cold water on the part. This water can be retained and added the salt bath.

2.7.2.3 Alkali hydroxide-based quench media

Quench hardening in molten mixtures of hydroxides of sodium and potassium media is called bright hardening. This is because hardened parts have a non-oxidized bright

surface. Alkali hydroxide mixtures have a lower melting point as compared to conventional nitrate-nitrite salt mixtures. Anhydrous molten mixtures are used when operating temperature is above 250°C. Pure molten NaOH are preferred quench media for operating temperature exceeding 350°C. Anhydrous mixtures have melting point ranging between 160°C (37%NaOH -63%KOH) and 360°C (KOH) can be obtained.

Torkamani et al. (Torkamani et al. 2014) compared mechanical properties of AISI D2 steel hardened in anhydrous 40%NaOH-60%KOH mixture at 230°C and oil at 60°C. The bright-hardened samples possessed higher hardness, toughness and ultimate tensile strength values than the oil-quenched samples.

Addition of water: Addition of water can significantly improve the quench performance of NaOH-KOH mixtures. Hydrated NaOH-KOH mixtures having melting points as low as 120°C can be obtained.

Rassizadehghani et al. (Rassizadehghani et al. 2006) compared mechanical properties of steel AISI 1045 quenched hardened in anhydrous and hydrous 40%NaOH-60%KOH quench media maintained at 205°C. Hardness and hardness distribution in the sample from the surface to the core were observed to be enhanced with addition of 5% water to anhydrous 40%NaOH-60%KOH quench media (Raygan et al. 2009).

Risks and limitations: The surface of parts quenched in these quenchants are highly susceptible to corrosion. Tri-sodium phosphate is added to NaOH-KOH mixture to increase the corrosion resistance of the quenched parts.

The service life and stability of the alkali hydroxide mixture media are lower in comparison to alkali nitrate/nitrite mixtures. Carbonates of sodium, potassium or barium (contaminant barium chloride from heating salt) are formed in the quench bath due to absorption of carbon dioxide from the environment. The dense carbonates in the bath modifies its composition as well as quenching power. Removal of clots formed, replenishing the bath with fresh salt and adding deoxidizers like potassium-ferrocyanide or/and borax are the remedies for above mentioned problems. Alkali chlorides, alkali carbonates, metallic scale and complexes are some of the insoluble contaminants that settle as sludge and are removed by filtration process.

Advantages: Hardening in molten nitrate-nitrite mixture media results in oxidation of quench-part surface. Bright surface of parts quenched in molten NaOH-KOH mixture baths need not be sand-blasted or etched. The residues of the bath should be washed out from their surface. Water added to the bath improves the quality of the quench-part surface.

2.7.3 Hot quenching oils

Martempering oils are formulated from refined paraffinic base oils with high thermal stability. Additives, which are carefully selected, and tested antioxidants are added to retard the aging process. The operating temperature for martempering oil range between 100°C to 250°C. These oils can be used for both modified and conventional martempering of steel parts. Some hot oils are also used for austempering certain grades of steel. Thermal aging and oxidation are thus main factors considered during selection of martempering oils.

The main problems often encountered in these quenchants are thermal and oxidation stability, which cause undesirable changes in viscosity of the oils thus, resulting in short service life. Oxidation stability of these oils can be improved by adding antioxidants. Designing the quench system that prevents overheating and ensures a protective, non-oxidizing environment can contribute in to increase thermal and oxidation stability respectively. The health and environmental concerns associated with toxic fumes that evolve when the part is quenched in hot oils and the high risk of fire hazard are the disadvantages associated with the hot oils.

The thermal degradation process in the mineral oils can be divided into 3 stages namely initiation, propagation and termination. During Chain Initiation, free alkyl radicals ($R\bullet$) are formed due to oxidation of base hydrocarbon ($R-H$) . These reactions are slow at room temperature but become increasingly faster as the temperature increase. During chain propagation, Alkyl radicals react with oxygen in the oil to form peroxy radicals ($ROO\bullet$). These peroxy radicals further react with additional hydrocarbon molecules to produce alkyl hydroperoxides ($ROOH$) and additional alkyl radicals. During termination stage, Hydroperoxides form aldehydes, ketones and alcohols. Carboxylic acids are formed by the oxidation of aldehydes and ketones. These oxidation products form, high

molecular weight oligomers which settle as sludge in quench tanks and increase viscosity of the oil (Rowland and MacKenzie 2018).

The unique feature of these oils is their high quench severity, even at high operating temperatures. There are 2 types of hot oils namely accelerated and non-accelerated hot oils.

- a) **Conventional hot oils:** Cooling performance depends on the viscosity of the oil.
- b) **High performance hot oils:** Cooling performance of these oils are independent of their viscosity rather cooling rate accelerating additives are added to the base oils which improves wetting and enhances quench heat transfer.

Since all the 3 stages of quenching are present, violent agitation is required during quenching in these quench media in order to ensure uniform heat transfer. Nevertheless, it also improves the cooling performance of the media.

Precautions: The heat density supplied by the quench steel parts should 10-150kW/m². The service life of hot oils is dependent on various operating conditions. The operating temperature and bath temperature after quenching should be substantially lower than flash point of the quench oil to avoid toxic fumes, fire hazard and accelerated degradation of oil.

The surface area of the quench oil in the tank in contact with the air should be reduced to minimum. Entering of air into the bath during agitation should be prevented. Violent agitation should be used only when parts are quenched in the bath. The rate of agitations should be decreased otherwise.

2.7.4 Fluidized-bed

Quench severities intermediate between those for still air and mineral oil quenchants are possible with fluidized bed quenching (Delano and Sype 1988; Doheim and Himmo 1988). A fluidized bed is generated by blowing gas through a bed of fine solid particles. Aluminium oxide, silicon carbide and quartz sand are used as solid particles. Nitrogen, argon, and carbon dioxide, helium, or hydrogen are used as gases. Generally, aluminium oxide provides the best heat-transfer capacity, thermal stability, and environmental compatibility. Traditionally, the most common gases for fluidized beds

were nitrogen and air. Hydrogen and helium provide greater potential for wider ranges of heat-transfer rates.

Flow rate of gas, particle size and compaction of particles considerably influences the quench performance of this media. In general, cooling rates increase as particle grain size increases. Generally, particles of size 100-150 μm are used. The flow rates are maintained at 2 to 5 times of critical flow rate i.e. flow rate at which loosening of bed particles start. The dimensions of the fluidized bed relative to the size and mass of the parts being quenched, and position of the part in the bed affect the cooling process.

For martempering and austempering, fluidized bed media are maintained at higher temperatures. The cooling rates decrease with increasing bed temperature. Apart from being environmentally friendly, the fluidized bed media provide an additional advantage of equal heat transfer throughout the range of temperature during quenching.

Limitations: Some of the disadvantages associated with the fluidized bed media are that, they have lower quench severity compared to molten salts. Also, some locations on the quenched part are shielded from the stream of particles known as shield effect which results in non-uniform heat extraction from the quenched part.

2.7.5 Alternative high temperature quench media

A large quantum of research on quench media are concerned with low temperature quench media. This section provides brief insight into the new class of alternative high temperature quench media suggested in this work.

2.7.5.1 Low melting point eutectic salt media

Bauer et al. (Bauer et al. 2012) enlists various eutectic low melting point ternary and quaternary mixtures of nitrates and nitrite salts with Na, K, Li and Ca cations. The lowest melting point of 75°C was observed in Li-K-Na nitrate-nitrite mixture. The chemical properties of the LiNO_3 - KNO_3 - NaNO_3 and $\text{Ca}(\text{NO}_3)_2$ - KNO_3 - NaNO_3 melts are similar to conventional KNO_3 - NaNO_3 melts. $\text{Ca}(\text{NO}_3)_2$ or LiNO_3 molten eutectic mixtures are thus not expected to intensify the corrosiveness of the conventional NaNO_3 - KNO_3 mixtures (Bradshaw et al. 2009).

When heated, molten nitrate salts undergo endothermic decomposition reaction. Decomposition reactions occur at the surface of the quenched steel part and contribute

to heat extraction process. The decomposition of nitrates occurs due to following 3 mechanisms (Bauer et al. 2013).

- 1) Nitrite formation in bath with oxygen release
- 2) Alkali metal oxide formation in melt with release of N_2 or nitrogen oxides
- 3) Vaporization of nitrate salts

Tao wang et al (Wang et al. 2013) studied decomposition of quaternary $LiNO_3$ - $NaNO_3$ - KNO_3 - $NaNO_2$ mixture. They concluded that contribution of vaporization mechanism during decomposition was insignificant.

The R.W. Bradshaw and D.E. Meeker (Bradshaw and Meeker 1990) investigated the chemical stability of low-melting, ternary molten salt mixtures of $NaNO_3$, KNO_3 and either $Ca(NO_3)_2$ or $LiNO_3$. They observed that the nitrate-nitrite decomposition reaction that occurs at lower temperatures in these ternary mixtures are comparable with that observed in equimolar $NaNO_3$ - KNO_3 melt. However high temperature decomposition reaction of nitrate/nitrite to oxide ions was observed to strongly dependent on the composition of ternary mixtures. Ternary mixtures containing lithium nitrate were more stable than those containing calcium nitrate.

2.7.5.2 Vegetable oil

Vegetable oils are mixture of various triglycerides of fatty acids. Based on the number of carbon-carbon double bonds in the fatty acid ester structural components of the different vegetable oil triglycerides are broadly classified into 3 types, 1) saturated, 2) monounsaturated and 3) poly unsaturated fatty acids.

Vegetable oils have a limitation of relatively poor oxidative stability properties. Oxidation of vegetable oils occurs in 3 stages namely initiation, propagation and termination. Vegetable oil oxidation is initiated by formation of free radicals ($R\bullet$). Free radicals react with oxygen to form a peroxy radical ($ROO\bullet$). The oxidation reaction is propagated by peroxy radical which attacks another lipid molecule to remove a hydrogen atom and forms hydroperoxide ($ROOH$) with an additional free radical. The strength of a carbon-hydrogen bond next to a carbon-carbon double bond is lower, and this hydrogen can be removed easily during oxidation reaction. Thus carbon-carbon bonds are active sites for oxidation reaction. In other words, oxidation stability of a vegetable oil decreases with increase in unsaturated fatty acid content. During

termination stage, hydroperoxides no longer remain stable and decompose to form numerous volatile and non-volatile secondary oxidation compounds. Hydroperoxides undergo polymerisation reactions leading to deposits and increase in viscosity of the oil.(Fox and Stachowiak 2007). The effect of oxidation results in grater variation in quench performance of vegetable oils relative to that observed in conventional petroleum oil quenchants (Canale et al. 2005). De Souza et al (de Souza et al. 2013) experimentally determined oxidative stability of various vegetable oils. The oxidative stability of vegetable oils was studied and was arranged in decreasing order as follows. Peanut< sunflower ~ cottonseed ~ soybean<coconut<corn oil.

2.8 Evaluating cooling performance of a quench media

Quenchometer test, hot wire test, Grossman technique, Rushman technique and interval five second test are some of the important tests that have been used in heat treatment industries to assess the cooling performance of various quench media. In recent years cooling curve has gained prominence and is the most widely used industrial practice for evaluating cooling performance of quench media. The method requires a standard probe equipped with thermocouples. The probe is heated to high temperature and quenched in the quench media. The time-temperature data in the quenched probe is obtained during cooling. The thermocouple may be placed at a single or multiple location to monitor the cooling at different locations of the probe. Researchers have tried standard probes of different shapes, sizes and materials. An Inconel 600 material cylindrical probe with 12.5 ϕ and 60mm length is proposed test probe for assessing performance of quench media in ISO9950 standard.

Cooling curve parameters obtained from quenching experiments using standard probe are as follows

- CR_{max} : Maximum cooling rate
- T_{max} : Temperature corresponding to CR_{max}
- CR_{705} : Cooling rate at 705°C (Temperature corresponding pearlitic transformation range)
- CR_{550} : Cooling rate at 550°C (Temperature corresponding to bainitic transformation range)

- CR300 and CR200: Cooling rate at 300°C and 200°C (Temperature corresponding to martensitic transformation range)
- $t_{760-230}$: Time to cool from 760°C to 230°C
- t_{A-B} : Time to transition from vapour blanket stage to nucleate boiling stage
- T_{A-B} : Temperature at transition from vapour blanket stage to nucleate boiling stage

Grossman's quench severity, Tamura's V-Value, hardening power (HP), Castrol index, V_s/V_c , and quench factor analysis are the other methods to characterize quench media. Some of these methods use steel probes for assessing of cooling performance of quench media.

2.9 Estimation of metal quenchant interfacial heat flux

Heat flux gage method, lumped heat capacitance method, temperature gradient method and Kobosko's method are some of the methods listed in the literature to estimate metal quenchant interfacial heat flux during quenching. Each of these methods have their own limitations related to size of the part used, modification quench part surface, etc.

Inverse heat conduction method has gained prominence lately and has proved to be a powerful tool to estimate quench heat flux based on the temperature data measured inside the quench part. Kumar (Babu and Prasanna Kumar 2012) developed a serial algorithm to estimate the individual boundary heat flux components, one by one, at the unknown boundary, based on the function specification method. Prabhu and Ramesh (Ramesh and Prabhu 2014b) used this method to determine spatially dependent heat flux transients during immersion quenching of the Inconel probe in brine and polymer media. Felde and Szénási (Felde and Szénási 2016) used a particle swarm optimization method to calculate the unknown HTC function during immersion quenching.

2.10 Summary

Conventional liquid immersion quenching is the process of immersing austenitized steel part in a single quenchant which may be gas or liquid. The quench media in this process is maintained near to room temperature. The high cooling rate in martensitic transformation range often results in quench defects in the heat-treated part.

Time quenching technique on the other hand involves use of two or more quenching media on a timed basis. This technique is practised to avoid quench defects in the heat-treated part. Martempering is one of the important industrial practice which is based on time quenching technique. The austenitized steel part is quenched in a medium maintained just above M_s , and the part is held in the quenchant until temperature is equalized throughout its cross section. Subsequently the part is air cooled. Large cross-section and low hardenable steel parts are subjected to modified martempering processes to obtain martensitic microstructure across the cross section.

Isothermal quenching technique involves quenching of austenitized steel part in a medium maintained at a specific predetermined temperature and holding at that temperature till transformation is completed. Austempering is a commercial example for this process which results in bainitic microstructure in the quenched steel part. Numerous variations of austempering process are practised to obtain a mixture of martensite and bainite in the microstructure of the steel part.

Selection of an appropriate quenching medium can certainly produce desired microstructure distribution in the quenched steel part with minimum quench defects. Based on the operating temperature, the quenching medium can be classified into low temperature and high temperature quenching medium.

The operating temperature for low temperature quench medium is less than 100°C . Brine, water aqueous polymer and mineral oils are the conventional low temperature quench media used in liquid immersion quenching technique. Quench media which can operate at temperatures greater than 100°C are classified as high temperature quench media. Hot petroleum oil, molten salts or alkali, low melting point alloys or metals and fluidized beds are suitable quench media for this purpose.

Molten salt baths possess properties such as wide operating temperature range, excellent thermal stability and tolerance for contaminants and hence been used in heat treating industry for more than 50 years. There are two main categories of quenching salts: nitrate/nitrite-based and chloride-based salts. Hydroxide and carbonate-based salts are not recommended for quenching or austenizing, because these materials adversely affect surface chemistry. The use of chloride-based salt is restricted for hardening tool steels which need quench bath maintained at 450°C - 600°C . Binary or

ternary mixtures of sodium and potassium nitrate/nitrite are conventionally used as high temperature quench media. Addition of small quantity of water to the molten salt bath results in a significant increase in quench performance of salt baths. Martempering oils/Hot oils which are refined paraffinic base oils with anti-oxidants and accelerators are also used as high temperature quenching applications.

Low melting point eutectic salt mixtures consisting nitrate/nitrites of Na, K, Li and Ca can serve as alternative high temperature quench media. The low melting point of these salt mixtures have an advantage of expanded operating temperature range. Vegetable oils are a possible alternative high temperature quench media which can effectively replace hazardous mineral based hot oil quench media.

Various methods have been developed by heat treatment researchers to assess cooling performance of quench media. Cooling curve analysis and estimation of metal quenchant interfacial heat flux are the most widely used methods characterize the cooling performance quench media.

Chapter 3 SCOPE

Quench part, quenching system and quenching medium are the three major factors which influence the properties of the quench hardened part. Of all these factors, quenching medium is the most critical factor. Hot oil and molten salt/alkali baths are widely used as quench media for austempering and marquenching heat treatment processes in industries.

A study on the cooling performance of conventional high temperature quench media like hot oils and molten salt mixtures is essential for better selection of quench medium. Cooling curve analysis and study of heat transfer at metal/quenchant interface provide a scientific basis for selecting quench media and would help in ensuring enhanced quality of the heat-treated product.

Heat transfer at the metal quenchant/interface is the driving force for metallurgical transformations, distortion and residual stress. The mechanism of heat extraction at metal/quenchant interface is complex. This is due to simultaneous existence of different stages of quench-heat extraction at the part surface which results in large variation in heat flux. The study of spatially dependent heat transfer at the metal/quenchant interface would provide a better perspective about the nature of cooling offered by the quenchant.

Low melting point eutectic salt mixture containing $\text{KNO}_3\text{-LiNO}_3\text{-NaNO}_3$ offers a wider operating temperature range as compared to conventional $\text{KNO}_3\text{-NaNO}_2\text{-NaNO}_3$ eutectic mixture. Non-edible vegetable oils are non-hazardous, and biodegradable, hence are perceived to be viable alternative to conventional mineral hot oils. The possibility of replacing conventional high temperature quench media by the vegetable oil and molten salt mixtures containing lithium nitrate needs to be investigated.

Metallurgical transformations that occur during quenching affects the thermal profile and the heat flow from the quenched part to the cooling medium. The heat transfer in standard Inconel probes used for characterization of quenchants is significantly different compared to that in steel probes wherein metallurgical transformations results in enthalpy change. An extensive study on the inter-relationship between the quench heat transfer characteristics and kinetics of metallurgical transformations that occur during quenching in high temperature quench media is therefore essential.

Chapter 4 OBJECTIVES

1. To assess the cooling performance of conventional hot oils and molten mixtures of KNO_3 , NaNO_3 and NaNO_2 quench media.
2. To calculate spatially dependent heat flux transients at the metal/quenchant interface.
3. To examine the possibility of replacing
 - a) Conventional hot oil with non-edible vegetable oil
 - b) Conventional molten salts with lithium nitrate based low melting eutectic salt mixture
4. To assess the effect of metallurgical transformations on cooling behavior of steel probes during quenching.
5. To propose a model to prediction of hardness as a function of bath temperature, part diameter, residence time and heat transfer coefficient.

Chapter 5 MATERIALS METHODS AND EXPERIMENTAL DESCRIPTION

5.1 Quench media

The quench media used for quenching experiments, respective bath temperatures and the material of the probe have been presented in Table 5.1. Pure NaNO_3 , NaNO_2 , KNO_3 and LiNO_3 were procured from Nice Chemicals private limited, Ernakulam India. Hot oil (martempering oil) was purchased from Hard Castle Petrofer and neem oil was purchased locally. Binary and ternary mixtures of salts listed in Table 5.1. They were prepared by mixing appropriate quantities of pure salt as per their indicated weight percentages. In Table 5.1, 'I' refers Inconel probe, 'S₁' and 'S₂' refers to steel probes of AISI-4140 and AISI-52100 grades respectively.

Table 5.1: Quenching experiment matrix

Quench media	Quench bath temperature (T _b) in °C								
	100	150	200	250	300	350	400	450	500
KNO_3 (0N)	-	-	-	-	-	I,S ₁	I	I	I
75% KNO_3 +25% NaNO_3 (25N)	-	-	-	-	I,S ₁	I,S ₁	I	I	I
55% KNO_3 +45% NaNO_3 (45N)	-	-	-	I,S ₁	I,S ₁	I,S ₁	I	I	I
25% KNO_3 +75% NaNO_3 (75N)	-	-	-	-	I,S ₁	I,S ₁	I	I	I
NaNO_3 (100N)	-	-	-	-	-	I,S ₁	I	I	I
39% NaNO_2 +7% NaNO_3 +54% KNO_3 (NaNO_2 Eutectic mixture)	-	I,S ₂	I,S ₂	I,S ₁	I,S ₁	-	-	-	-
26% LiNO_3 +20% NaNO_3 +54% KNO_3 (LiNO_3 Eutectic mixture)	-	I,S ₂	I,S ₂	I,S ₁	I,S ₁	-	-	-	-
Hot Oil	I,S ₂	I,S ₂	I,S ₂	-	-	-	-	-	-
Neem Oil	I,S ₂	I,S ₂	I,S ₂	-	-	-	-	-	-

5.2 Inconel probe dimensions

As shown in Figure 5.1, an Inconel cylindrical probe of 60mm height and 12.5mm diameter was used to evaluate the cooling performance of the quench media. The probe had 5mm length M16 thread at the top. Five holes of different depths and 1mm diameter

were EDM drilled in the probe. One hole was drilled at centre to a depth of 30mm and 4 holes drilled at 2mm from the surface of the probe (radial distance of 4.25mm from the centre) to depths of 7.5mm, 22.5mm, 37.5mm, and 52.5mm. These depths are exclusive of the 5mm threaded section at the top of the probe.

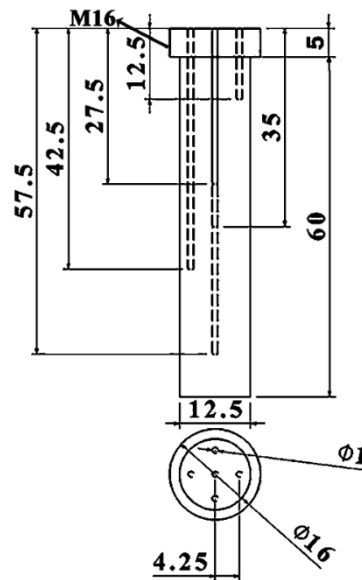


Figure 5.1: Dimensions of Inconel probe used for quenching experiments

5.3 Quenching experiments

1m long K-Type Inconel sheathed thermocouples were inserted into the 1mm holes in the Inconel probe through a 750mm length stainless steel tube. M16 thread of probe instrumented with thermocouples was fastened to the stainless-steel tube. The schematic of experimental setup is shown in Figure 5.2. Probe-stainless steel tube arrangement was transferred to a vertical tubular furnace. The thermocouples were connected to the NI-9213 data logger via compensating cables. Time-temperature data were acquired at a time interval of 0.1s in the computer. 2lts of quench medium was heated in stainless steel container and maintained at desired quench bath temperature in a quench bath furnace. Quench bath furnace was placed below vertical tubular furnace. The Inconel probe was heated to a temperature of 860°C. The SS tube was lowered through a guide and quenched into the concerned high temperature quench medium maintained at the required bath temperature.

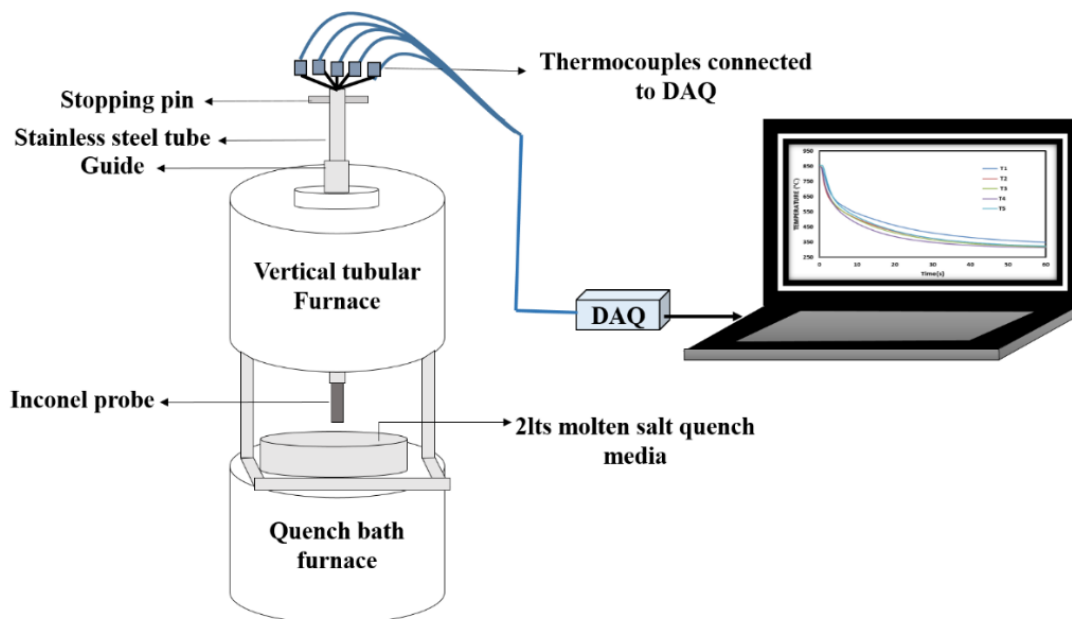


Figure 5.2: Schematic diagram for quenching experiment

5.4 Quenching of steel probe

Steel probes of AISI-52100 and AISI 4140 grades were machined to dimensions as shown in the Figure 5.3. The dimensions of the steel probe were similar to that of Inconel probe. However, two holes of 1.5mm diameter and 35mm depth were drilled at centre and 2mm from the surface of the probe.

Table 5.2 Composition of grade AISI 4140 and AISI 52100

	%C	%Si	%Mn	%Cr	%Ni	%Mo	%S	%P	%Fe
AISI 4140	0.429	0.238	0.64	1.1	0.161	0.195	0.0097	0.0082	Balance
AISI 52100	1.01	0.281	0.434	1.16	0.071	0.031	0.0042	0.0029	Balance

K-type stainless steel sheathed thermocouples of 1.5mm diameter and 1m long were inserted into the drilled holes. The setup for quenching experiment explained in section 5.3 was used for steel probe quenching experiments with some modifications. The instrumented steel probe was austenitized at 860°C for 20 minutes. The probe was subsequently quenched and held in the quenchant till the centre cooled to $(T_b+50^\circ\text{C})$ and $(T_b+20^\circ\text{C})$ in oil and molten salt media respectively. The steel probe was

subsequently removed from the quench medium and subjected to air cooling. The composition of AISI 4140 and AISI 52100 grades of steel used in probe has been provided in Table 5.2.

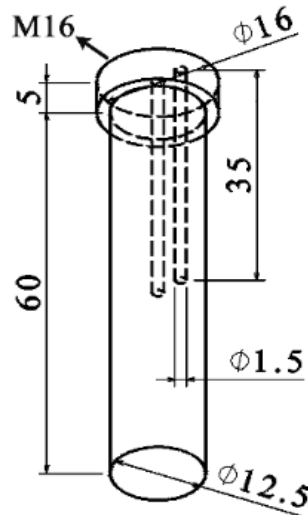


Figure 5.3: Dimensions of steel probe used for quenching experiments

5.5 Inverse heat transfer model for estimating heat flux

Inverse heat transfer model enables us to estimate the unknown metal-quenchant interfacial heat flux using the temperature data measured inside the Inconel probe. The cooling curve data recorded at the four locations near to the surface of the probe were used to calculate spatially dependent transient heat flux during quenching. Cooling curve data recorded at the geometric centre of the Inconel probe was not used for inverse calculation. It was used for validating the estimated heat flux.

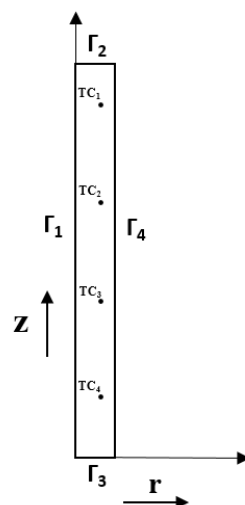


Figure 5.4: Axisymmetric model of the probe

$$\frac{1}{r} \frac{\partial}{\partial r} \left(kr \frac{\partial T}{\partial r} \right) + \frac{\partial}{\partial z} \left(k \frac{\partial T}{\partial z} \right) = \rho C_p \frac{\partial T}{\partial t} \quad (5.1)$$

Table 5.3: Boundary conditions for heat transfer model of the probe.

Boundary surface	Boundary condition
Γ_1	$q=0$ (Axisymmetric)
Γ_2	$q=0$
Γ_3	$q=0$
Γ_4	$q = p_1 z^3 + p_2 z^2 + p_3 z + p_4$

The heat transfer in the Inconel probe is governed by Fourier's heat conduction equation (Equation 5.1). The heat flow in the probe was assumed to be axisymmetric. The heat transfer model of the probe in cylindrical coordinates is described in Figure 5.4. The boundary conditions at surface $\Gamma_1, \Gamma_2, \Gamma_3$, and Γ_4 has been described in table 2. The probe was heated to 860°C before quenching, hence at time $t=0$, $T(r, z)=860^\circ\text{C}$. This was assumed to be the initial condition for solving inverse heat conduction model. The solution for Fourier heat conduction equation subject to these initial and boundary conditions, was obtained using finite element method (FEM). The rectangular axisymmetric model of the probe was discretized into 6000 rectangular elements of 0.25×0.25 mm mesh size. Temperature dependent thermal properties of Inconel 600 material used to in the FEM model are given in Table 5.4. These values were taken from the work published by Ramesh an Prabhu (Ramesh and Prabhu 2014d).

Table 5.4: Temperature dependent thermal properties of Inconel 600 alloy

T (°C)	200	250	300	350	400	450	500	550	600	650	700
K (W/mK)	16	16.9	17.8	18.7	19.7	20.7	21.7	-	25.9	-	30.1
C_p (J/kgK)	491	-	509	-	522	-	533	591	597	597	611
ρ (kg/m ³)	8340	-	8300	-	8270	-	8230	8190	8150	8100	8060

As shown in Table 5.1, top and bottom surfaces of probe was assumed to be insulated and heat transfer during quenching occurs only through boundary surface Γ_4 . The heat

flux at metal-quenchant interface (Γ_4) was modelled as a cubic function of distance z . The inverse problem is reduced to calculation of parameters p_1, p_2, p_3 and p_4 at each time step (t_s). Conjugate gradient method suggested in book by Ozisik and Orlande (Ozisik and Orlande 2000) was used to calculate these parameters.

Parameters were represented in vector form as P_{t_s} .

$$P_{t_s} = [p_{1,t_s} \ p_{2,t_s} \ p_{3,t_s} \ p_{4,t_s}] \quad (5.2)$$

$$q(P_{t_s}, z) = p_{1,t_s} z^3 + p_{2,t_s} z^2 + p_{3,t_s} z + p_{4,t_s} \quad \text{where } z \text{ varies between } 0 \text{ and } 60\text{mm} \quad (5.3)$$

The positions (r, z) of thermocouples TC_1, TC_2, TC_3, TC_4 and TC_C are (4.25, 7.5), (4.25, 22.5), (4.25, 37.5), (4.25, 52.5), (0, 30) respectively. Y_1, Y_2, Y_3, Y_4 and Y_C are the temperature data measured at TC_1, TC_2, TC_3, TC_4 and TC_C respectively.

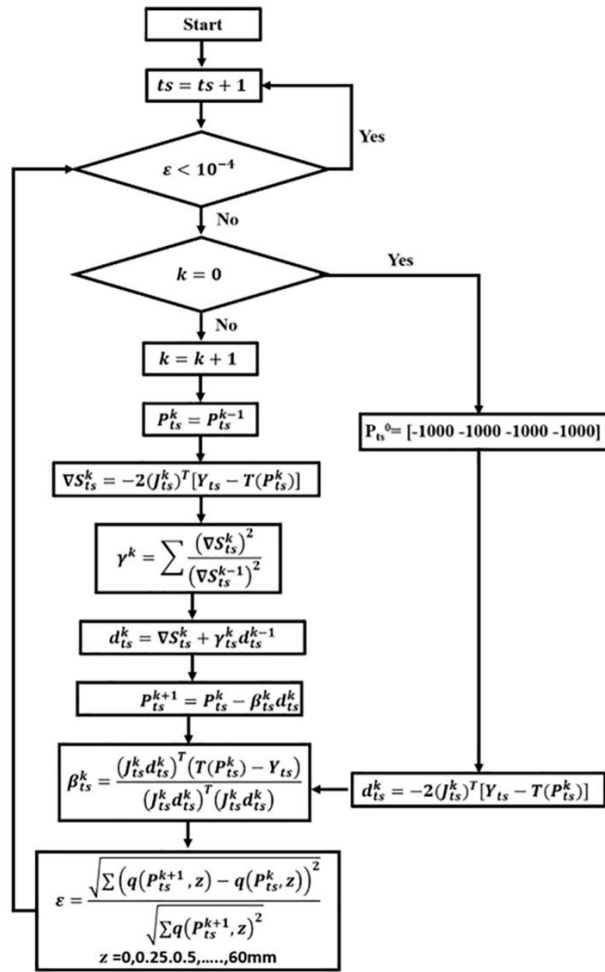


Figure 5.5: Flow chart for Inverse solution algorithm

Inverse problem was solved by calculating the values of parameters $p_{1,ts}$, $p_{2,ts}$, $p_{3,ts}$ and $p_{4,ts}$ for which the objective function S_{ts} was minimized.

$$S_{ts} = \sum_{i=1}^n \sum_{j=1}^m (Y_{i,ts+j-1} - T(P_{ts})_{i,ts+j-1})^2 \quad (5.4)$$

where $Y_{i,ts+j-1}$ is the temperature measured at i^{th} location (as in TC_i) and $ts+j-1^{\text{th}}$ time step. Since temperature was measured at four locations, $n=4$. $T(P_{ts})$ was calculated using FEM by assuming that heat flux remains constant for ‘m’ future time steps. j is a counting variable which varies from 1 to m.

i.e. $q(P_{ts}, z) = q(P_{ts+1}, z) = \dots = q(P_{ts+m}, z)$.

In the present work, the value number of future time steps was chosen to be 4.

In vector form, Equation 5.4 can be written as,

$$S_{ts} = [Y_{ts} - T(P_{ts}^k)]^T [Y_{ts} - T(P_{ts}^k)] \quad (5.5)$$

Where Y and T are vectors of measured and calculated vectors written as

$$Y_{ts} = [Y_{1,ts} \ Y_{1,ts+1} \ Y_{1,ts+2} \ \dots \ Y_{i,ts+j-1} \ \dots \ Y_{n,ts+m}]^T \quad (5.6)$$

$$T(P_{ts}^k) = [T_{1,ts} \ T_{1,ts+2} \ T_{1,ts+2} \ \dots \ T_{i,ts+j-1} \ \dots \ T_{n,ts+m}]^T \quad (5.7)$$

Iterative algorithm used to solve the inverse problem is shown in Figure 5.5. In Figure 5.5, β_{ts}^k , γ_{ts}^k and d_{ts}^k are search step size, conjugation coefficient and direction of decent respectively.

J_{ts}^k is the sensitivity matrix which was of dimension 16×4 (Equation 5.8)

$$J_{ts}^k = \begin{bmatrix} \frac{\partial T(P_{ts}^k)}{\partial p_{1,ts}} & \frac{\partial T(P_{ts}^k)}{\partial p_{2,ts}} & \frac{\partial T(P_{ts}^k)}{\partial p_{3,ts}} & \frac{\partial T(P_{ts}^k)}{\partial p_{4,ts}} \end{bmatrix} \quad (5.8)$$

Equation 5.9 illustrates forward differential method used to calculate first column of J_{ts}^k matrix.

$$\frac{\partial T(P_{ts}^k)}{\partial p_{1,ts}} = \frac{T([p_{1,ts}^k + \delta p_{1,ts}, \ p_{2,ts}^k, \ p_{3,ts}^k, \ p_{4,ts}^k]) - T([p_{1,ts}^k, \ p_{2,ts}^k, \ p_{3,ts}^k, \ p_{4,ts}^k])}{\delta p_{1,ts}} \quad (5.9)$$

Here, $\delta p_{1,ts} = 10^{-4} \times p_{1,ts}$

$T([p_{1,ts}^k + \delta p_{1,ts}, \ p_{2,ts}^k, \ p_{3,ts}^k, \ p_{4,ts}^k])$ and $T([p_{1,ts}^k, \ p_{2,ts}^k, \ p_{3,ts}^k, \ p_{4,ts}^k])$ in Equation 5.9 were evaluated by solving heat conduction equation using FEM. Similarly, forward

differential method was used to calculate other elements in the sensitivity matrix. The converged values of parameters, P_{ts} calculated for each time step was then used calculate spatially dependent heat flux, $q(P_{ts},z)$ using Equation 5.3.

5.6 Micrographs

The quenched-air cooled steel probes were cut at a depth of 35mm and subjected to metallographic polishing. Silicon carbide papers of grit size 300, 600, 800 and 1200 was used to roughly polish the surface. The roughly polished specimen was subjected to finely polish using diamond paste of particle size 3-4 μ m and 1-5 μ m to obtain a mirror finished surface.

The polished steel samples were etched with aqueous 10% potassium meta-bisuphite solution. The etching time was less than 10s. Karl Zeiss (Axioimager.A1m) microscope was used to observe the microstructure in these samples.

5.7 Hardness measurement

Micro Vickers hardness measurements were taken at different radial positions on the sectioned and polished steel probe surface. Shimadzu HMV G20ST hardness testing machine was used for hardness measurement. A load 0.5 kgf load and 15 seconds holding time were used for measuring hardness.

5.8 Contact angle measurement

0.2-0.25mm diameter spherical balls of NaNO₂ eutectic mixture and LiNO₃ eutectic mixture were prepared. The spherical salt balls were placed on the oxidized Inconel surface and bare AISI 4140 steel surface to study temperature dependent spreading characteristics of these salts.

Contact angle of these molten salts were measured at temperatures of 150°C, 200°C, 250°C, 300°C, 350°C and 400°C. The environment chamber was maintained at required temperature for an interval of 2 minutes at each temperature for attaining equilibrium. Kruss Drop Shape Analyser was used to measure the contact angle. The images were recorded at 26 fps and KRUSS advanced software was used to measure the contact angle.

5.9 Oxidation study and viscosity measurement

To study the effect of oxidation on viscosity, 30ml of hot and neem oil samples were heated in a hot air oven maintained at 120°C for a duration of 8,16,24,32,40 and 48hrs. After the oxidation treatment, viscosity of the hot oil and neem oil were measured using Brookfield LDV-IIIU viscometer with SC4-27 spindle. Thermosol accessory was used to heat 7ml of test oil sample to 40°C.

5.10 FEM based phase transformation model

The phase transformation during quench hardening of steel is a complex process which involves thermal field, metallurgical field and mechanical stress field interacting with each other. In the present model, the effect of mechanical stress field was neglected. The thermal field/ heat transfer in the steel, is the driving force for metallurgical transformations. The heat transfer during quench cooling of a 1-d cylinder is governed by Equation 5.10. The heat transfer equation coupled with phase transformation field was solved using FEM method.

$$\rho C_p \frac{\partial T}{\partial t} = \frac{1}{r} \frac{\partial}{\partial r} \left(kr \frac{\partial T}{\partial r} \right) + Q \quad (5.10)$$

The 2-physical phenomenon that results in interaction of phase transformation field with the thermal field are

1. Variation of thermo-physical properties of the steel with temperature and the phase composition of the steel.
2. Latent heat evolution associated with transformation of austenite to product phases.

Equation 5.11 shows linear mixture rule used to determine thermo-physical property of a mixture consisting of 'N' phases. P_k and ξ_k are the thermo-physical property and volume fraction of the phase 'k' respectively. Phase variable 'k' in equation 11 refers to austenite, ferrite, pearlite, bainite and martensite.

$$P(T, \xi_k) = \sum_{k=1}^N P_k \xi_k \quad (5.11)$$

In equation 5.12, Q is the latent heat that is generated when austenite transforms to any phase 'k' (ferrite, pearlite, bainitic, or martensite) and ΔH_k and $\dot{\xi}_k$ are the latent heat per unit volume and the rate of evolution of phase k from austenite respectively.

$$Q = \sum_{k=1}^N (\rho_k \Delta H_k \dot{\xi}_k) \quad (5.12)$$

Figure 5.6 shows the temperature dependent thermophysical properties of AISI 4140 steel. These properties were obtained from JMatPro software. ASTM grain size of 9 and composition of AISI 4140 steel probe presented in Table 5.2 were provided as input to JMatPro software to calculate thermophysical properties and TTT diagram. Figure 5.7 shows the TTT diagram and critical temperature obtained for 4140 steel.

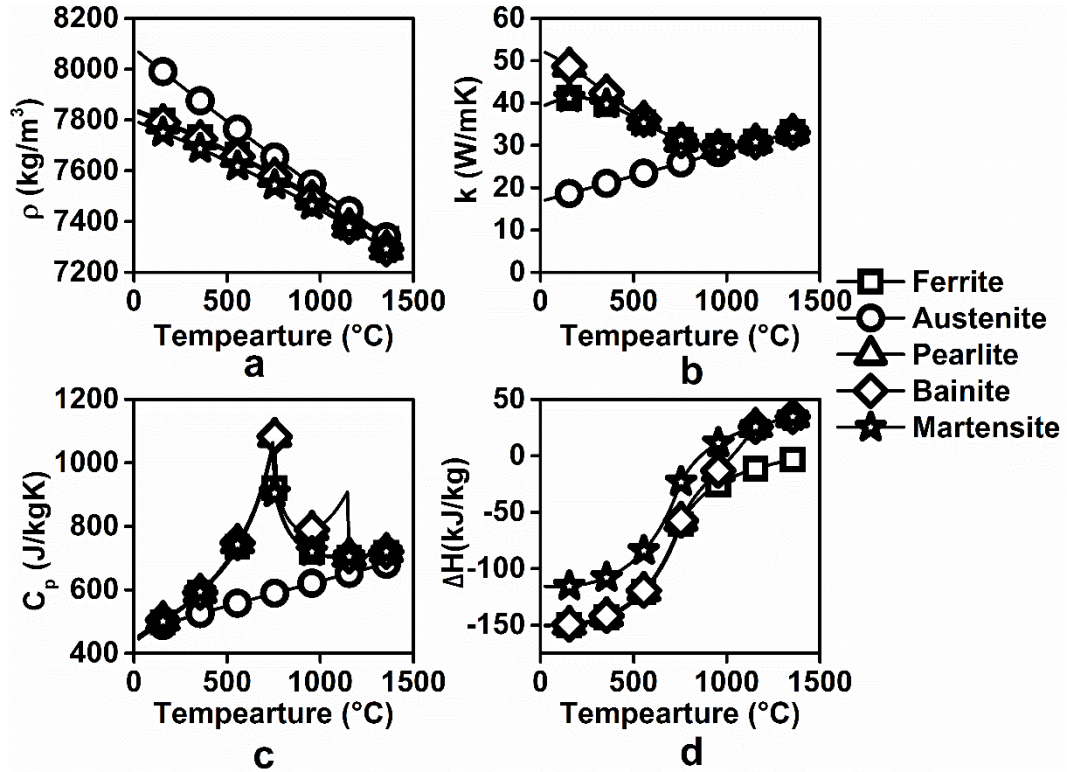


Figure 5.6: Temperature dependent variation of a) Density b) Thermal conductivity c) Specific heat d) enthalpy of transformations for different phases.

The transformation of austenite to ferrite, pearlite and bainite are diffusional transformations. Transformation of austenite to martensite is diffusion-less transformation. The isothermal diffusional transformations can be modelled using JMAK equation shown in equation 5.13.

$$\xi_k = (1 - \exp(-b_k(T)t^{n_k(T)})) \quad (5.13)$$

In equation 13, b_k and n_k are material parameters and were obtained from the TTT diagram. In the TTT diagram, transformation start phase fraction (ξ_{k_i}) and transformation finish phase fraction (ξ_{k_f}) were 0.1% and 99.9% respectively. Equation 14 and 15 show the formula used to calculate n_k and b_k respectively. t_i and t_f are the

transformation times corresponding to ξ_{k_i} and ξ_{k_f} respectively at a given temperature (T).

$$n_k = \frac{\ln\left(\frac{\ln(\xi_{k_i}-1)}{\ln(\xi_{k_f}-1)}\right)}{\ln\left(\frac{t_i}{t_f}\right)} \quad (5.14)$$

$$b_k = -\frac{\ln(\xi_{k_i}-1)}{t_i^{n_k}} \quad (5.15)$$

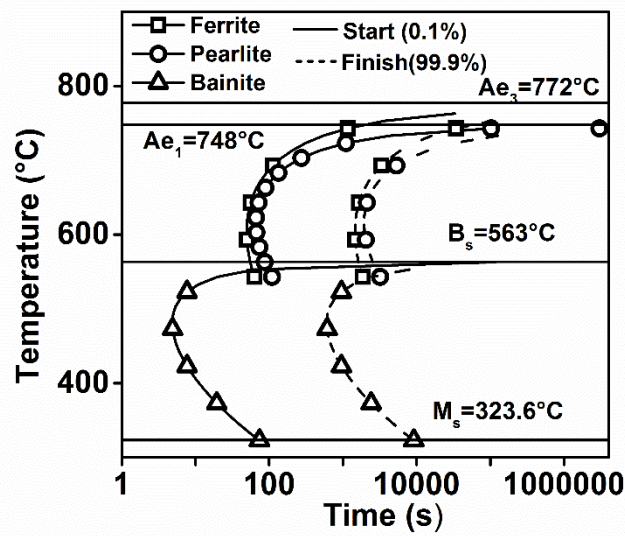


Figure 5.7: TTT diagram of AISI 4140 steel probe obtained from JMatPro

Diffusion based transformations occur in two stages, nucleation and growth. Schiel's additive rule was adopted to describe the non-isothermal nucleation process that occurs during quenching. The cooling was divided into small intervals of Δt_i . Time for start of transformation ($\tau(\xi_{k_i}, T_i)$) was extracted from TTT. Schiel's sum was then calculated at each time step as shown in Equation 5.16. When Schiel's sum exceeded the value of 1, the nucleation stage was presumed to be complete.

$$S_{k=f,p,b} = \sum_{i=1}^n \frac{\Delta t_i}{\tau_i(\xi_k, T)} \quad (5.16)$$

Subsequent to completion of nucleation stage, the growth of phases was modelled using JMAK (Johnson-Mehl-Avrami-Kolmogorov) equation as described in Equation 5.17- Equation 5.19. Fictitious time (τ_f) is defined as the time required for the formation of

phase fraction $\xi'_k(t)$ at constant temperature T. Later this fictitious time was used to calculate the phase fraction at next time step ($\xi_k^{t+\Delta t}$) as described in Equation 5.18.

$$\xi'_k(t) = \frac{\xi_k^t}{\xi_k^{max}(\xi_\gamma^t + \xi_k^t)} \quad (5.17)$$

$$\tau_f = \left(-\frac{\ln(1 - \xi'_k(t))}{b_k(T)} \right)^{\frac{1}{n_k(T)}} \quad (5.18)$$

$$\xi_k^{t+\Delta t} = \xi_k^{max}(\xi_\gamma^t + \xi_k^t)(1 - \exp(b_k(\tau_f + \Delta t)^{n_k})) \quad (5.19)$$

With known values of Ae₃ and composition, eutectoid composition and carbon equivalent of the AISI 4140 steel was calculated using Equation 5.20 (Kasuya and Hashiba 2007). Maximum ferrite composition (ξ_{Fe}^{max}) was calculated using lever rule. Maximum fraction transformed for pearlite and bainite was 1.

$$Ae_3 = 912 - 203 * \%C^{0.5} + 15.2 * \%Ni + 44.7 * \%Si - 104 * \%V + 31.5 * \%Mo + 13.1 * \%W - 30 * \%Mn - 11 * \%Cr - 20 * \%Cu + 700 * \%P + 400 * \%Al + 120 * \%As + 400 * \%Ti \quad (5.20)$$

The diffusion less martensitic transformation was modelled using Koistinen-Marburger model shown in equation 5.21. Ω in the equation was assumed to be 0.011.

$$\xi_M^{t+\Delta t} = (\xi_\gamma^t + \xi_M^t)(1 - \exp(-\Omega(M_s - T^{t+\Delta t}))) \quad (5.21)$$

5.11 Numerical experiment to simulate the effect heat transfer coefficient, bath temperature, section thickness and residence time on hardness during martempering:

As shown in Figure 5.8, a simulation study on the effect of four important process variables during martempering of AISI 4140 steel cylinders was performed. The four process variables considered were, heat transfer coefficient (h), quench bath temperature (T_b), diameter (D) and residence time (t_R).

The maximum residence time (t_{Rmax}) was defined as the time required to cool the quenched part surface from austenizing temperature (850°C) to quench bath temperature and subsequently reduce temperature difference between surface and centre of the steel part below 5°C. The part was subjected to air cooling at time greater than residence time. In order to ensure residence time is less than the maximum residence time, residence time fraction (f) was defined as ratio of residence time to

maximum residence time ($f=t_R/t_{Rmax}$). Ambient air temperature was assumed to be 30°C. The air heat transfer coefficient was obtained from (Kothandaraman and Subramayan 2010). The equation used to determine surface temperature dependent air heat transfer coefficient is given in Figure 5.8.

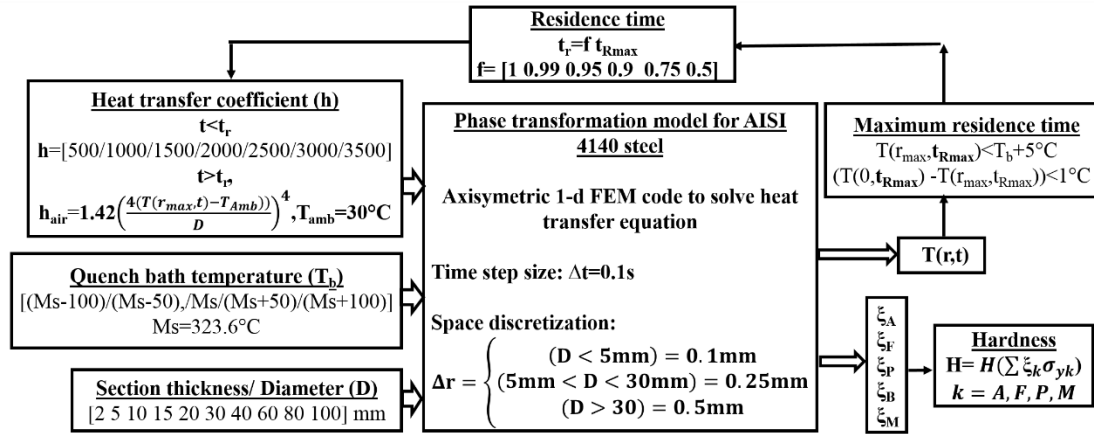


Figure 5.8: Flow chart of numerical experiment

Quench heat transfer coefficient was varied from 500W/m²°C to 3500W/m²°C in the steps of 500 W/m²°C. Bath temperature was varied in steps of 50°C from M_s-100 to M_s+100 in steps of 50°C. The section thickness (diameter) of the steel bar was varied in steps of 2mm,5mm,7.5mm,10mm,20mm,30mm,40mm,60mm, 80mm, and 100mm. The detailed description of time step size and mesh size used in FEM model are provide in Figure 5.8. At each node, kinetics of diffusion based and diffusion less transformations and phase dependent thermophysical properties were modelled as discussed in section 5.10 . The FEM based code to solve phase transformation coupled heat transfer equation was coded in MATLAB compiler. The calculation was stopped when temperature at centre of the probe decreased below M_s of the steel grade. As shown in Equation 5.22 and Equation 5.23, volume fraction of austenite and martensite at room temperature were assumed to be 5% and 95% of total austenite available for martensitic at each node at M_s.

$$\xi_A^{T=25^\circ C} = 0.05(\xi_A^{T=M_s}) \quad (5.22)$$

$$\xi_M^{T=25^\circ C} = 0.95(\xi_A^{T=M_s}) \quad (5.23)$$

Yield strength was calculated using linear mixture rule shown in Equation 22. The hardness (H) was modelled as a function of yield strength (σ_y). The hardness-yield

strength relation was obtained from JMatPro software and is shown in Figure 5.9. Table 5.5 shows yield strength at room temperature for different phases obtained from JMatPro.

$$H = \sum_{k=A,F,P,B,M} \sigma_k \xi_k \quad (5.24)$$

Table 5.5: Yield strength of different phases

Phase	Ferrite	Austenite	Bainite	Pearlite	Martensite
Yield strength (MPa)	245	273	850	586	1936

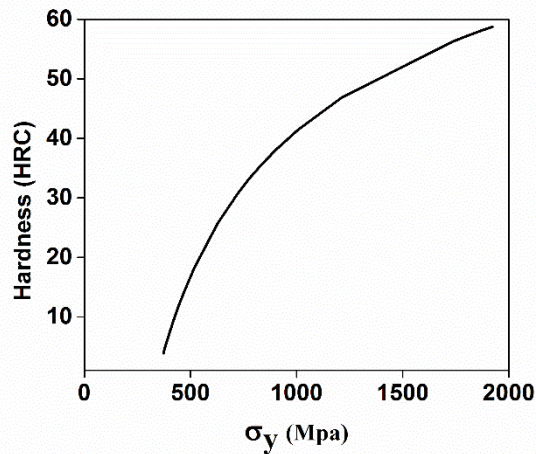


Figure 5.9: Hardness as a function of yield strength

The phase transformation coupled heat transfer equation was solved for all combinations of varying input variables shown in Figure 5.5. The total number of numerical experiments performed was $10 \times 7 \times 5 \times 6 = 2100$, where 10, 7, 5 and 6 are number of levels of input variables D , h , T_b and f respectively.

Chapter 6 RESULTS

6.1 Spatially dependent transient heat flux

The cooling curves obtained by quenching Inconel probe in a quench medium maintained at various temperatures were used to calculate the metal-quenchant interfacial heat flux. The measured temperature at the thermocouple locations TC₁, TC₂, TC₃, and TC₄ were used to calculate the cubic equation parameters at each time step. These parameters were used to define metal-quenchant interfacial heat flux as shown in Equation 5.3. Figure 6.1a-Figure 6.1c show the variation of measured temperature, inversely calculated cubic parameters and spatially dependent quench heat flux with time respectively. These plots were obtained for molten NaNO₃ quench medium maintained at 350°C. Similar plots were obtained during quenching experiments for quench media shown in Table 5.1. Transient variation of measured temperature at all thermocouple locations and spatially dependent transient heat flux calculated using inverse method have been provided in Appendix A and Appendix B respectively.

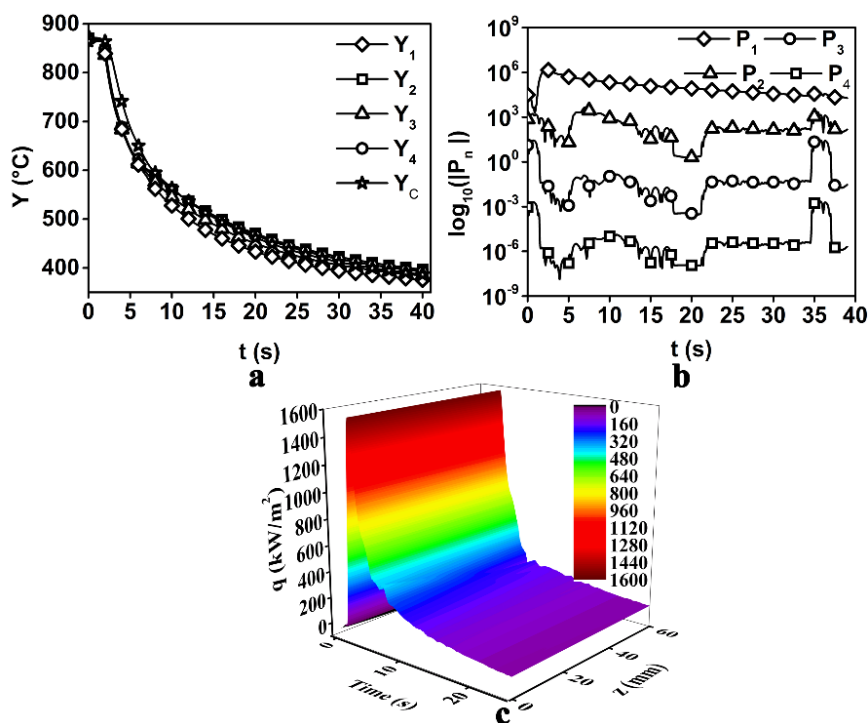


Figure 6.1: Transient variation of a) Measured temperature b) Cubic equation parameters calculated using Inverse method c) Spatially dependent quench heat flux for inconel probe quenched in NaNO₃ probe maintained at bath temperature of 350°C

6.2 Validation of calculated quench heat flux

Figure 6.2 shows a transient variation of % error calculated at all thermocouple locations in the Inconel probe quenched in molten NaNO_2 eutectic mixture quench medium maintained at 150°C bath temperature. As discussed in section 5.5 , temperature measured at the TCc location was used to validate the calculated metal-quenchant interfacial heat flux. Equation 6.1 shows the formula used to calculate time dependent %error between measured and calculated temperature at various thermocouple locations.

$$\%Error_i(t) = \frac{|Y_i(t) - T_i(t)| \times 100}{(T_{C_{meas}}(t))} \quad i = 1, 2, 3, 4, C \quad (6.1)$$

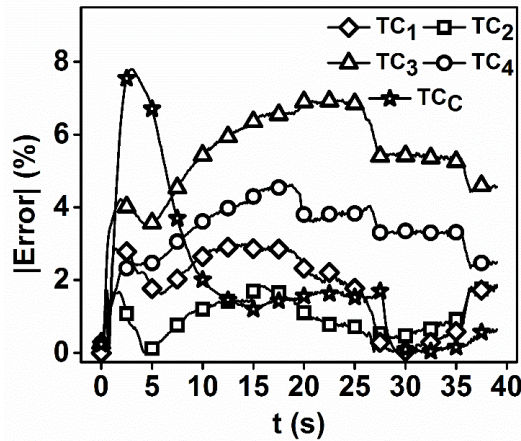


Figure 6.2: Error calculated at various thermocouple locations for Inconel probe quenched in NaNO_2 eutectic mixture maintained at quench bath temperature of 150°C

Table 6.1 and Table 6.2 shows maximum and mean %error calculated for inconel probe quenched in different quench media maintained at various bath temperatures. The error values were calculated for first 40s of quenching. The values of %error indicates the accuracy of spatially dependent transient quench heat flux calculated using inverse algorithm.

Table 6.1: Maximum %error calculated for inconel probe quenched in different quench media maintained at various bath temperatures

Quench medium	Quench bath temperature ($^\circ\text{C}$)								
	100	150	200	250	300	350	400	450	500
0N	-	-	-	-	-	2.9	1.4	2.2	1.8

25N	-	-	-	-	3.0	2.6	2.2	3.0	1.7
55N	-	-	-	5.3	1.6	1.5	1.5	1.6	-
75N	-	-	-	-	2.8	2.6	2.4	2.3	2.9
100N	-	-	-	-	-	1.3	2.5	2.1	1.7
NaNO₂ Eutectic	-	8.7	5.1	7.0	6.4	-	-	-	-
LiNO₃ Eutectic	-	7.8	10.1	14.2	9.7	-	-	-	-
Hot Oil	7.1	7.3	6.4	-	-	-	-	-	-
Neem Oil	7.2	9.0	7.4	-	-	-	-	-	-

Table 6.2: Mean %error calculated for inconel probe quenched in quench media maintained at various bath temperatures

Quench medium	Quench bath temperature (°C)								
	100	150	200	250	300	350	400	450	500
0N	-	-	-	-	-	0.6	0.4	0.9	0.4
25N	-	-	-	-	1.1	0.8	0.6	0.9	0.4
55N	-	-	-	2.9	0.8	0.7	0.5	0.5	-
75N	-	-	-	-	1.4	1.7	0.6	0.4	0.5
100N	-	-	-	-	-	0.6	0.7	0.7	0.5
NaNO₂ Eutectic	-	5.4	3.0	4.7	1.8	-	-	-	-
LiNO₃ Eutectic	-	5.0	3.0	3.6	2.4	-	-	-	-
Hot Oil	2.5	2.6	2.0	-	-	-	-	-	-
Neem Oil	3.4	2.5	2.6	-	-	-	-	-	-

6.3 Assessment of spatially dependent transient heat flux

The spatially dependent transient heat flux calculated at the metal/quenchant interface has two components

- 1) **Magnitude:** The magnitude of spatially dependent quench heat flux was assessed by calculating the average heat flux and average surface temperature over the metal/quenchant interface.
- 2) **Uniformity:** Uniformity of quench heat flux was assessed by studying the spatial variation of heat energy extracted per unit area.

Figure 6.3a shows the variation of average heat flux as a function of average surface temperature and Figure 6.3b shows the spatial variation of heat energy extracted per unit area calculated for Inconel probe quenched in 55N salt mixture maintained at 250°C.

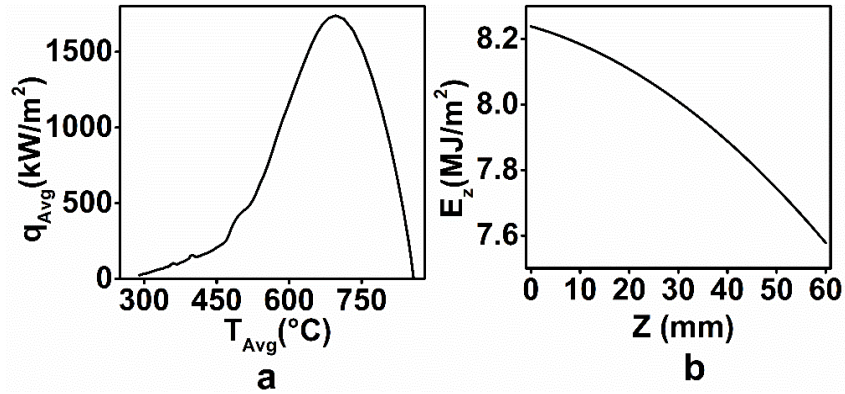


Figure 6.3: a) q_{Avg} as a function of T_{Avg} b) Spatial variation of heat energy extracted per unit area obtained for 55N salt mixture maintained at 250°C

6.3.1 Average heat flux

Equation 6.2 and Equation 6.3 are used to calculate average quench heat flux (q_{Avg}) and average quench heat flux (T_{Avg}) respectively. This was calculated using spatially dependent transient heat flux calculated using inverse algorithm. The integration was performed using trapezoidal method with step size of 0.25mm.

$$q_{Avg}(t) = \frac{1}{l} \int_0^l q(t, z) dz \quad l = 60mm \quad (6.2)$$

$$T_{Avg}(t) = \frac{1}{l} \int_0^l T(t, r_{max}, z) dz \quad r_{max} = 6.25mm, \quad l = 60mm \quad (6.3)$$

6.3.2 Uniformity of quench cooling

The energy extracted at the metal-quenchant interface was calculated using Equation 6.4. To obtain heat energy extracted per unit area during quenching as a function of space, the quench heat flux at each node on boundary Γ_3 was integrated for first 40s.

$$E_z(z) = \int_0^t q(t, z) dt \quad t = 40s \quad (6.4)$$

A Uniformity parameter (U) was defined to characterize the degree of uniformity of cooling offered by the quench medium during cooling of Inconel probe. As shown in Equation 6.6, uniformity parameter was defined as the root mean square variation of

heat energy with respect to the average heat energy extracted at the surface of the Inconel probe. A higher uniformity parameter suggests higher variation about the average heat energy extracted at the surface of the probe. This variation results in non-uniform cooling of the probe. Lower value of uniformity parameter thus indicates more uniform cooling.

In Equation 6.4-Equation 6.6 the integrations were performed using trapezoidal method. Integrations with respect to time(t) and space(z) were performed with a step size of 0.1s and 0.25mm respectively.

$$\bar{E}_z = \frac{1}{l} \int_0^l E_z(z) dz \quad l = 60mm \quad (6.5)$$

$$U = \frac{1}{l} \sqrt{\int_0^l (E_z(z) - \bar{E}_z)^2 dz} \quad l = 60mm \quad (6.6)$$

6.4 Simulation of effect of heat transfer coefficient, bath temperature and section thickness on phase evolution during martempering

The results of numerical experiment for a AISI 4140 steel cylinder of 60mm diameter, quenched in a medium which offers heat transfer coefficient of 1000W/m²K maintained at bath temperature of 323.6°C and held for a residence time of t_{Rmax} is shown in Figure 6.4. A sharp change in the thermal profile after residence time(t_r) was due to change of boundary condition to air cooling boundary condition. The volume % of austenite, ferrite, pearlite, bainite and martensite phases at room temperature were calculated to be 1.14%, 0.73%, 0%, 73.39% and 21.69% at the geometric centre.

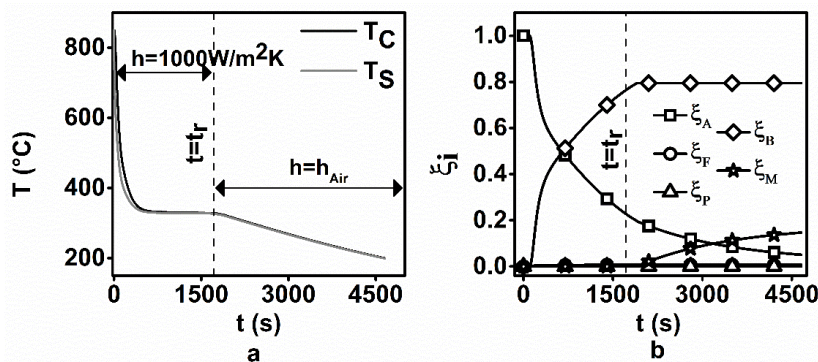


Figure 6.4: a) Transient variation of temperature at geometric center and surface of the cylinder and b) Volume fraction of various phases at geometric center of the cylinder obtained for numerical experiment with D=60mm, h=1000W/m²K, T_b=M_s (323.6°C) and f=1

Similarly, phase fractions were obtained at all the nodes of axisymmetric model of cylinder and these phase fractions were further used to predict hardness distribution in the cylinder. Figure 6.5a and Figure 6.5b shows the distribution of phase fractions and predicted hardness from surface to centre of the steel respectively. The detailed description of the procedure adopted for calculation of these phase fractions and predicting hardness has been provided in section 5.11 . The higher hardness near the surface of the cylinder was due to higher volume fraction of martensite near the surface.

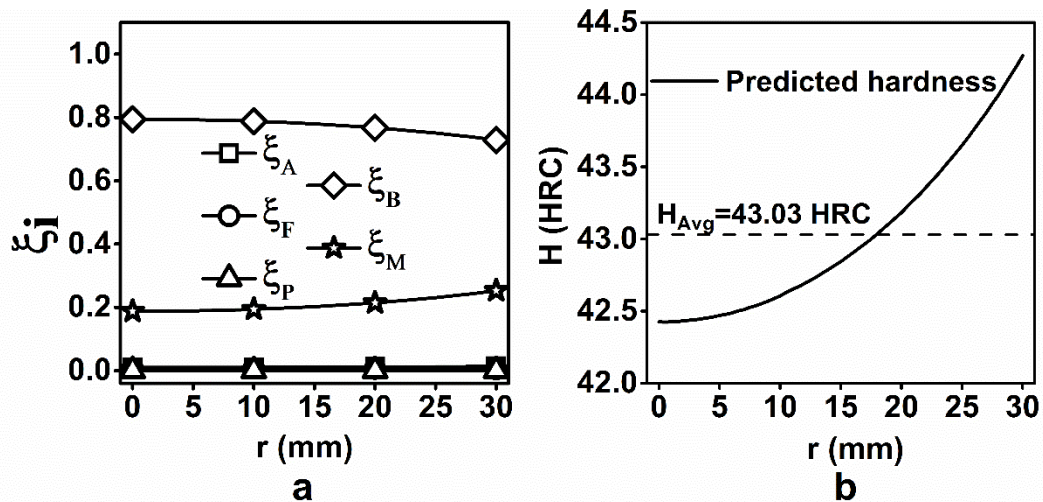


Figure 6.5: a)Phase fractions and b) Predicted hardness as a function of radial distance obtained for numerical experiment with $D=60\text{mm}$, $h=1000\text{W/m}^2\text{K}$, $T_b=M_s$ (323.6°C) and $f=1$

As shown in Figure 6.5, the average hardness, H_{Avg} was calculated based on the hardness distribution in the steel cylinder. Similar procedure was followed and the value of H_{Avg} was calculated for all 2100 numerical experiments. Appendix C shows the variation of average hardness in 4140 steel cylinders of different diameters with heat transfer coefficient, bath temperature and residence time fraction during martempering.

Chapter 7 DISCUSSION

The discussion of all the results in this work are discussed in six parts

- Comparison of cooling performance of hot oil and molten salt media.
- Effect of bath temperature on the cooling performance of eutectic $\text{KNO}_3\text{-NaNO}_3$ mixture.
- Effect of composition and bath temperature on the cooling performance of $\text{NaNO}_3\text{-KNO}_3$ mixtures.
- Cooling performance of molten $\text{KNO}_3\text{-LiNO}_3\text{-NaNO}_3$ eutectic mixture.
- Hot Neem Oil as alternative to Hot Mineral Oils for Martempering.
- Simulation of effect of heat transfer coefficient, bath temperature, residence time and thickness on hardness of martempered of AISI 4140 steel.

7.1 Comparison of cooling performance of hot oil and molten salt media

7.1.1 Heat extraction mechanism

Heat extraction process was observed to take place in two stages during quenching of Inconel probe in molten salt medium. The two stages being boiling and convective cooling stages. Contrary to this, heat extraction process during quenching of Inconel probe in hot oil occurred in three stages namely, vapour blanket stage, boiling stage and convective cooling stage. This is similar to the heat extraction mechanism observed in conventional low temperature quench media. Figure 7.1a and Figure 7.1b describe the heat extraction mechanism during quenching of Inconel probe in molten NaNO_2 eutectic mixture and hot oil. Both quench media were maintained at a bath temperature of 150°C .

Immediately after the immersion of Inconel probe at 860°C in the hot oil, a vapour layer encapsulates the Inconel probe. This prevents the heat transfer at the metal/quenchant interface and thus the heat flux is low during this stage. Vapor blanket stage occurs between points $p_0\text{-}p_1$. The duration of vapour blanket stage was observed to increase with increase in quench bath temperature. The decrease in surface temperature destabilizes vapour blanket and with rupture of vapour film (at point p_1), liquid hot oil comes in contact with the surface of the probe. Heat extraction from the probe at metal quenchant interface occurs by boiling of hot oil between points $p_1\text{-}p_2$ as shown in Figure

7.1a. During this stage, heat is extracted by boiling hot oil at the probe surface. The q_{Avg} thus rapidly increases to a maximum value at point p_2 . Further as T_{Avg} decreases, the average heat flux at the metal-quenchant interface also decreases and when the average surface temperature reaches point p_3 , the boiling of hot oil ceases, and heat extraction occurs by convective cooling stage. During convective stage, the average surface heat flux was observed to be very low. It should be noted that all three stages of heat transfer simultaneously exist at different locations on the surface of the probe. q_{avg} Vs T_{avg} plots were drawn by calculating the mean of spatially dependent heat flux transients.

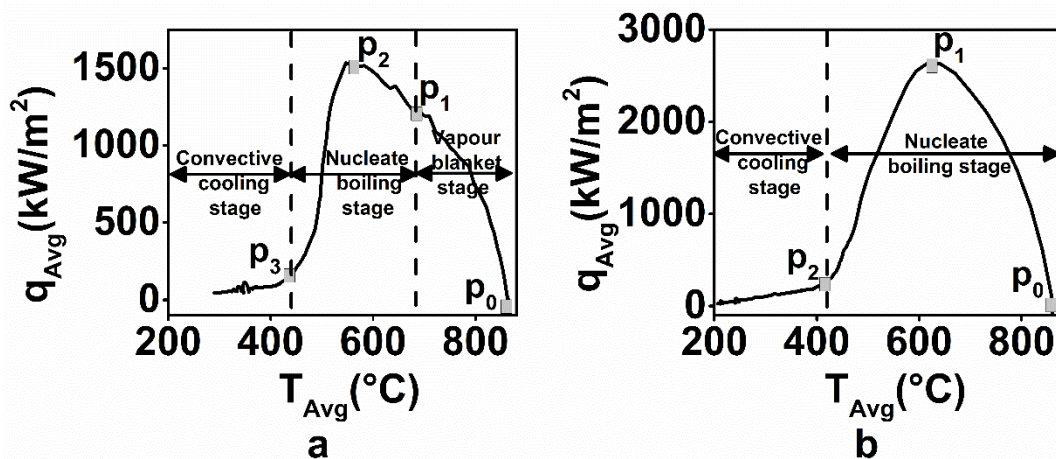


Figure 7.1: Heat extraction mechanism illustrated using q_{avg} plotted as a function of T_{avg} for Inconel probe quenched in a) Hot oil b) NaNO₂ maintained at 150°C

The heat transfer during quenching in molten NaNO₂ eutectic mixture salt medium was observed to take place in two stages as shown in Figure 7.1b. The vapor blanket stage was absent during quenching of Inconel probe in molten salt quench medium. Heat transfer occurred initially due to the boiling of the quenchant in contact with the probe surface. The average heat flux increased rapidly from point a to a peak at point p_1 and then decreased to point p_2 . At point ' p_2 ', transition of heat transfer mechanism from boiling stage to convection stage occurred. During convective cooling stage, the heat transfer at the metal/quenchant interface occurred due to natural convection. The magnitude of average heat flux during convection stage was observed to be very low in both the cases. As observed from Figure 7.1a and Figure 7.1b, the magnitude of heat extraction in Inconel probe quenched in hot oil is much lower compared to that of molten salt medium.

7.1.2 Uniformity of heat extraction along the surface of Inconel probe

Non-uniform cooling of the quenched part during quenching would invariably result in microstructure variation, distortion or residual stress in the quenched part. Figure 7.2a and Figure 7.2b show the spatial variation of the energy removed per unit area (E_z) and peak heat flux (q_{Peak}) respectively. The value of E_z was observed to be higher at the bottom portion and lower at the top portion of the quench probe. Thus, there exists a significant difference in heat transfer rates along the surface of the probe and more energy was removed in the bottom part as compared to the top part of the probe. The spatial variation of E_z observed in Inconel probe quenched in NaNO_2 eutectic mixture was much lower as compared to that in hot oil.

Peak heat flux during nucleate boiling stage is an important parameter which characterizes the heat transfer at the metal/quenchant interface. As shown in Figure 7.2b, the variation in peak heat flux along the surface was negligibly low in the case of molten NaNO_2 eutectic mixture medium maintained at 150°C . The variation in values of peak heat flux along the surface of the probe was very large in the case of hot oil medium maintained at 150°C . The values of peak heat flux were much higher in the bottom part of the probe as compared to the top part. This was attributed to early collapse of vapour blanket in the lower part of the probe.

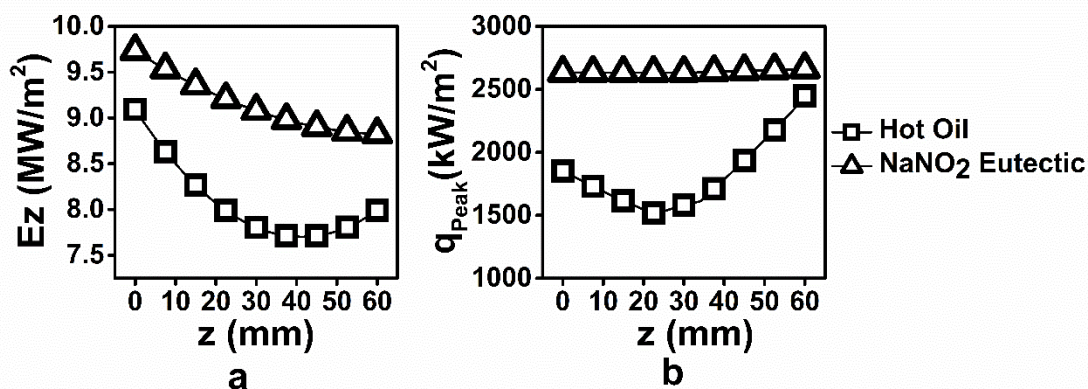


Figure 7.2: Spatial distribution of a) Energy extracted per unit area b) Peak heat flux during quenching of Inconel probe in hot oil and NaNO_2 eutectic mixture maintained at 150°C

A Stochastic parameter ' T_{Range} ' defined as the difference between maximum and minimum surface temperature was also used to quantify the transient variation of cooling non-uniformity. The range of surface temperature (T_{Range}) was calculated at

each time step. Figure 7.3 shows the variation of T_{Range} with T_{Avg} . The points O_1 , O_2 and O_3 are the points corresponding to end of vapour blanket stage, maximum average heat flux and end of convective cooling stage respectively. These points were plotted by extracting the values of T_{Avg} values of points p_1 , p_2 , and p_3 in Figure 7.1a. Similarly in Figure 7.3, points S_1 and S_2 represents maximum average heat flux and end of convective cooling stage respectively for NaNO_2 eutectic mixture maintained at 150°C . The T_{Avg} values of points S_1 and S_2 correspond to points p_1 and p_2 in Figure 7.1b.

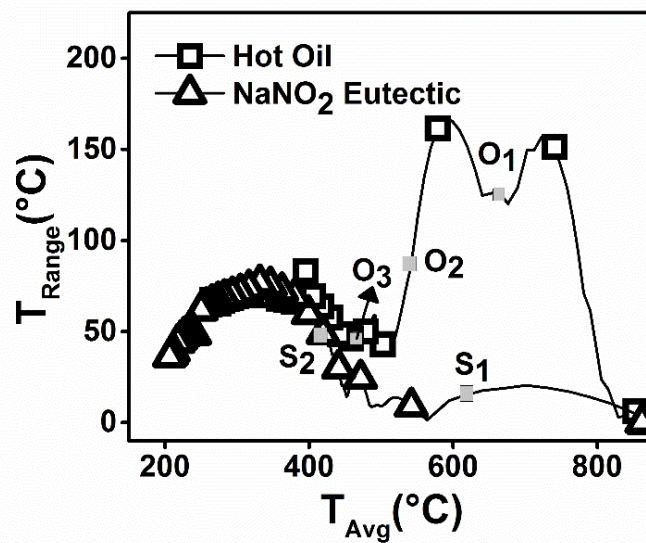


Figure 7.3: Variation of T_{Range} with T_{Avg} at the metal/quenchant interface for an inconel probe quenched in NaNO_2 and hot oil quench media maintained at 150°C

The non-uniformity in the surface temperature reaches first maximum value during nucleate boiling stage. Further, the non-uniformity in the surface temperature reduces to the local minima at the end of nucleate boiling and vapour blanket stages. This phenomenon was true for both hot oil and molten salt quench media. The non-uniformity in surface temperature increased to a maximum value during convective cooling stage and subsequently decreased. The peak non-uniformity in the surface temperature during nucleate boiling stage was higher than that observed in convective cooling stage in the case of hot oil quench media. However, the peak non-uniformity in the surface temperature during convective cooling stage was higher than that observed in nucleate boiling stage in the case of molten salt quench media.

The peak non-uniformity in the surface temperature during nucleate boiling and vapour blanket stage were nearly ~ten times higher in the case of hot oil quench medium as

compared nucleate boiling stage in molten salt medium. No significant difference in non-uniformity in the surface temperature was observed in hot oil and molten salt media during convective cooling stage.

7.1.3 Distribution of characteristic cooling time (t_{85}) in the Inconel probe

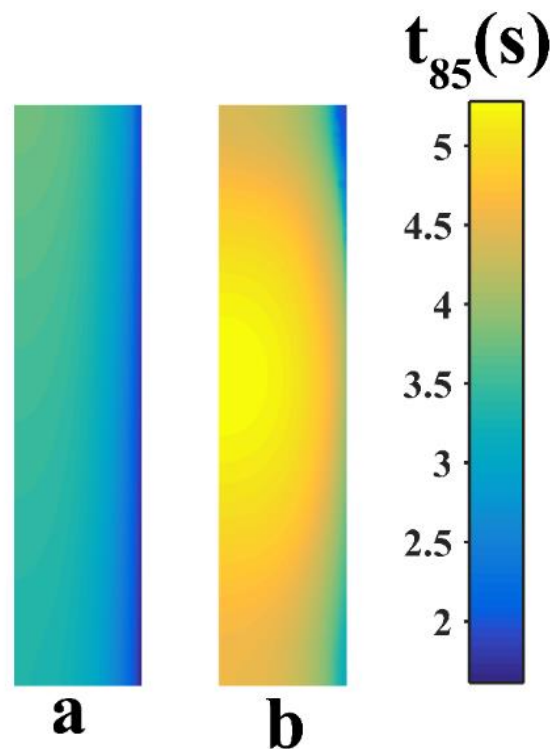


Figure 7.4: Distribution of t_{85} values in the Inconel probe quenched in a) molten eutectic NaNO_2 mixture b) Hot oil quench media maintained at 150°C

t_{85} is the characteristic cooling time, relevant for structure transformation for most structural steels (Smoljan 2006). t_{85} is the time required to cool from 800°C to 500°C . The temperature distribution in Inconel probe, determined using inverse algorithm was used to calculate t_{85} at all locations in the Inconel probe. Figure 7.4 shows the distribution of the t_{85} values in the Inconel probe quenched in molten NaNO_2 eutectic mixture and hot oil quench media maintenance at 150°C . The higher value of t_{85} values results in lower hardness in steel. If same distribution of t_{85} values is assumed to exist in steel probe of same dimension, the distribution of t_{85} values in the Figure 7.4 suggests higher hardness and uniform hardness distribution in the steel probe quenched in molten NaNO_2 eutectic mixture quench medium as compared to hot oil quench medium.

7.2 Effect of bath temperature on the cooling performance of eutectic KNO₃-NaNO₃ mixture.

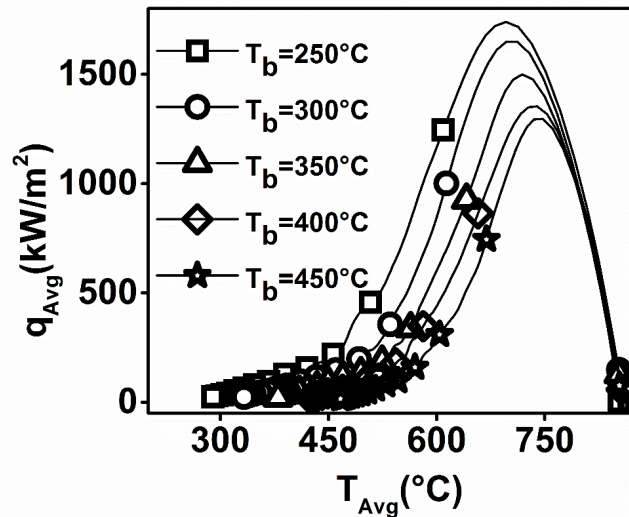


Figure 7.5: Variation of q_{Avg} with T_{Avg} calculate for inconel probe quenched in 55N salt mixture maintained at different quench bath temperatures.

55N salt is the eutectic mixture of KNO₃ and NaNO₃. This composition of KNO₃ and NaNO₃ salt mixture has the lowest melting point of 222°C. This salt thus offers a wide operating range. Figure 7.5 shows the variation of q_{Avg} as a function of T_{Avg} for Inconel probe quenched in 55N salt medium maintained at different quench bath temperatures. It was observed that irrespective of quench bath temperature, the curves followed the same trend.

Initially heat flux rapidly increased from zero to a maximum value, and then decreased. The rate of decrease of heat flux was initially high but decreased at the later stage. Molten eutectic KNO₃-NaNO₃ quench medium exhibits two stages of quench heat extraction namely nucleate boiling and convection stage.

7.2.1 Regression models to predict critical points at a given bath temperature

The nature of these curve are similar to that observed during quenching NaNO₂ eutectic mixture and discussed in section 7.1. Points p_1 and p_2 in Figure 7.1 are the critical points that have a significant effect on the heat transfer during quenching. The coordinates of points p_1 and p_2 are (q_{max}, T_{max}) and (q_{Conv}, T_{Conv}) respectively. q_{max} is the maximum value of average heat flux during nucleate boiling stage and T_{max} is the corresponding average

surface temperature. q_{Conv} is the value of average heat flux at the start of convective cooling stage and T_{Conv} is the corresponding average surface temperature.

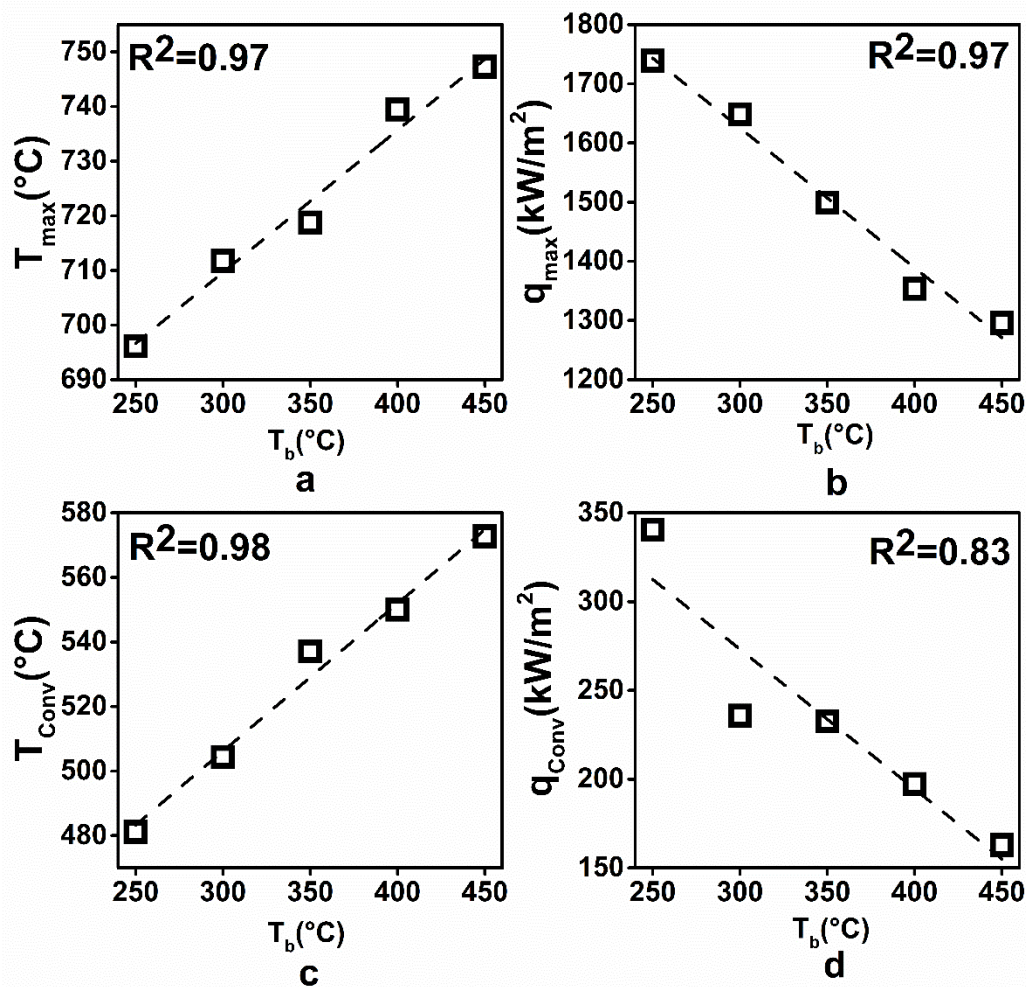


Figure 7.6: Linear regression models for variation of a) T_{max} b) q_{cax} c) T_{Conv} and d) q_{Conv} as a function of quench bath temperature for Inconel probe quenched in 55N salt mixture

It was observed that q_{max} decreased with increase in quench bath temperature (T_b). T_{max} decreased with increase in quench bath temperature (T_b). Equation 7.1 and Equation 7.2 were obtained by linear regression model presented in Figure 7.6a and Figure 7.6b respectively. These equations relate q_{max} (kW/m²) and T_{max} (°C) with quench bath temperature (T_b in °C) respectively.

$$T_{max} = 0.26T_b + 631.4 \quad (7.1)$$

$$q_{max} = -2.362T_b + 2333.92 \quad (7.2)$$

Further it was observed that T_{conv} increased with increase in quench bath temperature and q_{Conv} decreased with increase in quench bath temperature. Equation 7.2 and Equation 7.3 and relates T_{conv} ($^{\circ}C$) and q_{Conv} (kW/m^2) with quench bath temperature. It can be observed that all regression models in Figure 7.6a-Figure 7.6d have a high R^2 value. This validates the proposed linear regression model.

$$q_{Conv} = -0.7873 T_b + 509.338 \quad (7.3)$$

$$T_{Conv} = 0.4578 T_b + 368.92 \quad (7.4)$$

7.2.2 Characteristic cooling time in the Inconel probe

7.2.2.1 Regression model to predict the maximum value of t_{85} as a function of quench bath temperature

t_{85} values were obtained at each node of axisymmetric model of Inconel probe. Equation 7.5 presents a regression model to predict maximum value of t_{85} in the Inconel probe quenched in molten eutectic $NaNO_3-KNO_3$ media maintained at a given quench bath temperature. As shown in Figure 7.8, the maximum t_{85} value in the Inconel probe increased linearly with increase in quench bath temperature.

$$t_{85} = 0.09485 T_b - 18.77565 \quad (7.5)$$

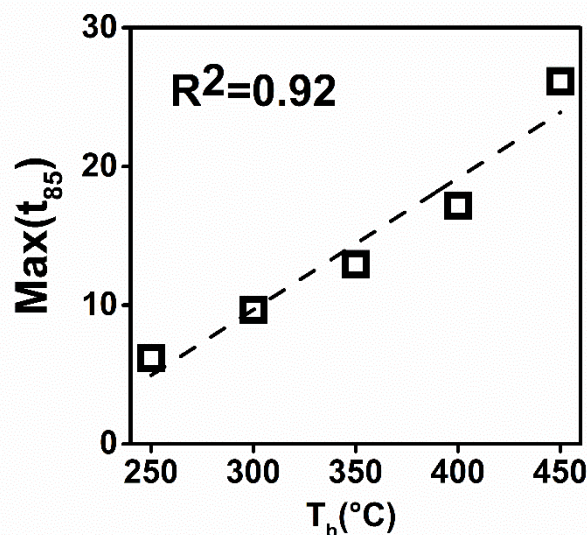


Figure 7.7: Linear regression model to predict the maximum t_{85} value for the Inconel probe quenched in 55N salt mixture as a function of bath temperature.

7.2.2.2 Distribution of t_{85} in the Inconel probe

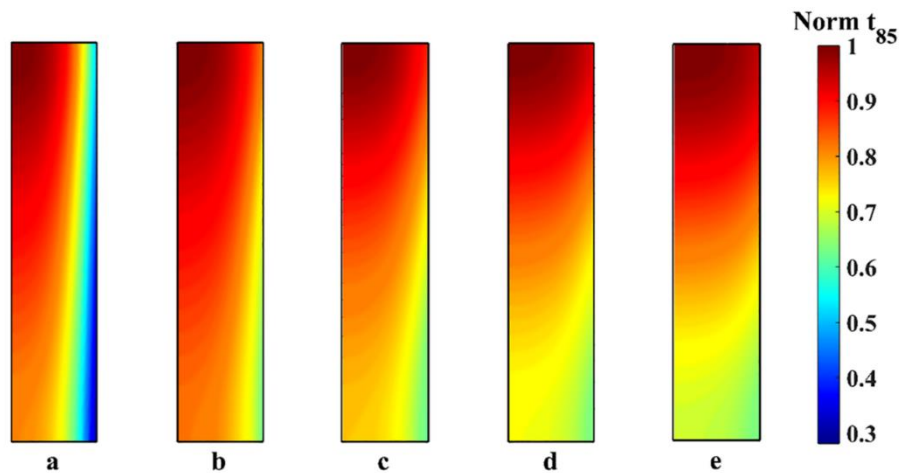


Figure 7.8: Normalized t_{85} distribution in axisymmetric hot Inconel probe quenched in eutectic $\text{NaNO}_3\text{-KNO}_3$ quench medium maintained at a) 250°C b) 300°C c) 350°C d) 400°C e) 450°C

The t_{85} values were obtained at each node of axisymmetric model of Inconel probe were normalized by dividing them with the maximum value of t_{85} in the probe. The normalization of t_{85} values facilitates the comparison of distribution of t_{85} values irrespective of their magnitude. Figure 7.8 shows the distribution of normalized t_{85} in the axisymmetric model of the Inconel probe quenched in the 55N salt quench medium maintained at different bath temperatures.

It was observed that the variation of normalized t_{85} along the length of the probe increased with increase in the bath temperature of the quench medium. The values of normalized t_{85} was observed to be lower in the bottom part of the probe compared to the top part of the probe. The non-uniform distribution of t_{85} was attributed to the variation of heat transfer characteristics along the surface of the probe.

7.3 Effect of composition and bath temperature on the cooling performance of $\text{NaNO}_3\text{-KNO}_3$ mixtures.

7.3.1 Average surface heat flux

Figure 7.9 shows the variation of q_{Avg} with T_{Avg} for Inconel probe quenched in molten $\text{NaNO}_3\text{-KNO}_3$ mixtures maintained at different bath temperatures. Table 5.1 provides the compositions of 100N, 75N, 55N, 25N and 0N salts and their respective bath temperatures.

Figure 7.9 shows the variation of q_{Avg} with T_{Avg} for Inconel probe quenched in molten $NaNO_3-KNO_3$ mixtures maintained at different bath temperatures. The heat extraction mechanism in all the mixtures were observed to be similar. As illustrated in Figure 7.9a, during the nucleate boiling stage, the average heat flux swiftly increased to a peak value of q_{max} corresponding to an average surface temperature of T_{max} . The magnitude of heat flux decreased subsequently. The second stage of heat extraction process was the convective cooling stage. The rate of heat extraction was very low during this stage. In Figure 7.9a, the average heat flux and average surface temperature at the point of transition from boiling to the convective stage are denoted by q_{conv} and T_{conv} respectively.

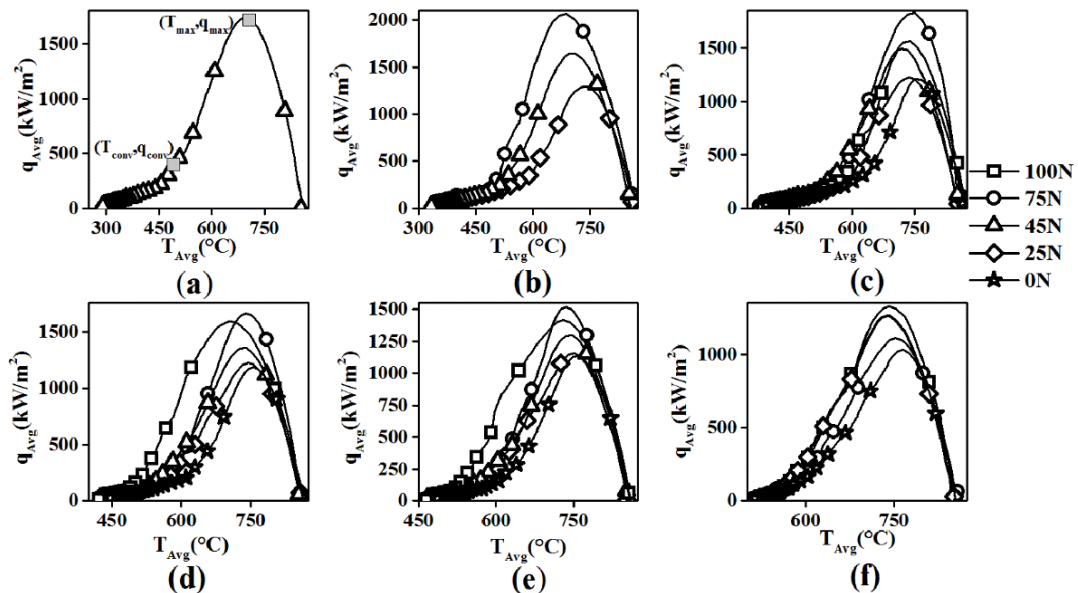


Figure 7.9: Variation of average surface temperature with average surface heat flux for Inconel probe quenched in molten $NaNO_3-KNO_3$ mixtures at a) 250°C, b) 300°C c) 350°C C) d)400°C e)450°C f) 500°C

7.3.2 Variation of critical points with composition and bath temperature

Peak heat extraction rate during nucleate boiling stage and the point of transition from nucleate boiling stage to convective cooling stage were chosen as critical points to assess cooling performance of these quench media. The coordinates of these points i.e., q_{max} , T_{max} , q_{conv} , and T_{conv} were used to characterize the quench performance of molten $NaNO_3-KNO_3$ mixtures. Figure 7.10a-Figure 7.10d were generated using the data obtained from the quenching experiments.

The peak average heat flux decreased with increase in KNO_3 concentration and bath temperature in the quenching medium. T_{max} increased with increase of KNO_3 concentration and bath temperature in the quenching medium.

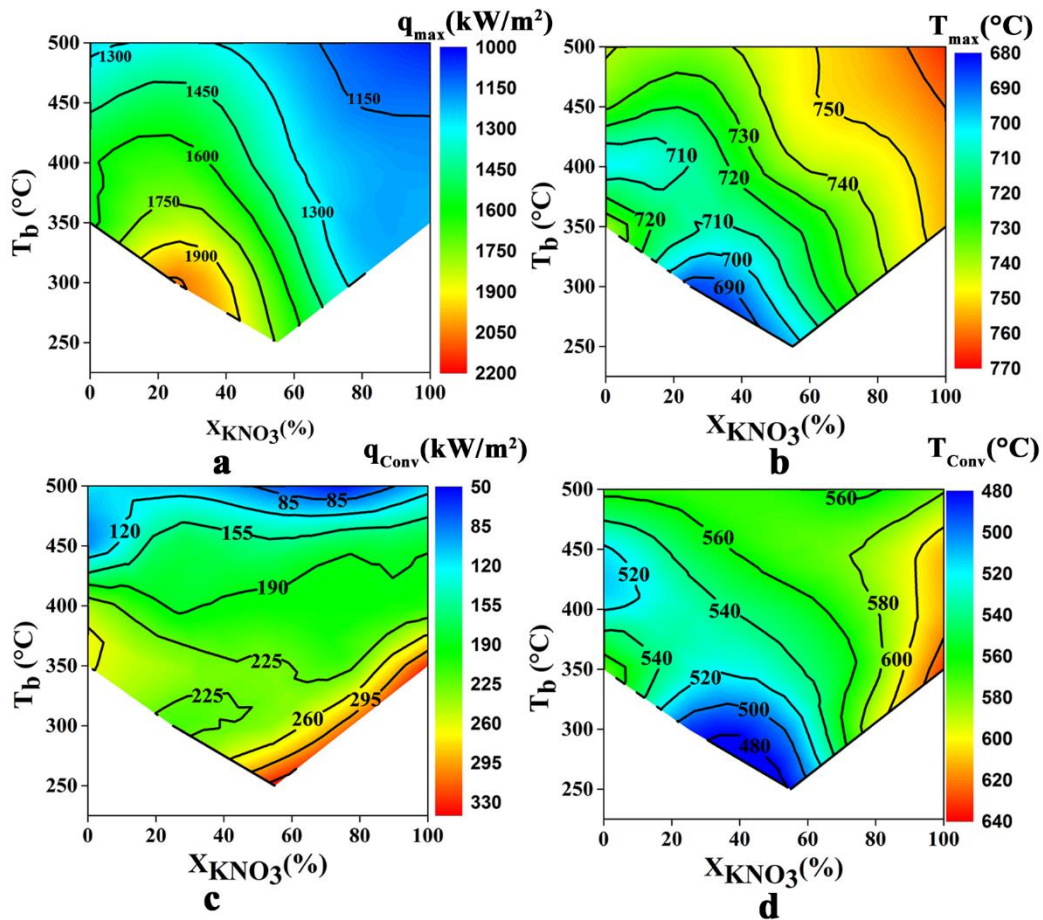


Figure 7.10: Contour plots presenting variation of average heat flux curve parameters, a) q_{max} , b) T_{max} , c) q_{conv} and d) T_{conv} with respect to the composition and quench bath temperature in molten $\text{NaNO}_3\text{-KNO}_3$ mixtures

q_{conv} remained nearly constant for all compositions at bath temperatures greater than 400°C . At bath temperatures below 350°C , q_{conv} increased with KNO_3 composition in the molten salt medium. T_{conv} increased with increase of KNO_3 concentration and bath temperature in the quenching medium. The overall cooling performance of the molten $\text{NaNO}_3\text{-KNO}_3$ mixtures can be thus enhanced by changing its composition.

A higher value of q_{max} and q_{conv} and lower values of T_{conv} during quenching results in increased hardness in the quenched steel part. A higher value of q_{max} indicate the increased cooling rate thereby avoiding pearlitic nose of steel in TTT diagram.

T_{\max} should ideally be close to but below the pearlite nose of the steel in the TTT diagram. The lower value of T_{conv} and higher value of q_{conv} avoids bainitic transformation during quenching of steel parts.

Higher peak heat flux also ensures higher heat transfer rates up to the start of the convective cooling stage. Higher heat transfer rates between T_{\max} and T_{conv} temperatures suppresses the transformation of austenite to bainite and pearlite.

7.3.3 Steel probe quenching

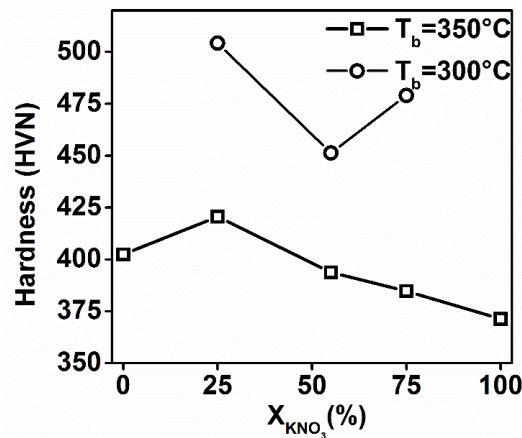


Figure 7.11: Average hardness of AISI 4140 steel probe quenched in molten $\text{NaNO}_3\text{-KNO}_3$ mixtures with varying KNO_3 composition maintained at 300°C and 350°C

7.3.3.1 $T_b = 300^\circ\text{C}$

The decrease in hardness in AISI 4140 steel probe quenched in 75N and 45N quench media maintained at 300°C was attributed to the large decrease in the magnitude of q_{\max} . No significant change in q_{conv} and T_{conv} was observed but T_{\max} increased with the change in composition.

The increase in hardness value between AISI 4140 steel probe quenched in 45N and 25N quench media was related to the increase in the value of q_{conv} . This resulted in increased cooling rate during convective cooling stage and bainitic transformation of austenite was thus suppressed. The increase in the value of q_{\max} with the change in composition was observed to have no significant effect on the hardness of the steel part in this case.

7.3.3.2 $T_b=350^\circ\text{C}$

The hardness value of AISI 4140 steel probe quenched in $\text{NaNO}_3\text{-KNO}_3$ mixtures maintained at 350°C was observed to be significantly affected by the change in composition of the bath. With change in composition, there was significant variation in q_{\max} . Unlike the bath maintained at 300°C , the benefit from higher values of q_{conv} at higher concentrations of KNO_3 in the molten bath was negated by the early commencement of convective cooling stage as indicated by higher values of T_{conv} .

7.3.4 Uniformity of quench cooling of Inconel probe

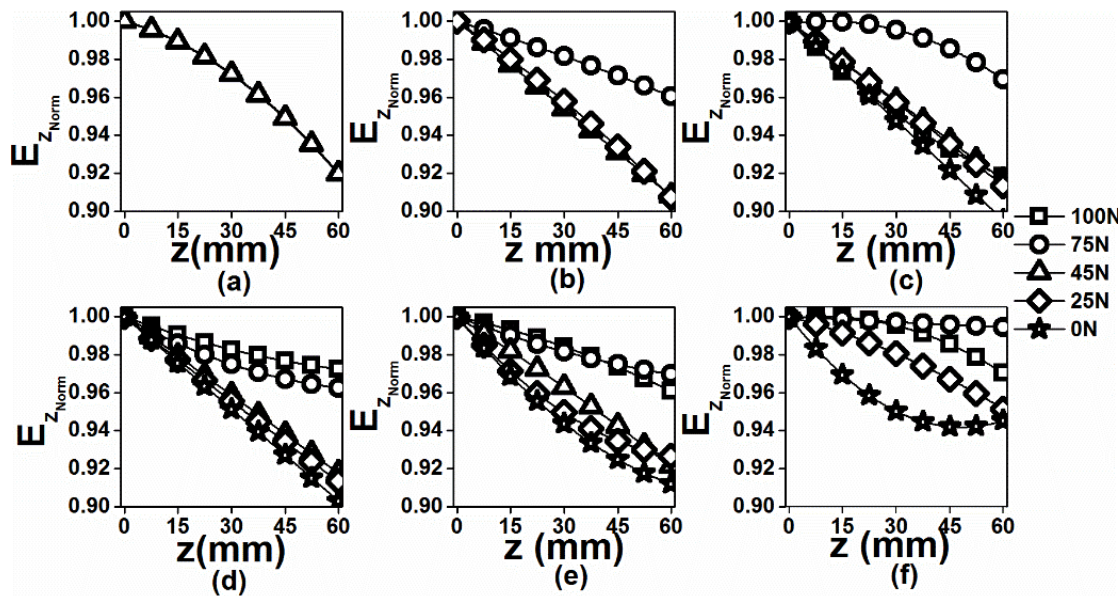


Figure 7.12: Spatial variation of normalized heat energy along the surface for Inconel probe quenched in molten $\text{NaNO}_3\text{-KNO}_3$ mixtures maintained at a) 250°C , b) 300°C c) 350°C C) d) 400°C e) 450°C f) 500°C

The normalized energy extracted at the metal-quenchant interface was calculated using equation 7.6.

$$E_{zNorm} = \frac{E_z(z)}{\max(E_z(z))} \quad (7.6)$$

The spatial variation of normalized heat energy reflects on the nonuniformity in heat extraction along the surface of the probe. This variation would result in nonuniform hardness and defects in the quenched steel parts. The uniformity of cooling along the surface of the Inconel probe was observed to decrease with increase in KNO_3 concentration in the quenching medium.

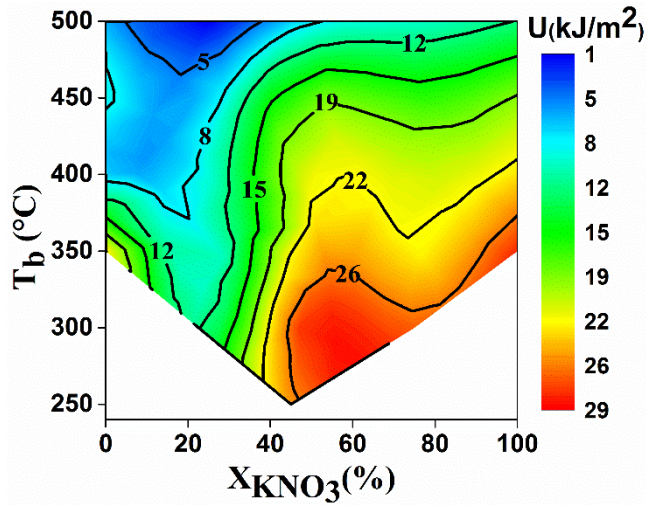


Figure 7.13: Contour plots presenting variation of uniformity with respect to the composition and quench bath temperature in molten NaNO₃-KNO₃ mixtures

Figure 7.13 shows the variation of uniformity parameter with bath temperature and composition of KNO₃-NaNO₃ mixtures. Uniformity parameter quantifies the spatial variation of energy extracted per unit area at the metal quenchant interface with respect to the average energy extracted per unit area. Lower value of uniformity parameter thus indicates more uniform heat extraction.

It was observed from the figure that uniformity of heat extraction improved with the increase in bath temperature and decrease in KNO₃ composition in the quench bath. Uniformity in quench heat extraction ensures even distribution of hardness along the specimen and lowers the propensity of quench defects.

7.3.5 Thermo chemical decomposition of salt and boiling heat transfer

The heat extraction during boiling stage mainly occurs due to decomposition of molten KNO₃-NaNO₃ mixtures at the surface of hot probe during quenching. The endothermic reversible chemical reaction that are responsible for high heat extraction rates during the boiling stage in NaNO₃ and KNO₃ are given in Equations 7.7- 7.8 and Equations 7.9-7.10 respectively. Free convection and turbulence due to gas evolution also contributes to the quench heat transfer during boiling stage. However, boiling/decomposition reaction of the nitrates at the probe surface is the main heat extraction mechanism.





NaNO_3 melts without decomposition to a liquid which is stable in air to at least 500°C and begins to decompose slowly at 600°C . Between 600°C and 750°C , a pseudo equilibrium is established between air and a liquid containing NaNO_3 and NaNO_2 whose composition is temperature dependent.



at least 530°C . When heated in air, it begins to decompose near 650°C and quasi-equilibrium is set up between 550°C and 750°C (Bartholemew 1966).

The nitrate-oxide reactions shown in Equations 7.8 and Equations 7.10 occur only at temperatures above 750°C . Thus, the contribution of nitrate-oxide reaction to boiling quench heat extraction can be neglected.

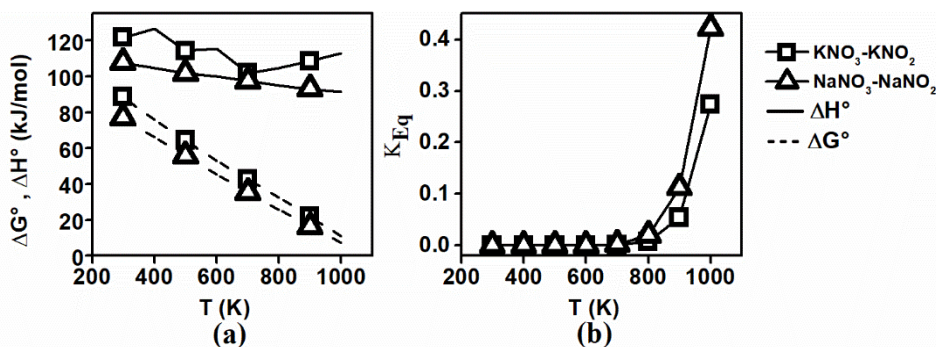


Figure 7.14: a) Change in standard enthalpy and standard Gibbs free energy b) Equilibrium constant for nitrate-nitrite decomposition of NaNO_3 and KNO_3

Figure 7.14 shows variation of enthalpy and free energy during the nitrate-nitrite reactions (Equation 7.7 and Equation 7.9). These values have been taken from the book authored by Stern (Stern 2001). Figure 7.14a shows that the standard free change for decomposition of KNO_3 is higher than NaNO_3 . The spontaneity of decomposition of NaNO_3 at any given temperature is more than KNO_3 . Therefore, an extended boiling regime is observed during quenching in a eutectic NaNO_3 mixture. Figure 7.14 also shows that change in standard enthalpy for decomposition of KNO_3 is higher than NaNO_3 . The equilibrium constant for decomposition of NaNO_3 was higher than KNO_3 . This indicates that the rate of decomposition of NaNO_3 at a given temperature, surface

condition and pressure is potentially higher compared to the rate of decomposition of KNO_3 .

$$K_{Eq} = \frac{[\text{MNO}_2][\text{O}_2]^{\frac{1}{2}}}{[\text{MNO}_3]} \quad \text{M can be K or Na} \quad (7.11)$$

The nitrite-nitrate ratio increases with bath temperature and from equation 7.11, the presence of nitrite in the quench bath suppresses the decomposition of nitrate salt.

During the boiling stage, concentration of nitrites increases near the surface of the quenched probe. This creates a concentration barrier and decreases the rate of decomposition of nitrates. Subsequently, the boiling stage ends when the heat energy supplied from the probe falls below the heat energy required for decomposition of nitrate

7.4 Cooling performance of molten KNO_3 - LiNO_3 - NaNO_3 eutectic mixture.

7.4.1 Quench heat flux parameters

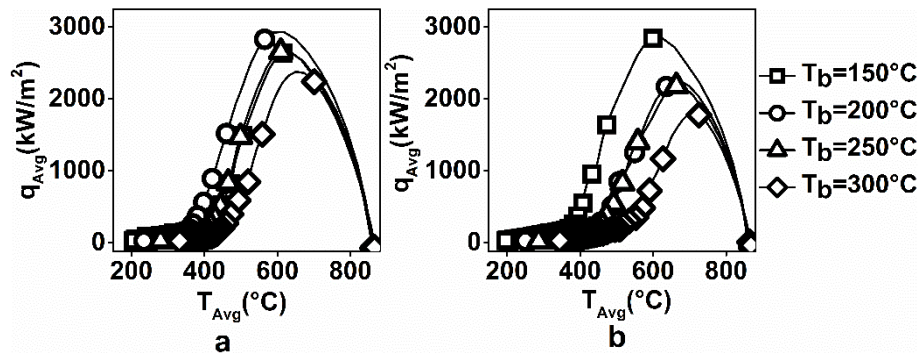


Figure 7.15: Variation of q_{Avg} with T_{Avg} for Inconel probe quenched in molten a) NaNO_2 b) LiNO_3 eutectic mixtures maintained at different quench bath temperatures

Figure 7.15a and Figure 7.15b show the variation of average heat flux with average surface temperature at the Inconel probe surface during quenching in molten eutectic mixtures of NaNO_2 and LiNO_3 maintained at various bath temperatures. The cooling was observed to occur in 2 stages. In the first stage, heat flux reaches a maximum value due to boiling of quench media. During boiling stage, nitrates in the molten salt decompose to nitrites and nitrites oxidize to form metal oxides. The high cooling rates during this stage are due to the absorption of heat for these endothermic reaction in the quench medium. Once the surface temperature drops, the decomposition reaction of salt

mixtures ceases, and convective cooling stage starts. The start of convective cooling stage was marked by sudden drop in slope of heat extraction rate to low value.

The points corresponding to the peak heat flux (q_{\max}, T_{\max}) and start of convective cooling stage ($q_{\text{Conv}}, T_{\text{Conv}}$) on the q_{Avg} v/s T_{Avg} plot were chosen as parameters to characterize the cooling performance of these quench media maintained at different bath temperatures. The values have been tabulated in Table 7.1.

During quenching of Inconel probe in molten eutectic NaNO_2 mixture, q_{\max} increased with bath temperature when it was increased from 150°C to 200°C . However, with further increase in the bath temperature to 250°C and 300°C , resulted in decrease of q_{\max} . An opposite trend was observed in the values of q_{Conv} and T_{Conv} . The values of q_{Conv} and T_{Conv} decreased when bath temperature was increased from 150°C to 200°C and these values decreased with further increase in bath temperature to 250°C and 300°C . No significant changes in the value of T_{\max} was observed for the probe quenched in molten NaNO_2 eutectic mixture maintained at 150°C , 200°C and 250°C . For bath maintained at 300°C , a significant increase in the values of T_{\max} was observed.

q_{\max} values were observed to monotonously decrease with increase in bath temperature for Inconel probe quenched in molten LiNO_3 eutectic mixture. The difference in the values of q_{\max} , q_{Conv} , T_{Conv} , and T_{\max} for the bath temperatures of 200°C and 250°C was however observed to be negligibly small. The values of T_{Conv} and T_{\max} increased when the bath was heated to 300°C . The value of q_{Conv} increased with increase in bath temperature to 300°C .

Higher values of q_{\max} , low values of T_{\max} and T_{Conv} indicate better cooling performance of quenching medium. From Table 7.1, it can thus be inferred that at bath temperature of 150°C , molten LiNO_3 eutectic mixture offered better cooling performance compared to molten NaNO_2 eutectic mixture. At bath temperatures at and above 200°C , molten NaNO_2 eutectic mixture offered better cooling performance compared to molten LiNO_3 eutectic mixture.

Table 7.1: Quench heat flux parameters for Inconel probe quenched in molten NaNO_2 and LiNO_3 eutectic mixtures quench media maintained at different bath temperatures

T_b (°C)	Eutectic mixture	q_{max} (kW/m ²)	T_{max} (°C)	q_{conv} (kW/m ²)	T_{conv} (°C)	U (kJ/m ²)
150	NaNO ₂	2632	615	302	428	35
	LiNO ₃	2840	599	291	384	26
200	NaNO ₂	2931	617	228	364	21
	LiNO ₃	2244	675	270	468	26
250	NaNO ₂	2652	609	248	420	27
	LiNO ₃	2178	664	255	466	36
300	NaNO ₂	2376	650	153	440	29
	LiNO ₃	1797	707	188	511	36

7.4.2 Uniformity of cooling

Figure 7.16 shows the spatial variation of heat energy extracted per unit area during Inconel probe quenched in molten LiNO₃ and NaNO₂ eutectic mixtures maintained at different bath temperatures. The spatial variation of heat energy extracted per unit area was used to calculate the uniformity parameter.

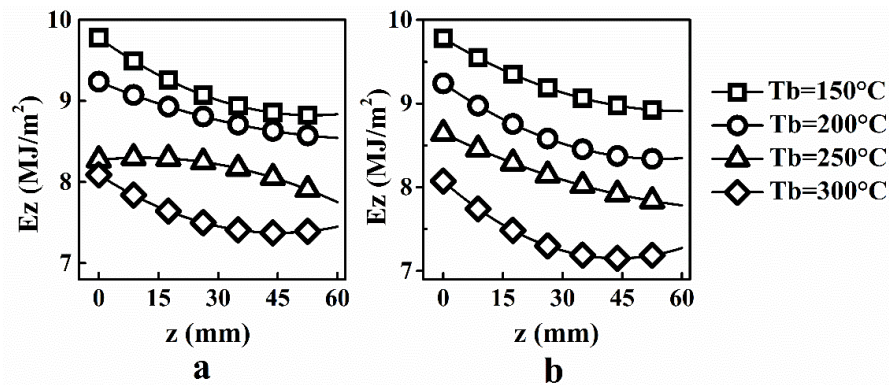


Figure 7.16: Variation of heat energy removed per unit area along the surface of the Inconel probe quenched in a) NaNO₂ b) LiNO₃ eutectic mixtures maintained at different quench bath temperatures

The values of uniformity parameter are tabulated in Table 7.1. A comparison of uniformity parameter values suggests that at bath temperatures of 200°C, 250°C and 300°C, Inconel probe quenched in NaNO₂ eutectic mixture was cooled more uniformly compared to LiNO₃ eutectic mixtures. For bath temperature of 150°C, LiNO₃ eutectic mixture cooled the Inconel probe more uniformly.

7.4.3 Hardness of steel probes

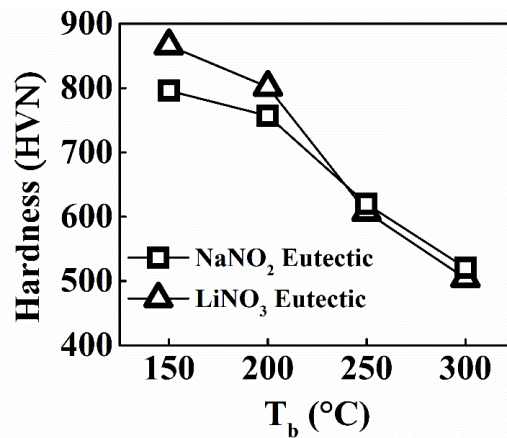


Figure 7.17: Average hardness measured in steel probes quenched in molten NaNO₂ and LiNO₃ eutectic mixtures maintained at varying bath temperatures

Average hardness of steel probes quenched in LiNO₃ eutectic mixture was higher than that in NaNO₂ eutectic mixture for bath temperatures of 150°C and 200°C. Hardness measured in steel probes quenched in NaNO₂ eutectic mixture were slightly higher compared to those quenched in LiNO₃ eutectic mixture for bath temperatures of 250°C and 300°C. These hardness values do not follow the trend of exceptionally higher heat transfer rates observed in Inconel probe quenched in NaNO₂ eutectic mixture when compared to LiNO₃ eutectic mixture for bath temperatures greater than 150°C. In order to study the reason for discrepancy in these results, the cooling data at the geometric centre of Inconel and steel probe during quenching were compared.

7.4.4 Centre cooling data for Inconel and steel probes

Figure 7.18 and Figure 7.19 show the cooling curves and cooling rate vs temperature curves acquired at the geometric centre for Inconel and steel probes quenched in LiNO₃ and NaNO₂ eutectic mixtures maintained at different bath temperatures respectively. The temperature for start convective cooling stage shifted to lower temperature in steel probe compared to Inconel probe quenched in molten LiNO₃ eutectic mixture. The magnitude of shift increased with increase in quench bath temperature. At bath temperature of 300°C, maximum cooling rate was observed to be nearly 50% higher in steel probe as compared to Inconel probe. In contrast to this, a very small difference was observed between cooling curves obtained for Inconel and steel probes quenched in molten NaNO₂ eutectic mixture.

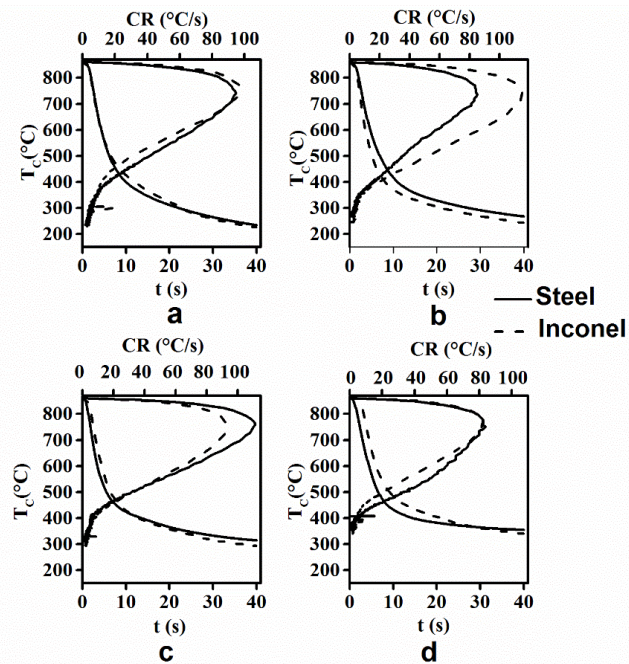


Figure 7.18: Time temperature and cooling rate curves measured at the geometric centre during quenching of Inconel and steel probes quenched in molten NaNO_2 eutectic mixture maintained at a) 150°C b) 200°C c) 250°C d) 300°C

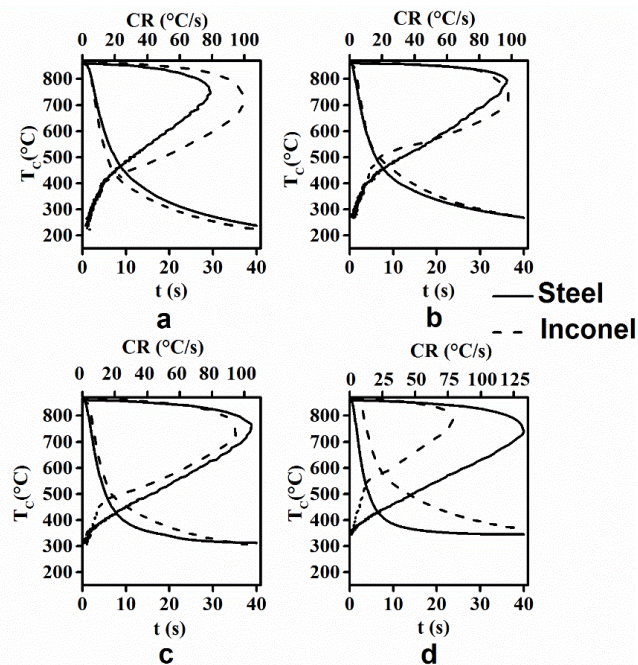


Figure 7.19: Time temperature and cooling rate curves measured at geometric centre during quenching of Inconel and steel probes quenched in molten LiNO_3 eutectic mixture maintained at a) 150°C b) 200°C c) 250°C d) 300°C

7.4.5 Equilibrium contact angle

























	150°C	200°C	250°C	300°C	350°C	400°C
NaNO ₂ Eutectic Inconel	 θ=76.00°	 θ=85.65°	 θ=88.55°	 θ=95.70°	 θ=52.75°	 θ<10°
NaNO ₂ Eutectic AISI-4140 Steel	 θ=90.95°	 θ=96.35°	 θ=84.20°	 θ=84.15°	 θ=35.20°	 θ<10°
LiNO ₃ Eutectic Inconel	 θ=87.55°	 θ=84.10°	 θ=85.75°	 θ=79.75°	 θ=64.45°	 θ<10°
LiNO ₃ Eutectic AISI-4140 Steel	 θ=71.95°	 θ=77.85°	 θ=81.45°	 θ=81.35°	 θ=52.25°	 θ=16.7°

Figure 7.20: Contact angle for spreading of LiNO₃ and NaNO₂ eutectic mixtures maintained at different temperatures on Inconel and AISI-4140 steel surfaces

The observations of centre cooling curves suggest that the behaviour of molten LiNO₃ eutectic on steel and oxidized Inconel surface is different. To confirm this, temperature dependent contact angle was studied. Figure 7.20 shows the photographs of LiNO₃ and NaNO₂ droplets spreading on steel and oxidized Inconel surfaces. The furnace was heated in stages to temperatures of 150°C, 200°C, 250°C, 300°C, 350°C and 400°C and held for roughly 2 minutes and equilibrium contact angle (θ) was measured. The details of contact angle measurement have been provided in section 5.8 .

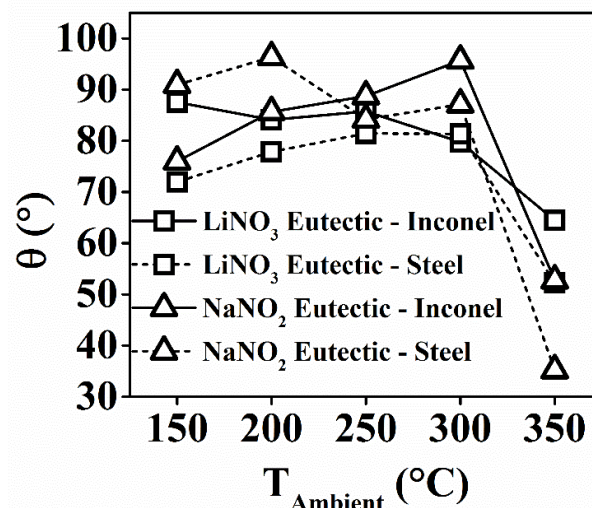


Figure 7.21: Variation of equilibrium contact angle with ambient temperature for spreading of LiNO₃ and NaNO₂ eutectic mixtures on Inconel and AISI-4140 steel surfaces

Figure 7.21 shows variation of equilibrium contact angle with ambient temperature. In case of NaNO_2 eutectic drop heated on oxidized Inconel surface, when the ambient temperature was increased from 150°C to 300°C , dilation of NaNO_2 eutectic droplet was observed. This was due to the evolution of O_2 gas as a result of the decomposition of nitrates to nitrites. The dilation of the droplet stopped and spreading started when the ambient temperature was further increased to 350°C . Further no dilation was observed when ambient temperature was raised from 350°C to 400°C . No boiling of liquid droplet was observed at 350°C and 400°C . NaNO_2 eutectic mixture droplets heated on steel surface also followed the same trend. The contact angles in this case were lower than that observed on oxidized Inconel surface.

In the case of LiNO_3 eutectic mixture droplet on oxidized Inconel surface, the droplet started inflating after the ambient temperature was increased to 250°C . The shape of droplet deformed when ambient temperature was increased to 300°C . The droplet started spreading when ambient temperature was increased to 350°C . Boiling of LiNO_3 eutectic mixture droplet was observed during spreading at 350°C and 400°C . This led to repeated rise and fall of the droplet height on the surface.

Contact angles observed during spreading of LiNO_3 eutectic mixture droplet on steel surface were lower compared to that observed on oxidized Inconel surface. The spreading of LiNO_3 eutectic mixture droplet observed on Inconel surface at ambient temperature of 200°C was not observed on steel surface. The dilation of LiNO_3 eutectic droplet continued when temperature was increased to 200°C , 250°C and at 300°C . Spreading of the droplet started when ambient temperature was increased from 300°C to 350°C . Similar to Inconel surface, boiling of LiNO_3 eutectic mixture droplet was observed during spreading at ambient temperature of 350°C and 400°C on the steel surface.

As compared to spreading of LiNO_3 eutectic mixture on oxidized Inconel surface, lower contact angle and extended temperature range of dilation of droplet on the steel surface were observed. Fernandes and Prabhu (Fernandes and Prabhu 2008) suggested increased wettability (decrease in contact angle) results in better heat extraction rates. Apart from this, boiling stage stabilized on the steel surface over an increased

temperature range. These two-phenomena resulted in increased quench heat transfer during quenching of steel probe compared to Inconel probe.

7.5 Hot Neem Oil as alternative to Hot Mineral Oils for Martempering.

7.5.1 Heat extraction mechanism

As shown in Figure 7.22, in the initial stage of quenching, the rate of increase of mean heat flux in the case of Inconel probe quenched in hot oil was not as sharp as that observed in neem oil. This suggests the presence of an unstable vapour blanket stage. An unstable vapour blanket stage was also observed in neem oil maintained at 200°C bath temperature. In the case of hot oil and neem oil maintained at 200°C, the heat flux increased to a peak value during nucleate boiling stage subsequent to vapour blanket stage. Further, the heat flux decreased with temperature and convective cooling stage started at lower temperatures (<500°C). In contrast to the conventional 3-stage cooling observed during quenching in hot oil, the heat transfer during quenching in neem oil maintained at 100°C and 150°C occurred in only two stages namely boiling and convective cooling stage.

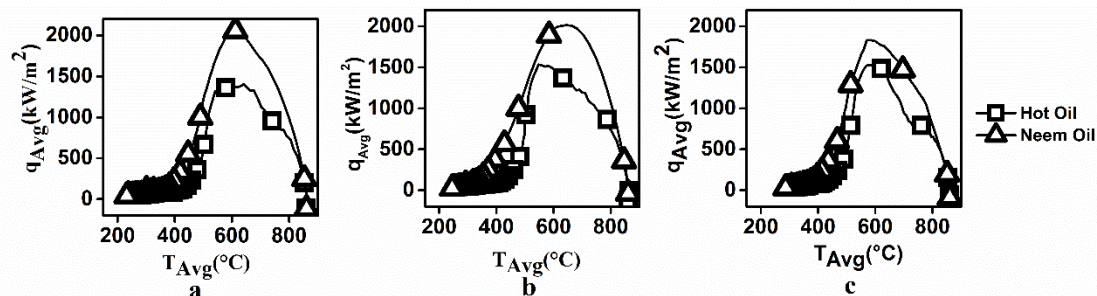


Figure 7.22: Mean heat flux v/s mean surface temperature in inconel probe cooling in hot oil and neem oil maintained at a) 100°C b) 150°C c) 200°C

7.5.2 Uniformity of heat extraction

Figure 7.23 shows the spatial variation of quench heat energy at the metal/quenchant interface extracted in the first 40s of quenching of Inconel probe. The values were obtained by integrating spatially dependent heat flux over time. Higher energy was extracted from the top portion of the probe compared to that from bottom portion of the probe. However, the variation in the hot oil was much higher compared to hot oil.

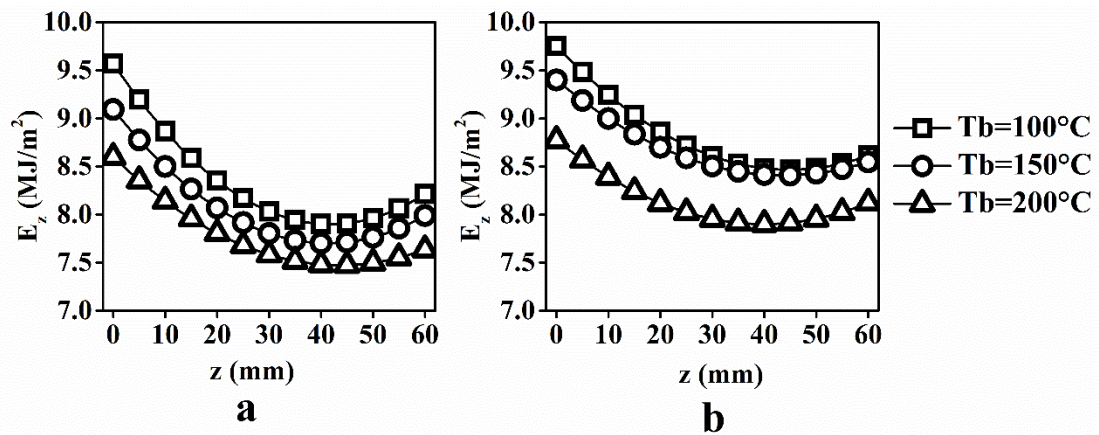


Figure 7.23: Spatial variation of heat energy for inconel probe quenched in a) hot oil b)neem oil maintained at different bath temperatures

7.5.3 Quench heat flux parameters

Table 7.2 shows the quench heat flux parameters calculated for hot oil and neem oil maintained at various quench bath temperatures. q_{\max} , T_{\max} , q_{Conv} , T_{conv} and uniformity parameter (U) were the parameters calculated from spatially dependent transient quench heat flux.

Table 7.2: Quench heat flux parameters calculated for Inconel probe quenched in hot oil and neem oil quench media maintained at different bath temperatures

Medium	T_b (°C)	q_{\max} (kW/m ²)	T_{\max} (°C)	q_{Conv} (kW/m ²)	T_{conv} (°C)	U (kJ/m ²)
Hot Oil	100	1404	640	220	458	60
	150	1535	547	225	454	50
	200	1532	581	204	461	41
Neem Oil	100	2072	629	293	412	48
	150	2014	645	239	369	36
	200	1832	585	267	420	31

The values of q_{conv} and q_{\max} in neem oil was higher than hot oil. Higher values of q_{\max} and values of T_{\max} near pearlite nose of steel are conducive to avert high temperature diffusion-based transformation of austenite to ferrite, pearlite and cementite. No significant difference in the values of T_{conv} was observed in the case of hot oils. T_{conv}

values for hot oil were significantly higher as compared to that for neem oil. The start of convective cooling stage at higher surface temperature would result in slow cooling of steel part in bainitic and martensitic transformation range and result in lower hardness.

Uniformity parameter decreased with bath temperature in hot oil and neem oil. The degree of uniform cooling thus decreased with bath temperature in both quench media. For a given bath temperature, Inconel probe quenched in neem oil was cooled with more uniformly as compared to that in hot oil. From Table 7.2, it can be concluded that neem oil offered higher cooling rates with increased uniformity of cooling as compared to hot oil at all bath temperatures.

7.5.4 Quenching of steel probes

Figure 7.24 shows the cooling and rate curves for Inconel and AISI-52100 steel probes measured at the geometric centre of the probe. The difference in cooling profiles of Inconel and steel probes are due to the difference in thermo physical properties and the evolution of latent heat of transformation associated with the transformation of austenite in the course of cooling of steel probe. Vapour blanket stage was not observed during quenching of steel probes in hot oils maintained at 100°C and 150°C.

Significant effect of latent heat of transformation was observed in steel probe quenched in hot oil maintained at 200°C. The latent heat of transformation of austenite to pearlite, cementite, bainite and martensite in the probe resulted in the increase of temperature at geometric centre of the probe. This resulted in the loop observed in cooling rate curve observed in Figure 7.24c.

Figure 7.25b shows the variation of measured hardness of AISI-52100 steel probes with bath temperature. Higher hardness values were observed in neem oil compared to hot oil. TTT diagram shown in Figure 7.25a was generated using JMatPro software. Steel probes quenched in neem oil maintained at 200°C and hot oil maintained at 150°C were observed to have highest hardness in the respective quench media.

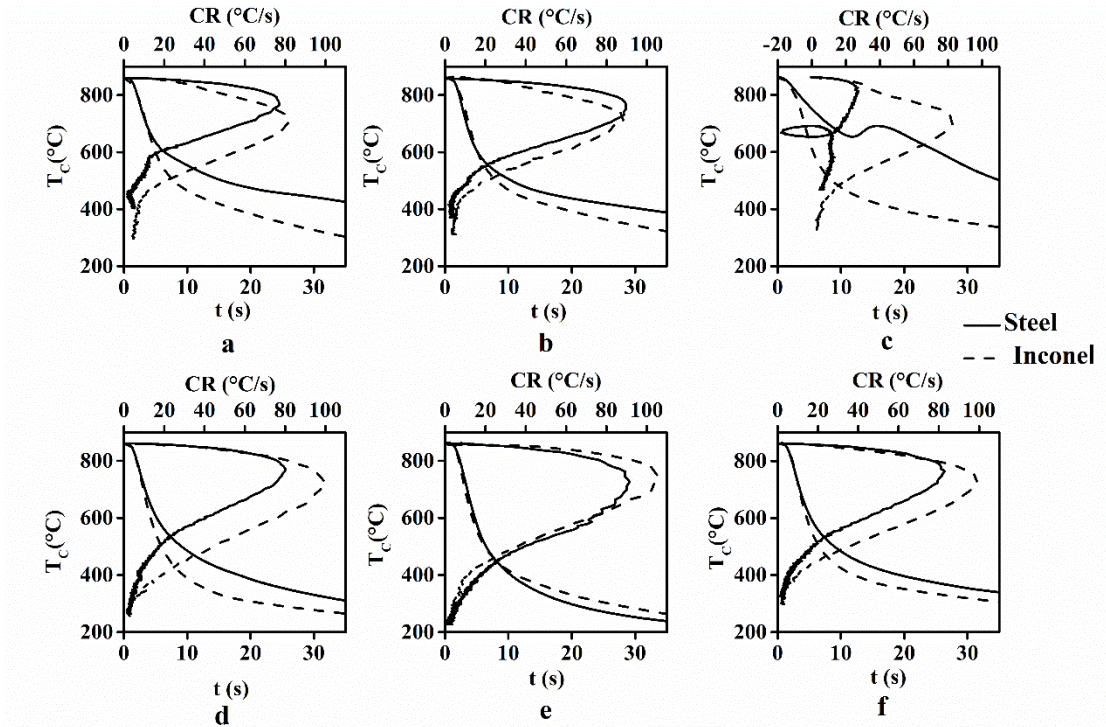


Figure 7.24: Cooling and rate curves obtained at the geometric centre of Inconel and AISI-52100 quenched in hot oil maintained at a) 100°C b) 150°C c) 200°C and neem oil maintained at d) 100°C e) 150°C f) 200°C

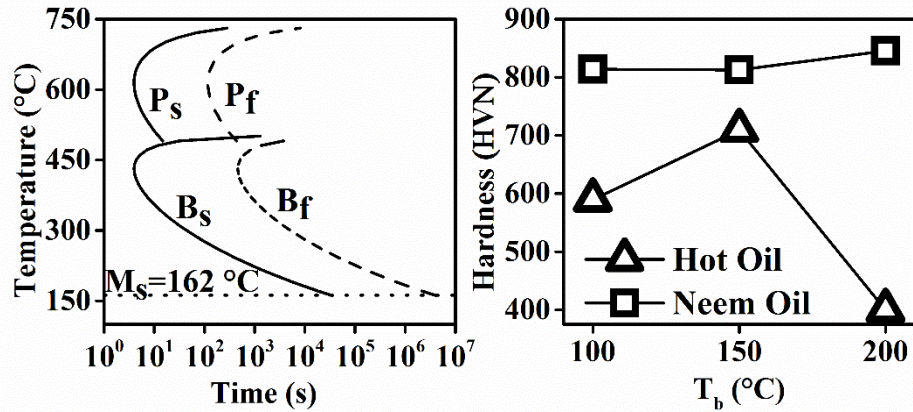


Figure 7.25: a) TTT diagram for AISI-52100 steel and b) variation of average measured in steel probe quenched in hot oil and neem oil

Figure 7.26-Figure 7.28 show the micrographs for AISI-52100 steels quenched in hot oil and neem oil maintained at 100°C, 150°C and 200°C respectively.

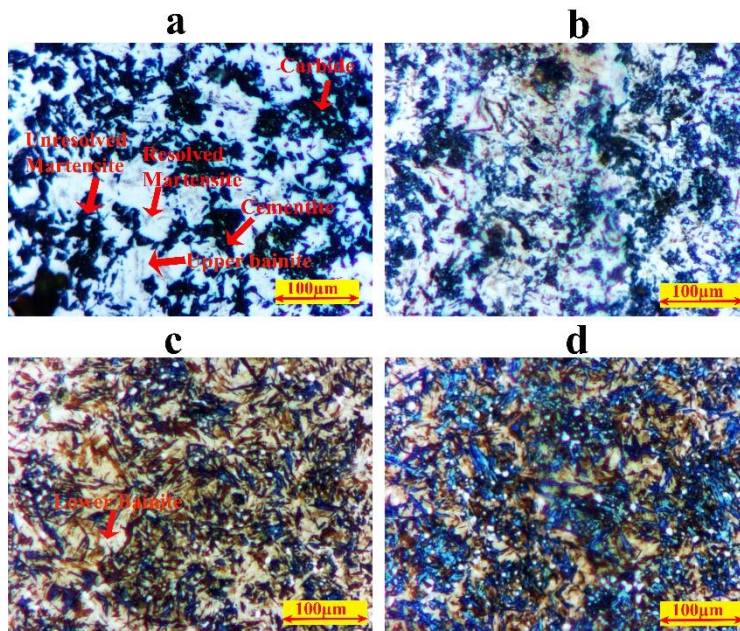


Figure 7.26: Micrographs of AISI-52100 probe quenched in hot oil at a)center b) near surface and neem oil at a)center b) near surface for bath temperature of 100°C

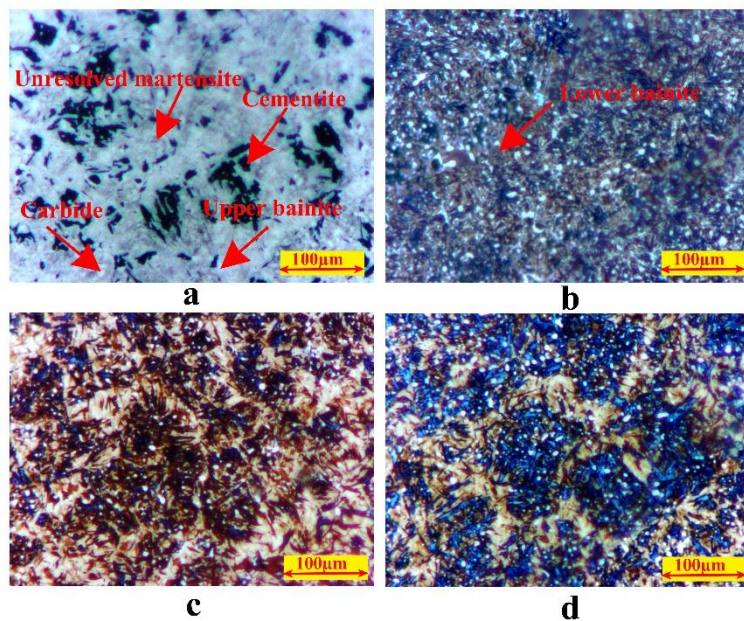


Figure 7.27: Micrographs of AISI-52100 probe quenched in hot oil at a)center b) near surface and neem oil at a)center b) near surface for bath temperature of 150°C

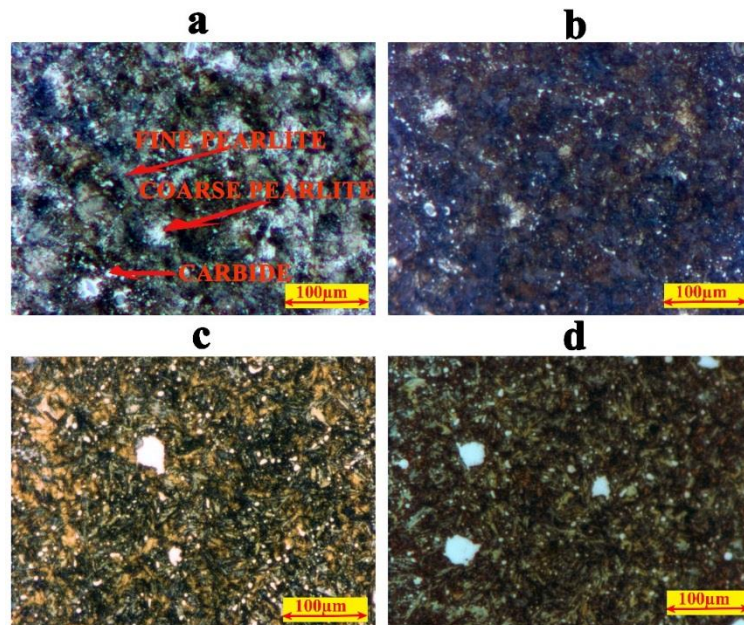


Figure 7.28: Micrographs of AISI-52100 probe quenched in hot oil at a)center b) near surface and neem oil at a)center b) near surface for bath temperature of 200°C

From the cooling curves for steel probe quenched in hot oil maintained at 100°C, a significant drop in the cooling rate was observed below 600°C. This region corresponds to pearlite nose in the TTT diagram. The latent heat of transformation of austenite to carbide, lower pearlite and upper bainite was the reason for decrease in the cooling rate. Un-resolved martensite, resolved martensite, carbides and upper bainite were observed in the microstructure. The volume fraction of martensite was higher at the surface. A mixture of martensite, bainite and small grains of carbides was observed in steel samples quenched in neem oil maintained at 100°C.

The volume fraction of unresolved martensite observed at the centre of the steel sample quenched in hot oil maintained at 150°C was higher than that observed in steel sample quenched in hot oil maintained at 100°C bath temperature. A mixture of lower bainite, small carbide and martensite was observed near the surface of these samples. The microstructure in steel samples quenched in neem oil maintained at 150°C was similar to that observed in steel samples quenched in neem oil maintained at 100°C.

In steel samples quenched in hot oil maintained at 200°C bath temperature, a mixture of pearlite and cementite phase was observed. In the case of samples quenched in neem oil maintained at 200°C, a mixture of bainite, martensite and large carbide was

observed. The increase in hardness is due to the evolution of large carbides observed in the microstructure.

7.5.5 Oxidation of oils

Figure 7.29 shows the change in appearance of the oil due to oxidation. Both oils became observed to darker with progress of oxidation.

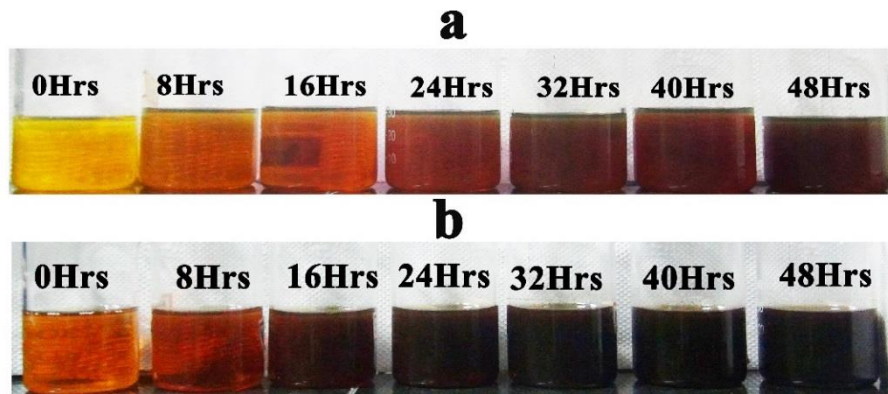


Figure 7.29: Photographs of a) hot oil and b) neem oil oxidized in hot air oven

Fluid viscosity is the thermo-physical property with greatest effect on heat transfer during quenching (Elmi Hosseini et al. 2015). Figure 7.30 shows the effect of oxidation on viscosity of hot oil and neem oil. No significant effect of oxidation was observed on viscosity of hot oil. A marginal change of 4% was observed. In neem oil, the viscosity increased by 15% after 24hrs of oxidation. No significant increase in viscosity was observed during the next 24hrs. The viscosity of neem oil sample thus stabilized after initial oxidation

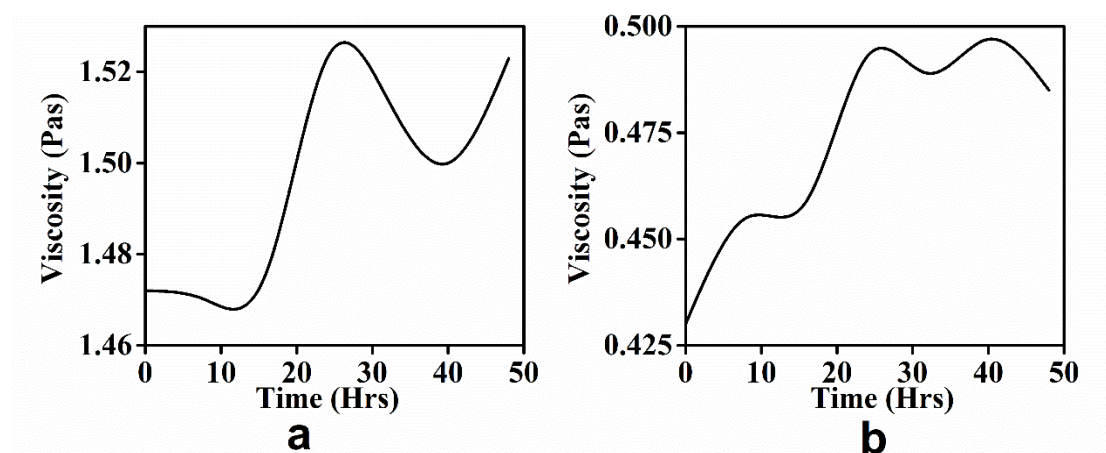


Figure 7.30: Effect of oxidation on dynamic viscosity of a) hot oil and b) neem oil

The effect of oxidation of neem oil on the cooling performance was also assessed. Figure 7.31 compares the temperature dependent cooling rate curve at the geometric centre of Inconel probe quenched in non-oxidized and oxidized neem oil maintained at 150°C. The neem oil was oxidized by subjecting it to multiple cycles of quenching and maintaining bath temperature in the range of 100°C-200°C. The viscosity of the oxidized neem oil was 0.465Pas. The viscosity was ~10% higher as compared to the viscosity of non-oxidized neem oil which was 0.43Pas at 40°C.

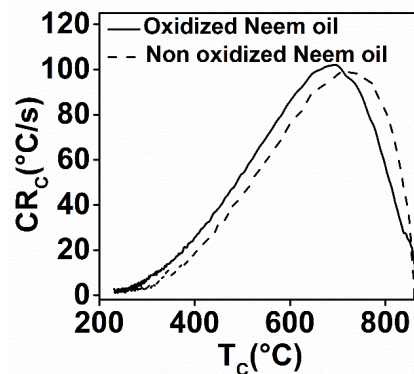


Figure 7.31: Cooling rate v/s measured temperature curve at the geometric centre of an Inconel probe quenched in oxidized and non-oxidized neem oil quench media maintained at 150°C.

The peak cooling rate was marginally higher in the case of oxidized neem oil but the temperature corresponding to peak cooling rate was ~40°C lower than non-oxidized neem oil. This lowering of peak cooling rate temperature was due to the occurrence of vapour blanket stage. Thus, the oxidation of neem oil resulted in change of two stage heat extraction mechanism (boiling and convective cooling stages) observed in non-oxidised neem oil to 3 stage heat extraction mechanism (vapour blanket, boiling and convective cooling stages). Further, the oxidation of neem oil lead to decreased cooling rate in the initial stage of quenching. Subsequently, the cooling rate in oxidized neem oil was higher as compared to the non-oxidized neem oil. The increased cooling rate at the lower temperature would be helpful to suppress bainitic transformation of austenite. However, the decreased cooling rate at the higher temperatures increases the propensity towards transformation of austenite to pearlite, cementite and ferrite phases

Oxidized neem oil has its own advantages and disadvantages. On one the hand oxidation of oil prevents transformation of bainite whereas on the other it increases the

propensity of transformation to pearlite. However, the effect of oxidation of neem oil on the overall quench heat extraction was observed to be minimal.

7.6 Effect of Section thickness, heat transfer coefficient, bath temperature and residence time on hardness of AISI 4140 steel cylinders during martempering

Appendix C shows the variation of mean hardness in AISI 4140 steel probes of different diameters (D) with bath temperature (T_b), heat transfer coefficient (h) and residence time fractions (f).

For cylinders of diameters lesser than 5mm, variation in the h , T_b and f did not have a significant effect on hardness evolution. The mean hardness in this case was observed to be very high.

For cylinders of diameter greater than 10mm, significant drop in hardness was observed for low values of h and high values T_b . This effect of lower of hardness at lower h and high T_b increased with increase in diameter. This was evident from the increase in lower mean hardness area in the h v/s T_b contour plots with increasing diameters.

There was no significant effect of residence time fraction (f) on the hardness was observed for cylinders with diameter lesser than 10mm. The decrease in the value of f resulted in decrease in the mean hardness values in cylinders with diameters greater than 15mm. This decrease in mean hardness was initially observed to be concentrated in low heat transfer coefficient and high bath temperature region. However, with increase in diameter of cylinder, the effect of 'f' on mean hardness was observed in high heat transfer coefficient and low bath temperature region. From the contour plots it is very clear that the mean hardness is significantly affected by all the 4 process parameters and the variation was observed to be non-linear in nature. Modelling such a complex process is thus not possible using conventional regression models.

7.6.1 Variation of maximum residence time

Residence time is one of the important process variables during matempering of steel parts. Figure 7.32 shows the variation of maximum and minimum values of t_{Rmax} with diameter, heat transfer coefficient and bath temperature. The maximum and minimum values of t_{Rmax} were observed to be significantly dependent on the diameter of cylinder. The minimum values of t_{Rmax} was observed to decrease with increase in heat transfer

coefficient and bath temperatures. The maximum value of t_{Rmax} was observed to be independent of heat transfer coefficient and bath temperature

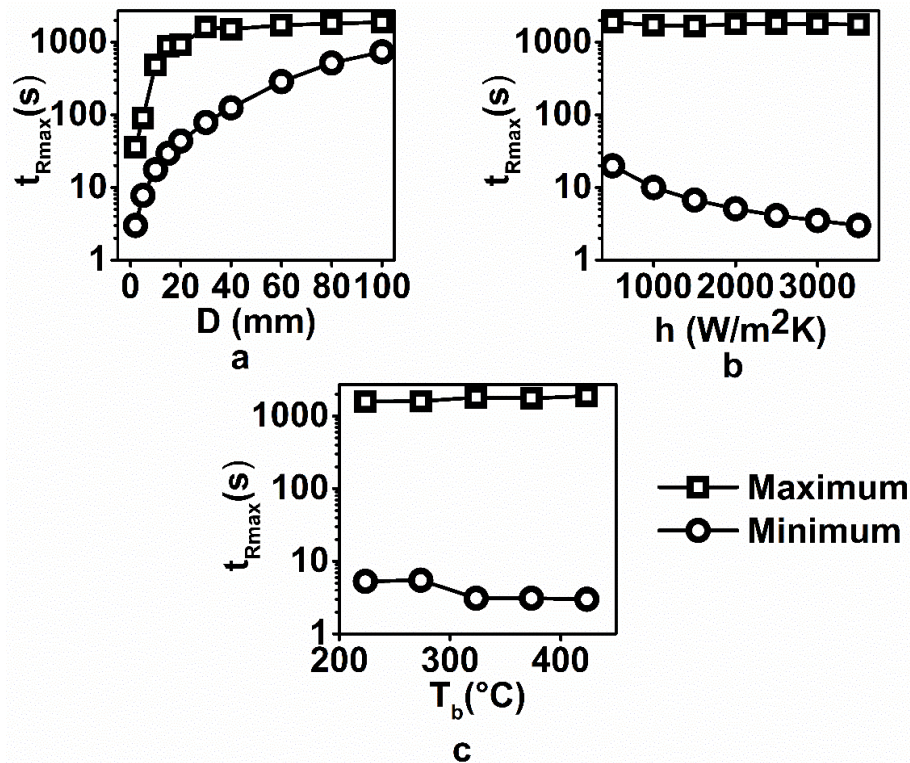


Figure 7.32: Variation of maximum residence time with a) diameter of steel cylinder b) heat transfer coefficient c) bath temperature

7.6.2 Artificial neural network model for predicting hardness distribution in AISI 4140 steel cylinder

Artificial neural network (ANN) is a powerful machine learning algorithm which is inspired by biological neuronal networks in animal brains. Neural network toolbox in MATLAB was used to model the hardness in the AISI 4140 steel cylinder during martempering. Figure 7.33 shows the architecture of artificial neural network model used to predict hardness distribution in martempered AISI 4140 steel cylinders

As described in section 6.4 , 2,100 simulation experiments were performed for AISI 4140 steel cylinders by varying diameter, heat transfer coefficient, bath temperature and residence time fractions. The hardness values were extracted at various radial locations in the cylinder of radius r_o . These locations were defined by the dimensionless radial location (r/r_o). The hardness values were extracted at 11 equally spaced radial locations between centre ($r/r_o=0$) and surface ($r/r_o=1$) for each simulation experiment

with incremental steps of 0.1. The total number of input/output data set available for training neural network model was thus 23,400 (2,100 simulation experiments \times 11 radial locations).

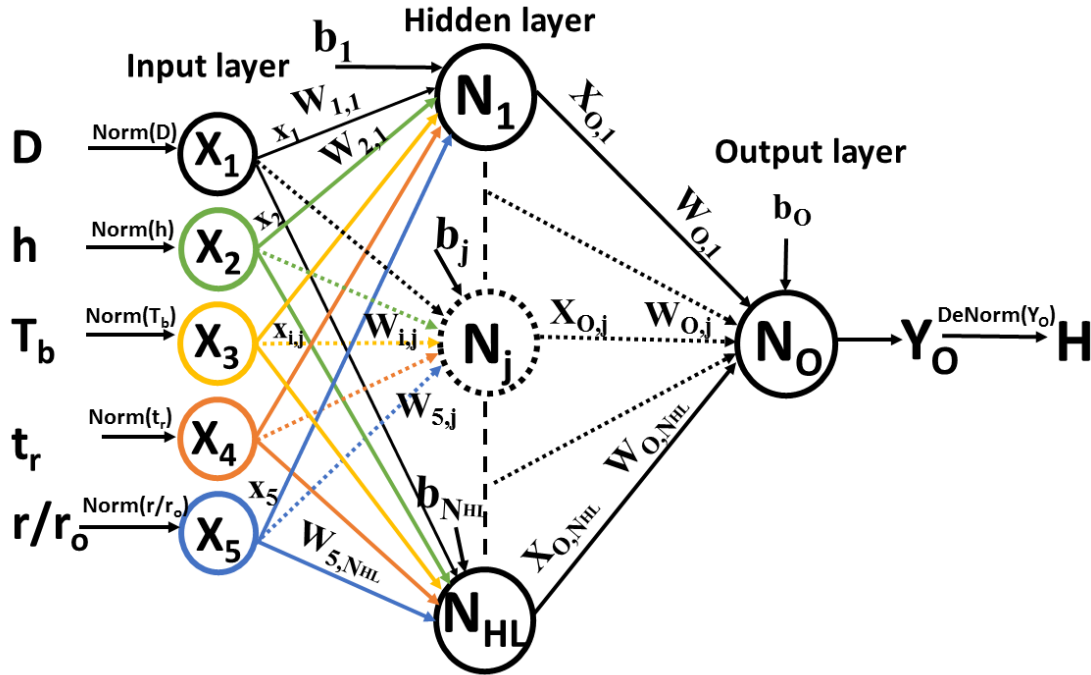


Figure 7.33: Architecture of artificial neural network model used to predict hardness distribution in martempered AISI 4140 steel cylinders

A single hidden layer neural network architecture shown in Figure 7.33 was used to model hardness distribution in martempered AISI 4140 steel cylinders. The neural network consists of 3 layers namely input, hidden and output layers. Equation 7.12 shows the scheme adapted to calculate the weighted summation of normalized input (x_i) for each neuron (N_j) in the hidden layer. $W_{i,j}$ and b_j corresponds to weight and bias for i^{th} input variable and j^{th} hidden layer neuron respectively. z_j is the input to the hidden layer.

$$z_j = b_j + \sum_{i=1}^5 (W_{i,j} x_i) \quad (7.12)$$

The output from the hidden layer $X_{0,j}$ was calculated by applying tan sigmoidal activation function on z_j in Matalab algorithm as shown in Equation 7.13.

$$X_{0,j} = \frac{e^{z_j} - e^{-z_j}}{e^{z_j} + e^{-z_j}} \quad (7.13)$$

A linear activation function was applied on the weighted sum of $x_{o,j}$ in the output layer to calculate the output Y_o as shown in Equation 7.14. The output of the ANN model is the normalized hardness value (Y_o).

$$Y_o = b_o + \sum_{j=1}^{N_{HL}} (W_{o,j} x_{o,i}) \quad (7.14)$$

7.6.2.1 Data pre-processing

There is a large difference between the magnitude of different input/output variables used in the ANN model. For instance, h varies between 3500 and 500 whereas D varies between 2 and 100. In order to avoid the adverse effects of magnitude on convergence of network parameters, the input and output variable were normalized and scaled between 0 and 1. The maximum and minimum values of input and output variables used for normalization are shown in Table 7.3. Equation 7.15 shows the formula used to normalize the values of D , h , T_b , t_r ($f \times t_{Rmax}$) r/r_o and H .

$$X_{Norm} = \frac{(X_{Norm} - X_{Min})}{(X_{Max} - X_{Min})} \quad (7.15)$$

Normalization of input and output data is a very important step in training neural network. However for the prediction of hardness, normalized output data, Y_o needs to be denormalized. Equation 7.16 shows the formula used to calculate the hardness value from the normalized output from ANN model.

$$X = X_{Norm}(X_{Max} - X_{Min}) + X_{Min} \quad (7.16)$$

Table 7.3: Parameters used to normalize inputs and outputs of ANN model

	D (mm)	h (W/m²K)	T_b (°C)	t_r (s)	r/r_o	H (HRC)
X_{Min}	2	500	223.6	1.5	0	12.82
X_{Max}	100	3500	423.6	1887.4	1	57.86

7.6.2.2 Training and validation of ANN model

Training a neural network involves calculation of weights ($W_{i,j}$ and $W_{o,j}$) and biases (b_j and b_o) by minimizing the error in output the output variable. Matlab uses Levenberg–Marquardt algorithm to minimize the error of the output variable and calculate weights and biases.

In order to avoid overfitting, 70% of total data set was randomly selected to train the neural network. The balance 30% of total data was equally divided and used to validate and test the neural network model.

Numbers of neurons in the hidden layer (N_{HL}) is an important parameter which defines the architecture of an ANN model. Equation 7.17 shows the procedure adapted to calculate the mean square error (MSE). Mean square error was calculated by using whole data set consisting 23400 input/output data set.

$$MSE = \frac{1}{n} \sum_{i=1}^n (H_{Sim} - H_{ANN})^2 \quad n = 23400 \quad (7.17)$$

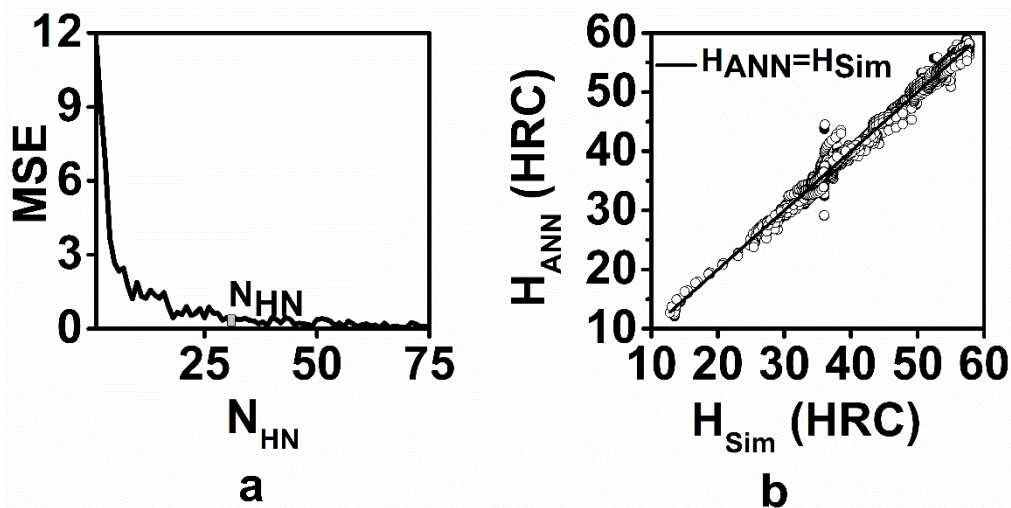


Figure 7.34: a) Variation of standard error with number of neurons in the hidden layer b) Error plot for $N_{HL}=43$

As shown in Figure 7.34a, the mean square error decreased with the number of neurons in hidden layer. Beyond 30 neurons in hidden layers, there is no significant reduction in the mean square error with further increase in number of neurons in hidden layer.

A single hidden layer neural network with 30 neurons was thus used to model the hardness distribution in AISI 4140 cylinders during martempering. Figure 7.34b shows the error between, hardness values over the entire range. The hardness values predicted by ANN model was in fair agreement with hardness values from simulation experiment.

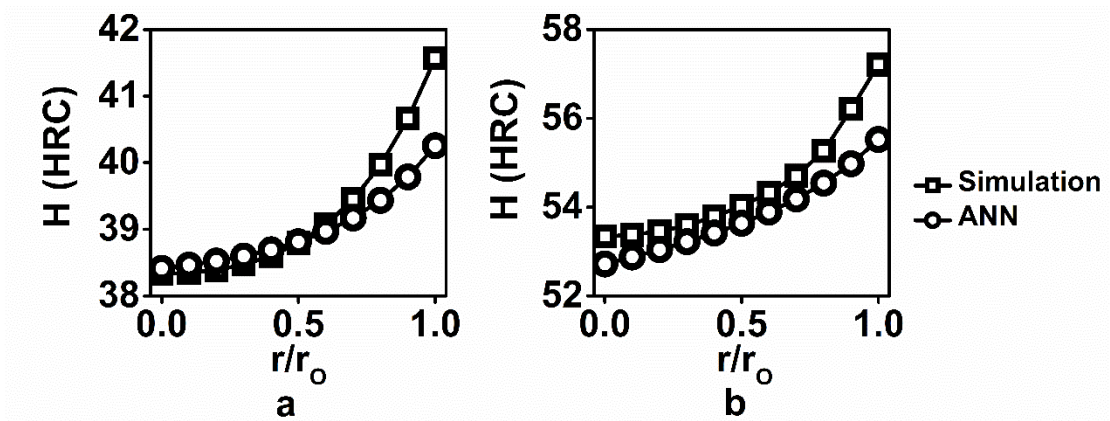


Figure 7.35: Distribution of hardness predicted by simulation experiment and ANN model in AISI 4140 cylinder of a) 80mm diameter and $h=1000\text{W/m}^2\text{K}$ $T_b=373.6^\circ\text{C}$ and $f=0.99$ b) 100mm diameter and $h=3000\text{W/m}^2\text{K}$ $T_b=273.6^\circ\text{C}$ and $f=0.5$

Figure 7.35 shows the hardness distribution in AISI 4140 steel cylinders as predicted using simulation experiment and ANN model. The process variables leading to hardness distribution in Figure 7.35a and Figure 7.35b were chosen to demonstrate the accuracy of hardness prediction in low and high average hardness regimes respectively.

7.6.3 Relative importance of input variables

Appendix D presents values of all weights and biases of the suggested neural network model. Equation 7.18 shows the procedure suggested by Ibrahim (Ibrahim 2013) to calculate relative importance (RI) of input variables based on the connection weights in the neural network. Table 7.4 shows the relative importance of parameters calculated for all input variables neural network model.

$$RI_i = \frac{\sum_{j=1}^{N_{HL}} |W_{i,j} W_{o,j}|}{\sum_{i=1}^5 (\sum_{j=1}^{N_{HL}} |W_{i,j} W_{o,j}|)} \quad (7.18)$$

Table 7.4: Relative importance parameter calculated for input variables of neural network model.

Inputs	D	h	T_b	t_r	r/r_o
Relative importance (RI _i)	8.989	4.640	9.613	6.190	0.568

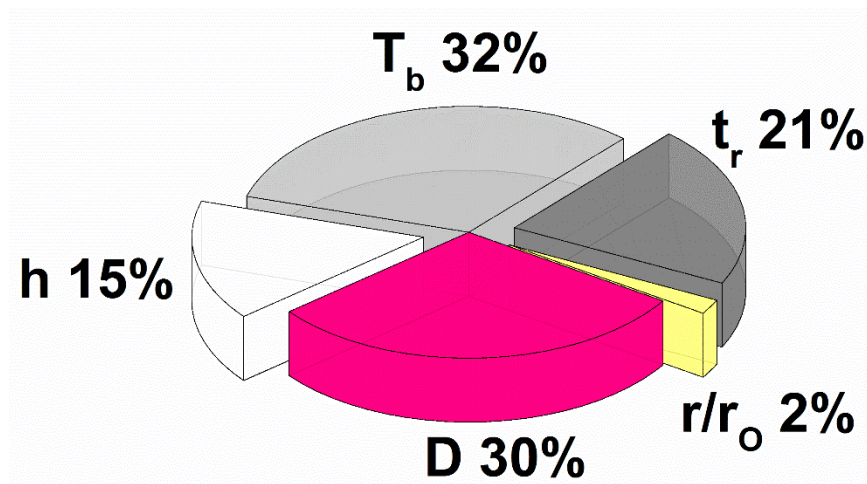


Figure 7.36: Pie chart showing percentage of relative importance input variables

From Figure 7.36, it is clear that bath temperature and diameter are the most important input variables followed by the residence time and heat transfer coefficient. Dimensionless radial position was the least important input variable in the neural network model. The relative importance of input variables should be analysed in conjunction with the observation from figures in Appendix C. Increase in bath temperature, diameter and residence time results in decrease in hardness whereas, increase in heat transfer coefficient results in increase of average hardness in martempered AISI 4140 cylinders. Also from Figure 7.35a and Figure 7.35b, it was observed that hardness increased with increase in r/r_o .

Chapter 8 CONCLUSIONS

The following are the conclusions based on the investigation of high temperature quench media for industrial heat treatment.

1. Comparison of cooling performance of hot oil and molten salt media

- 1.1. The heat extraction mechanism in hot oil was similar to conventional vaporizable quench media and occurred in three stages, namely, vapor blanket, nucleate boiling and convective cooling stages. However, the heat extraction mechanism in molten $\text{KNO}_3\text{-NaNO}_2\text{-NaNO}_3$ eutectic mixture was observed to occur only in boiling and convective cooling stages.
- 1.2. The magnitude of heat extraction rate was significantly higher in the case of molten salt media and q_{\max} was ~85% higher as compared to hot oil medium.
- 1.3. Molten salt medium offered more uniform cooling as compared to hot oil medium.
- 1.4. The non-uniformity in surface temperature during boiling stage in Inconel probe was 10 times lower in molten salt medium as compared to that in hot oil medium. However, the non-uniformity in surface temperature during the convective cooling stage in both the media were comparable.
- 1.5. Higher and uniform hardness distribution is predicted in steel parts quenched in molten salt as compared to those quenched in hot oil

2. Effect of bath temperature on the cooling performance of eutectic $\text{KNO}_3\text{-NaNO}_3$ mixture

- 2.1. Linear regression models to predict q_{\max} , T_{\max} , q_{Conv} , T_{Conv} and maximum t_{85} for a given bath temperature in molten 55N salt has been proposed
- 2.2. T_{\max} , T_{Conv} and maximum t_{85} increased with increase in bath temperature where as q_{\max} and q_{Conv} , decreased with increase in bath temperature.
- 2.3. t_{85} parameter suggested lower hardness and improved hardness distribution for steel parts quenched in 55N medium with increase in bath temperature.

3. Compositional and bath temperature effects on heat transfer during quenching in molten NaNO_3 – KNO_3 salt mixtures

- 3.1. Contour plots showing the variation of q_{\max} , T_{\max} , q_{conv} and T_{conv} to predict the cooling performance of molten NaNO_3 - KNO_3 molten salt mixtures at different bath temperature were constructed. The contour plots serve as the basis for predicting the variation of average hardness in the AISI 4140 probe.
- 3.2. The degree of uniformity of cooling of the Inconel probe increased with decrease in KNO_3 concentration in the quenching medium.
- 3.3. During quench boiling, the heat extraction occurs primarily by endothermic decomposition of nitrates to nitrites
- 3.4. The equilibrium concentration of nitrites in nitrate-nitrite mixtures increases with bath temperature. This reduces heat transfer during boiling stage at higher bath temperature.
- 3.5. The increase of concentration of nitrites near the quench probe surface in the course of boiling stage decreases the rate of decomposition of nitrates.
- 3.6. The convective cooling stage starts when the heat supplied by the probe becomes insufficient for decomposition of nitrates in the presence of high nitrite concentration barrier near the probe surface.

4. Cooling performance of molten KNO_3 - LiNO_3 - NaNO_3 eutectic mixture

- 4.1. During quenching of Inconel probe, LiNO_3 eutectic mixture maintained at 150°C , offered higher cooling rate. However, NaNO_2 eutectic mixture maintained at 200°C , 250°C and 300°C bath temperatures offered higher cooling rates.
- 4.2. Inconel probe quenched in NaNO_2 eutectic mixture maintained at 200°C , 250°C and 300°C is cooled more uniformly
- 4.3. Hardness measured in steel probes quenched in LiNO_3 eutectic mixture maintained at 150°C and 200°C were higher as compared to that obtained with NaNO_2 eutectic mixture. For higher bath temperatures, hardness values were found to be comparable.
- 4.4. The analysis based on Inconel heat flux parameters and the hardness values measured in quenched steel probe were found to be contradictory. However, the wettability study on steel indicated improved spreading and early dilation of

LiNO₃ eutectic droplet leading to an extended boiling stage resulting in higher hardness values.

5. Hot neem oil as alternative to hot mineral oils for martempering

5.1. Neem oil offered higher cooling rates and cooled the Inconel probe more uniformly as compared to hot oil.

5.2. Quenching in neem oil resulted in higher hardness for AISI-52100 steel probes as compared to that obtained with quenched in hot oil.

5.3. Pearlite in microstructure of AISI-52100 steel probe quenched in hot oil maintained at 200°C negates the purpose of hardening. Hot oil is thus unsuitable as quench medium at this bath temperature.

5.4. The effect of oxidation on viscosity of neem oil is more pronounced compared to that of hot oil. The effect of oxidation on the viscosity of neem oil stabilized after 24 hours of oxidation.

5.5. Oxidation of neem oil resulted in vapor blanket stage and decreased T_{max} and cooling rate at higher temperatures.

5.6. Peak cooling rate and cooling rate at lower temperatures was higher in the case of oxidized neem oil.

5.7. Oxidation had a very limited effect on the cooling performance hot neem oil quench medium and can be considered as an effective replacement for hot oil.

6. Simulation of the effect of heat transfer coefficient, bath temperature and section thickness on hardness of martempered of AISI 4140 steel

6.1. Increase in bath temperature, diameter and residence time results in decrease in hardness whereas, increase in heat transfer coefficient results in increase of average hardness in martempered AISI 4140 cylinders.

6.2. Artificial neural network model was trained to predict hardness distribution in martempered AISI 4140 steel cylinders.

6.3. The weights of neural network were used to calculate the relative importance parameter for each input variable. The ability of input variables to influence the hardness is arranged in the following increasing order: $T_b > D > t_r > h > r/r_0$

6.4. The proposed model for prediction of hardness considers the effects of bath temperature, part diameter, residence time along with heat transfer coefficient.

REFERENCES

- A guide to the safe use of molten salt baths.* (1996). Park Thermal International corp., Buffalo, New York, USA.
- ASM Handbook Committee. (1998). *ASM hand book volume 4 heat treating.* ASM International.
- Babu, K., and Prasanna Kumar, T. S. (2012). “Optimum CNT Concentration and Bath Temperature for Maximum Heat Transfer Rate during Quenching in CNT Nanofluids.” *J. ASTM Int.*, 9(5), 104442.
- Bartholemew, R. F. (1966). “A Study of the Equilibrium $\text{KNO}_3(\text{l}) \rightleftharpoons \text{KNO}_2(\text{l}) + 1/2\text{O}_2(\text{g})$ over the Temperature Range 550-750°.” *J. Phys. Chem.*, 70, 3442.
- Bates, C. E., Totten, G. E., and Brennan, R. L. (1991). “Quenching.” *ASM Handb. Vol. 4 Heat Treat.*, ASM Handbook Committee, ed., ASM International.
- Bauer, T., Breidenbach, N., and Eck, M. (2012). “Overview of Molten Salt Storage Systems and Material Development for Solar Thermal Power Plants.” *World Renew. Energy Forum 2012*, 1–8.
- Bauer, T., Pflieger, N., Doerte laing, Wolf-dieter steinmann, Eck, M., and Kaesche, S. (2013). “High temperature molten salts for solar power application.” *Molten Salts Chem. From Lab to Appl.*, F. Lantelme and H. Groult, eds., Elsevier Science, 415–438.
- Boyer, H. E., and Cary, P. R. (1988). *quenching and distortion control.* ASM International.
- Bradshaw, R. ., and Meeker, D. . (1990). “High Temp Stability of Ternary Nitrate Molten Salts for Solar Thermal Energy Systems.” *Sol. Energy Mater.*, 21, 51–60.
- Bradshaw, R. W., Cordaro, J. G., and Siegel, N. P. (2009). “Molten Nitrate Salt Development for Thermal Energy Storage in Parabolic Trough Solar Power Systems.” *3rd Int. Conf. Energy Sustain.*, San Francisco: ASME, 615–624.
- Canale, L. de C. F., Fernandes, M. R., Agostinho, S. C. M., Totten, G. E., and Farah, A. F. (2005). “Oxidation of vegetable oils and its impact on quenching performance.” *Int. J. Mater. Prod. Technol.*, 24(1/2/3/4), 101.
- Dean, S. W., Prabhu, K. N., and Fernandes, P. (2009). “Heat Transfer During

- Quenching and Assessment of Quench Severity—A Review.” *J. ASTM Int.*, 6(1), 101784.
- Delano, M. A., and Sype, J. Van Den. (1988). “Fluid Bed Quenching of Steels: Applications Are Widening.” *Heat Treat.*, 1–4.
- Dexter, G. W. (n.d.). “Hardening high speed steels: Metallurgical benefits of salts.” <<http://www.ppunch.com/wp-content/uploads/2015/05/heat1.pdf>> (Aug. 30, 2017).
- Doheim, M. A., and Himmo, R. M. (1988). “Effect of Fluidized Bed Parameters on Quenching of Steel Sections.” *Mater. Sci. Technol.*, 4, 371–376.
- Dubal, G. P. (1999). “Salt bath quenching.” *Adv. Mater. Process.*
- Elmi Hosseini, S. R., Zabett, A., and Li, Z. (2015). “Cooling Curve Analysis of Heat Treating Oils and Correlation With Hardness and Microstructure of a Low Carbon Steel.” *Mater. Perform. Charact.*, 3(4), 20130067.
- Felde, I., and Szénási, S. (2016). “Estimation of temporospatial boundary conditions using a particle swarm optimisation technique.” *Int. J. Microstruct. Mater. Prop.*, 11(3/4), 288.
- Fernandes, P., and Prabhu, K. N. (2007). “Effect of section size and agitation on heat transfer during quenching of AISI 1040 steel.” *J. Mater. Process. Technol.*, 183(1), 1–5.
- Fernandes, P., and Prabhu, K. N. (2008). “Comparative study of heat transfer and wetting behaviour of conventional and bioquenchant for industrial heat treatment.” *Int. J. Heat Mass Transf.*, 51(3–4), 526–538.
- Fox, N. J., and Stachowiak, G. W. (2007). “Vegetable oil-based lubricants-A review of oxidation.” *Tribol. Int.*, 40(7), 1035–1046.
- Hassan, S. B., J.B, A., Aigbodion, V. S., and Williams, E. J. (2011). “Hardening Characteristics of Plain Carbon Steel and Ductile Cast Iron Using Neem Oil as Quenchant.” *Journal Miner. Mater. Charact. Eng.*, 10(2), 161–172.
- Hilder, N. A. (1988). “The behaviour of polymer quenchant.” Aston University.
- Ibrahim, O. M. (2013). “A comparison of methods for assessing the relative importance

- of input variables in artificial neural networks.” *J. Appl. Sci. Res.*, 9(11), 5692–5700.
- Kasuya, T., and Hashiba, H. (2007). *Carbon equivalent to assess hardenability of steel and prediction of HAZ hardness distribution*.
- Kothandaraman, C. P., and Subramayan, S. (2010). *Heat and mass transfer data book*. New Age International publishers.
- Liščić, B., and Singer, S. (2014). *Calculation of the Heat Transfer Coefficient Based on Experiments by the Liscic Probes. Compr. Mater. Process*.
- Lisicic, B., Tensi, H. M., and Canale, L. C. . (Eds.). (2010). *Quenching Theory and Technology*.
- MacKenzie, D. S. (2003). “Advances in Quenching.” *Proc. 22nd Heat Treat. Soc. Conf. 2nd Int. Surf. Eng. Congr.*, (Stage C), 228–239.
- Mathews, N. G., Pranesh, R. K. M., Nayak, U. V., and Prabhu, K. N. (2019). “Comparison of Cooling Behaviour of Carbon Steels in Polymer, Oil and Carbonated Quench Media.” *Trans. Indian Inst. Met.*, 1–4.
- Mehrkam, Q. D. (1967). “An Introduction To Salt Bath Heat Treating.” *Tool. Prod. Mag. Repr. N° 182, Ajax Electr. company, Philadelphia, USA*.
- Narazaki, M., Totten, G. E., and Webster, G. M. (2002). “Hardening by reheating and quenching.” *Handb. residual Stress Deform. steel*, G. E. Totten, M. Howes, and T. Inoue, eds., ASM International, 248–295.
- Nayak, U. V., and Prabhu, K. N. (2015). “Heat transfer during immersion quenching in MWCNT nanofluids.” *Mater. Sci. forum*, 172–176.
- Nayak, U. V., and Prabhu, K. N. (2016a). “Heat transfer and quench performance of aqueous CuO nanofluids during immersion quenching.” *Int. J. Microstruct. Mater. Prop.*, 11, 186–202.
- Nayak, U. V., and Prabhu, K. N. (2016b). “Wetting Behavior and Heat Transfer of Aqueous Graphene Nanofluids.” *J. Mater. Eng. Perform.*, 25(4), 1474–1480.
- Nayak, U. V., and Prabhu, K. N. (2018). “Heat Transfer during Quenching of Inconel Probe in Non-Edible Vegetable Oils Wärmeübertragung während des Abschreckens

der Inconel-Sonde in nicht essbaren Pflanzenölen.” *Heat Treat. Mater.*, 73(5), 283–291.

Nayak, U. V., Pranesh, R. K. M., Pai, M. A., and Prabhu, K. N. (2016). “Carbonated aqueous media for quench heat treatment of steels.” *J. Mater. Eng. Perform.*, (Ref 6).

Ozisik, M. N., and Orlande, H. R. B. (2000). “Techniques for solving inverse heat transfer problems.” *Inverse heat Transf. Fundam. Appl.*, 35–114.

Pai, A., Nayak, U. V., Pranesh, R. K. M., and Prabhu, K. N. (2015). “Wetting Kinetics and Cooling Performance of PAG Polymer Quenchants.” *Mater. Sci. forum*, 156–159.

Prabhu, K. N., Fernades, P., and Kumar, G. (2009). “Effect of substrate surface roughness on wetting behaviour of vegetable oils.” *Mater. Des.*, 30(2), 297–305.

Prabhu, N. K., U, V. N., and Rao, K. M. P. (2016). “Polymer quenchants for Industrial Heat Treatment.” *Adv. Polym. Mater. Technol.*, A. Srinivasan and S. Bandyopadhyay, eds., CRC Press.

Pranesh Rao, K. M., and Prabhu, K. N. (2015). “Assessment of Wetting Kinematics and Cooling Performance of Select Vegetable Oils and Mineral-Vegetable Oil Blend Quench Media.” *Mater. Sci. Forum*, 830–831, 160–163.

R.W. Foreman. (1993). “New Developments in Salt Bath Quenching.” *Ind. Heat.*, 60(3), 41–47.

Ramesh, G., and Prabhu, K. N. (2011). “Review of thermo-physical properties , wetting and heat transfer characteristics of nanofluids and their applicability in industrial quench heat treatment.” 1–15.

Ramesh, G., and Prabhu, K. N. (2012). “Cooling Characteristics of Liquid Quenchants for Heat Treatment of Castings.” *indian foundary J.*, 58(12), 23–29.

Ramesh, G., and Prabhu, K. N. (2013a). “The Effect of Addition of Copper Nanoparticles on Wetting Behaviour of Water During Immersion Quenching.” *Trans. Indian Inst. Met.*, 66(August), 375–379.

Ramesh, G., and Prabhu, K. N. (2013b). “Wetting kinematics and spreading behaviour of water based aluminium nanofluids during immersion quenching.” *Int. heat Treat. surafce Eng.*, 7(2).

Ramesh, G., and Prabhu, K. N. (2014a). “Wetting and Cooling Performance of Mineral Oils for Quench Heat Treatment of Steels.” *ISIJ Int.*, 54(6), 1426–1435.

Ramesh, G., and Prabhu, K. N. (2014b). “Comparative Study of Wetting and Cooling Performance of Polymer – Salt Hybrid Quench Medium With Conventional.” *Exp. Heat Transf.*, 28(May 2014), 464–492.

Ramesh, G., and Prabhu, K. N. (2014c). “Wetting kinetics , kinematics and heat transfer characteristics of pongamia pinnata vegetable oil for industrial heat treatment.” *Appl. Therm. Eng.*, 65(1–2), 433–446.

Ramesh, G., and Prabhu, N. K. (2014d). “Spatial Dependence of Heat Flux Transients and Wetting Behaviour During Immersion Quenching of Inconel 600 Probe in Brine and Polymer Media.” *Metall. Mater. Trans. B*, 45(4), 1355–1369.

Rassizadehghani, J., Raygan, S., and Askari, M. (2006). “Comparison of the quenching capacities of hot salt and oil baths.” *Met. Sci. Heat Treat.*, 48(5), 193–198.

Raygan, S., Rassizadehghani, J., and Askari, M. (2009). “Comparison of Microstructure and Surface Properties of AISI 1045 Steel After Quenching in Hot Alkaline Salt Bath and Oil.” *J. Mater. Eng. Perform.*, 18, 168–173.

Reid, B. (1996). *Heat Treating In Molten Salt*. Park Thermal International corp. Buffalo, New York, USA.

Rowland, E., and MacKenzie, D. S. (2018). “Proper Care of Quench Oil Leading to Consistent Part Quality.” *Therm. Process. Motion*, ASM International, 98–105.

Salawa, F., Napierala, R., and Suarez, C. (n.d.). *Best Practices for the Application of Quenching Oils*.

Sidney.H. Avner. (1997). *Introduction to physical metallurgy*. Tata McGraw-Hill; New Delhi; India.

Şimşir, C., and Gür, C. H. (2008a). “A FEM based framework for simulation of thermal treatments: Application to steel quenching.” *Comput. Mater. Sci.*, 44, 588–600.

Şimşir, C., and Gür, C. H. (2008b). “3D FEM simulation of steel quenching and investigation of the effect of asymmetric geometry on residual stress distribution.” *J. Mater. Process. Technol.*, 207(1–3), 211–221.

- Smoljan, B. (2006). "Prediction of mechanical properties and microstructure distribution of quenched and tempered steel shaft." *J. Mater. Process. Technol.*, 175(1–3), 393–397.
- Souza, E. C. de, Fernandes, M. R., Augustinho, S. C. M., Canale, L. de C. F., and Totten, G. E. (2009). "Comparison of Structure and Quenching Performance of Vegetable Oils." *J. ASTM Int.*, 6(9), 102188.
- Souza, E. C. de, Friedel, L. F. O., Totten, G. E., and Canale, L. C. F. (2013). "Quenching and Heat Transfer Properties of Aged and Unaged Vegetable Oils." *J. Pet. Sci. Res.*, 2(1), 42–48.
- Stern, K. H. (2001). *High Temperature Properties and Thermal Decomposition of Inorganic Salts with Oxyanions*. CRC Press.
- Stitch, A., and Tensi, H. M. (1990). "Effect of wetting process on cooling behaviour and hardness distribution in immersion cooled work pieces." *VII Int. Congr. heat Treat. Met.*, Moscow, 136–150.
- Sudheer, R., and Prabhu, K. N. (2016). "A Computer Aided Cooling Curve Analysis method to study phase change materials for thermal energy storage applications." *Mater. Des.*, 95, 198–203.
- Torkamani, H., Raygan, S., and Rassizadehghani, J. (2014). "Comparing microstructure and mechanical properties of AISI D2 steel after bright hardening and oil quenching." *Mater. Des.*, 54, 1049–1055.
- Totten, G. E. (2007). *Steel Heat treatment Hand book*. Taylor and Francis Group, New York, USA.
- Totten, G. E., Bates, C. E., and N. A. Clinton (Eds.). (1993). *Handbook of quenchants and quenching technology*. ASM International.
- Totten, G. E., Liščić, B., I, kobasko N., Han, S. W., and SUN, Y. H. (1998). "Advances in polymer quenching technology." <https://www.researchgate.net/publication/267806983_Advances_in_polymer_quenching_technology> (Feb. 17, 2017).
- Totten, G. E., M. Howes, and Inoue, T. (2002). *Handbook of residual stress and*

deformation of steel. ASM International.

Totten, G. E., Tensi, H. M., and Canale, L. de C. F. (2003). “Chemistry of quenching: Part I –fundamental interfacial chemical processes involved in quenching.” *Proc. 22nd Heat Treat. Soc. Conf. 2nd Int. Surf. Eng. Congr.*, ASM International, Indianapolis, USA, 148–154.

Totten, G. E., Tensi, H. M., and Lainer, K. (1999). “Performance of vegetable oils as a cooling medium in comparison to a standard mineral oil.” *J. Mater. Eng. Perform.*, 8(4), 409–416.

Wang, T., Mantha, D., and Reddy, R. G. (2013). “Novel low melting point quaternary eutectic system for solar thermal energy storage.” *Appl. Energy*, 102, 1422–1429.

Webster, H., and Liard, W. j. (1991). *ASM hand book volume 4 heat treatinge*. (ASM Handbook Committee, ed.), ASM International.

APPENDIX A: TIME TEMPERATURE CURVES MEASURED DURING QUENCHING OF INCONEL PROBE

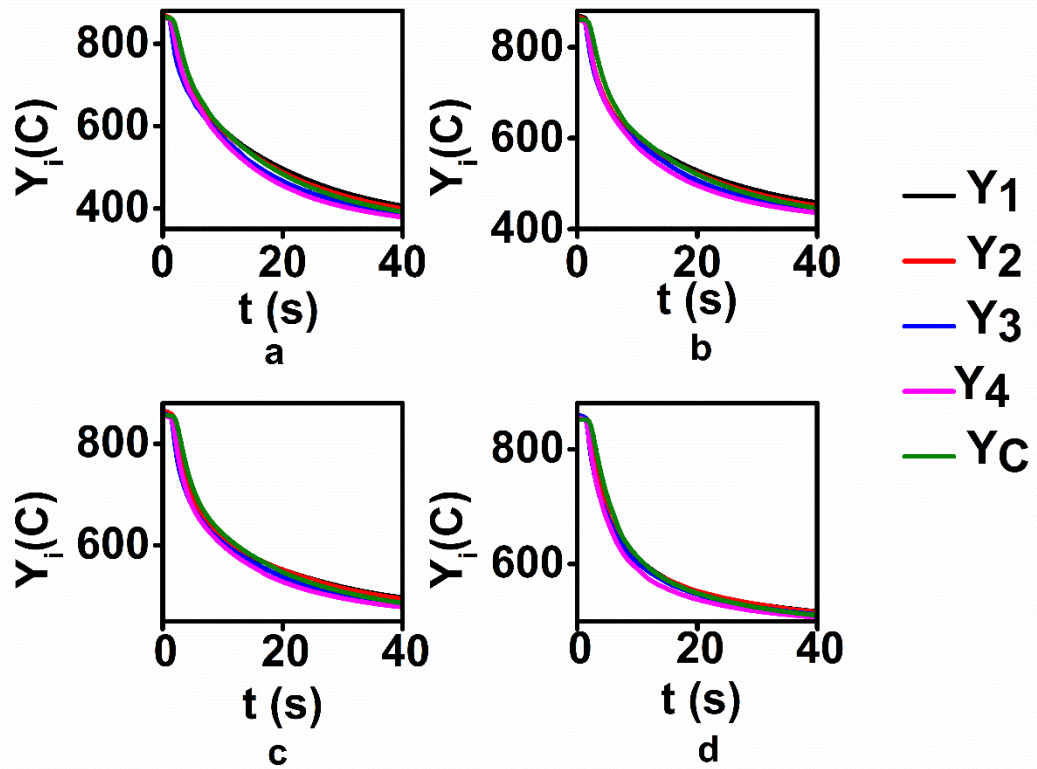


Figure A.1: Time temperature curves measured at different locations in Inconel probe quenched in 0N salt maintained at a)350°C b)400°C c)450°C d)500°C

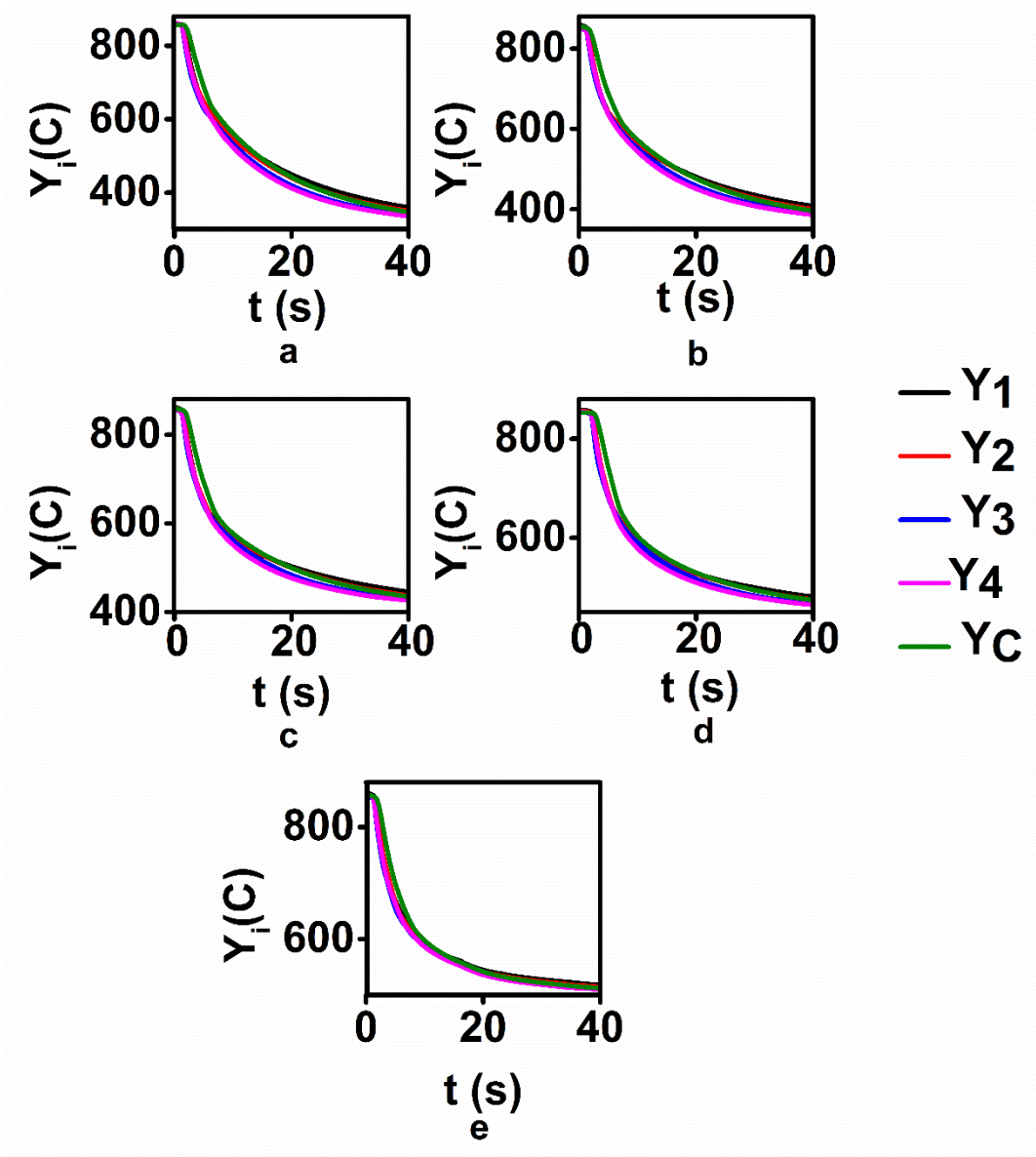


Figure A.2: Time temperature curves measured at different locations in Inconel probe quenched in 25N salt maintained at a)300°C b)350°C c)400°C d)450°C e)500°C

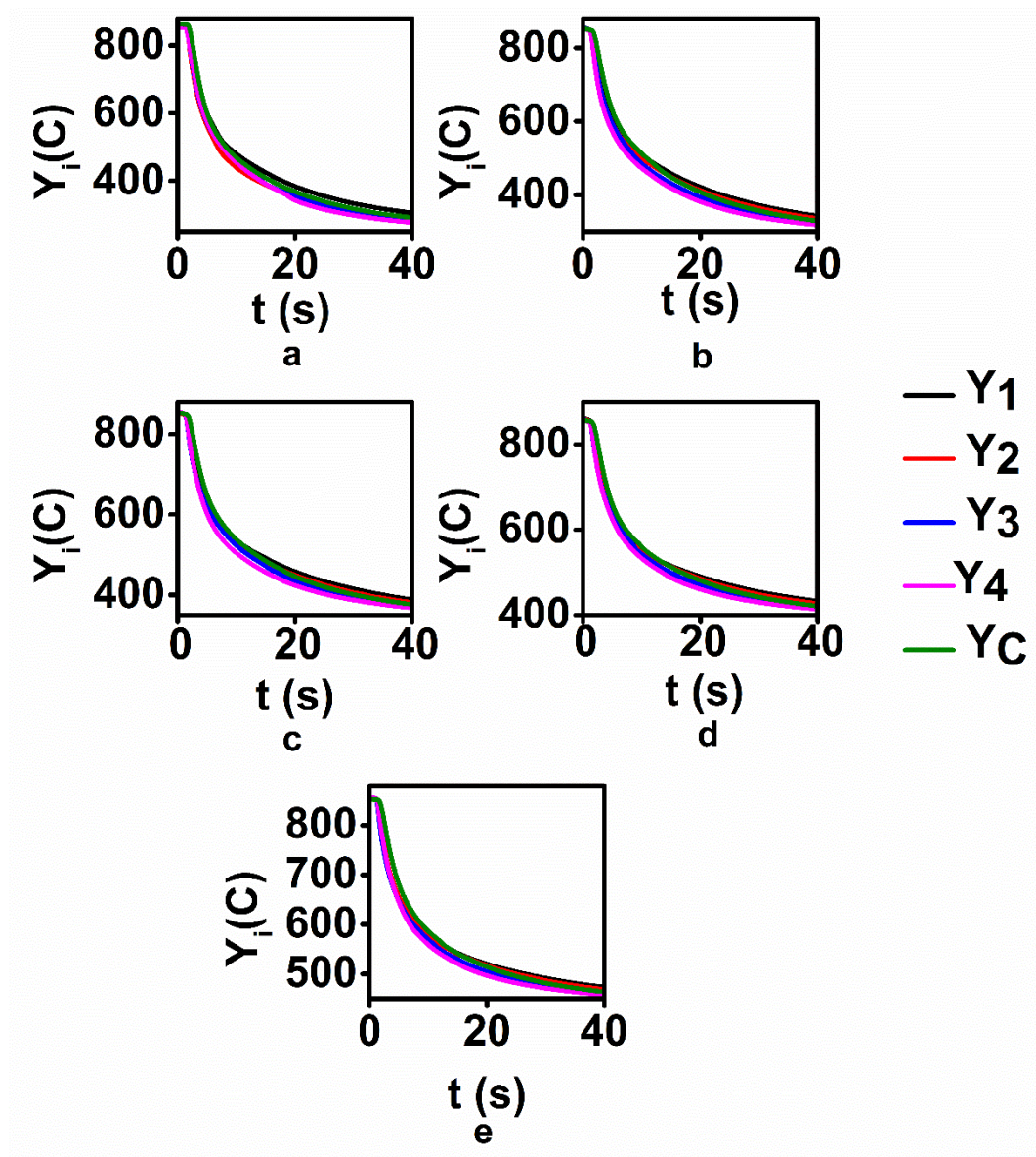


Figure A.3: Time temperature curves measured at different locations in Inconel probe quenched in 45N salt maintained at a)250°C b)300°C c)350°C d)400°C e)450°C

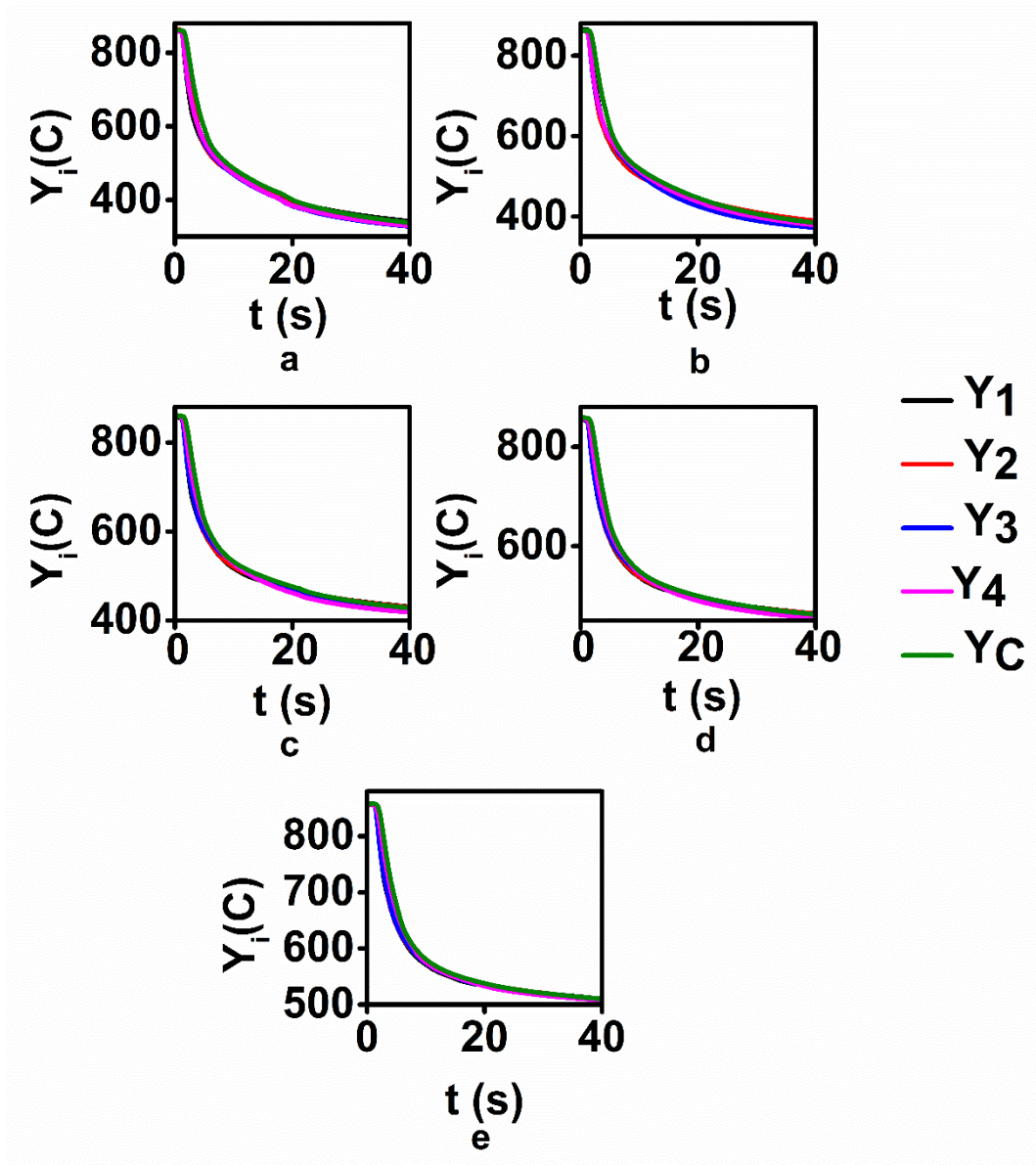


Figure A.4: Time temperature curves measured at different locations in Inconel probe quenched in 75N salt maintained at a)300°C b)350°C c)400°C d)450°C e)500°C

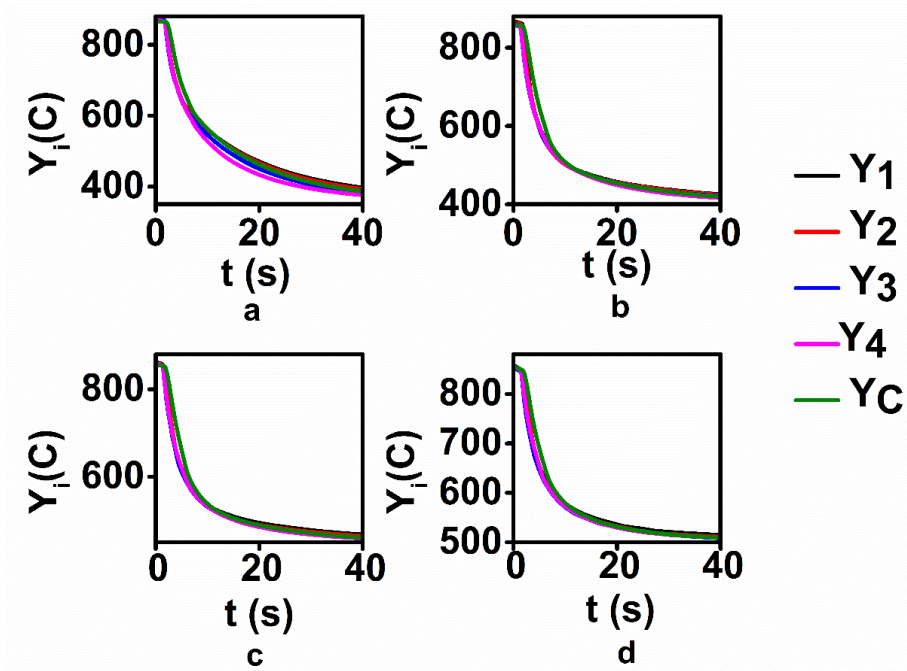


Figure A.5: Time temperature curves measured at different locations in Inconel probe quenched in 100N salt maintained at a)350°C b)400°C c)450°C d)500°C

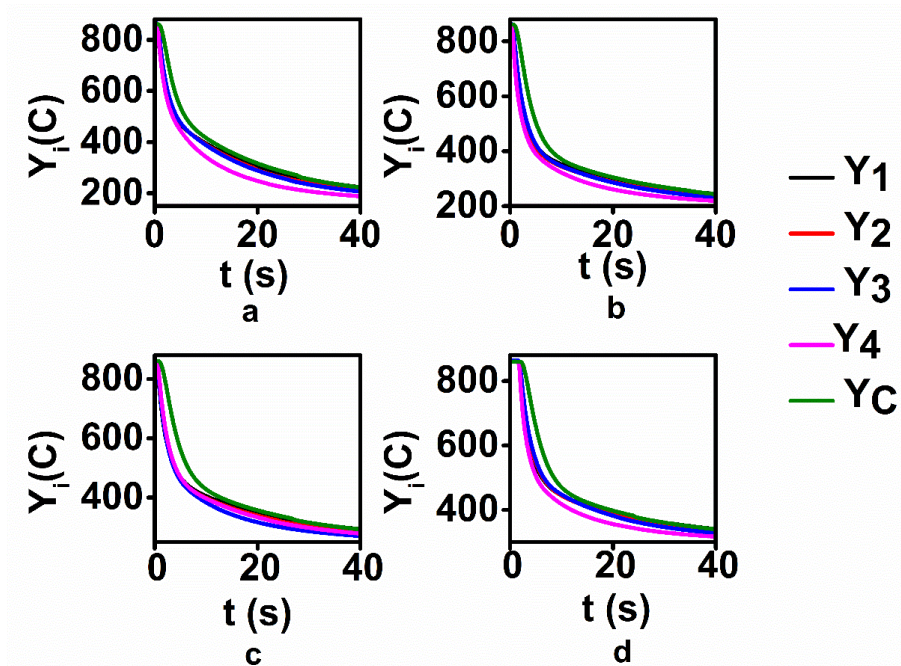


Figure A.6: Time temperature curves measured at different locations in Inconel probe quenched in NaNO₂ eutectic salt mixture maintained at a)150°C b)200°C c)250°C d)300°C

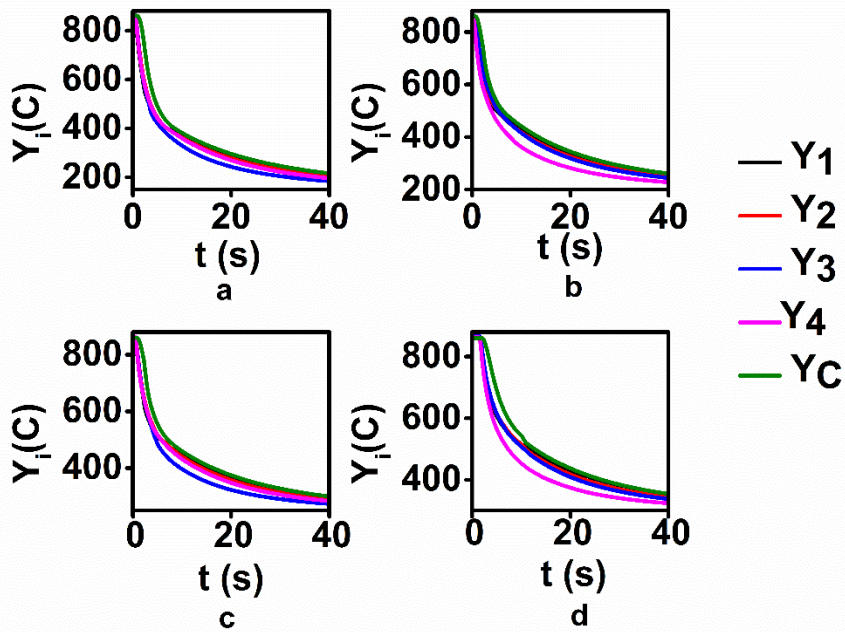


Figure A.7: Time temperature curves measured at different locations in Inconel probe quenched in LiNO₃ eutectic salt mixture maintained at a)150°C b)200°C c)250°C d)300°C

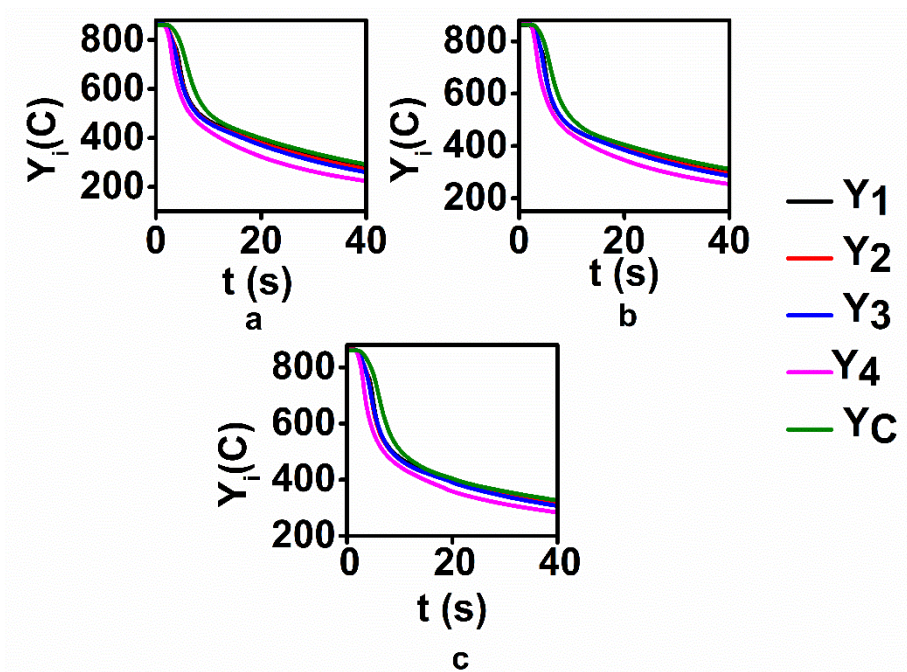


Figure A.8: Time temperature curves measured at different locations in Inconel probe quenched in hot oil maintained at a)100°C b)150°C c)200°C

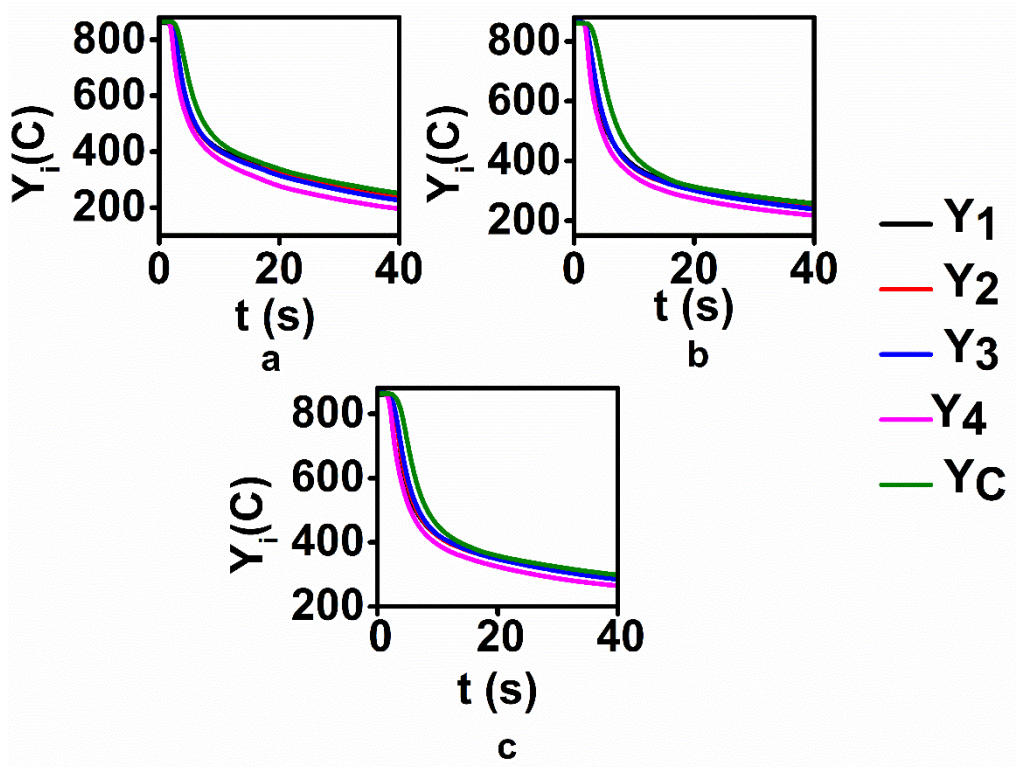


Figure A.9: Time temperature curves measured at different locations in Inconel probe quenched in hot oil maintained at a)100°C b)150°C c)200°C

APPENDIX B: SPATIALLY DEPENDENT TRANSIENT QUENCH HEAT FLUX CALCULATED USING INVERSE METHOD FOR INCONEL PROBE

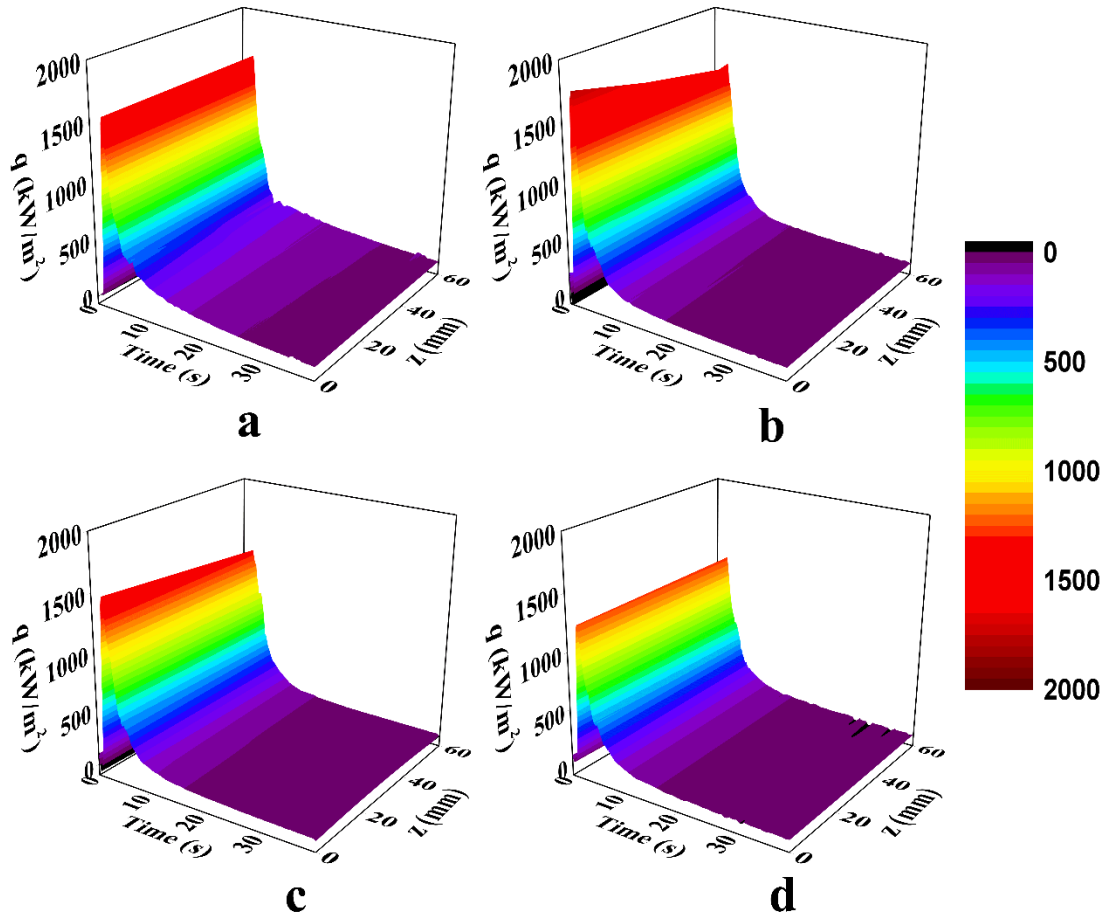


Figure B.1: Spatially dependent transient heat flux for inconel probe quenched in 100N salt mixture maintained at a)350°C b) 400°C c) 450°C d)500°C

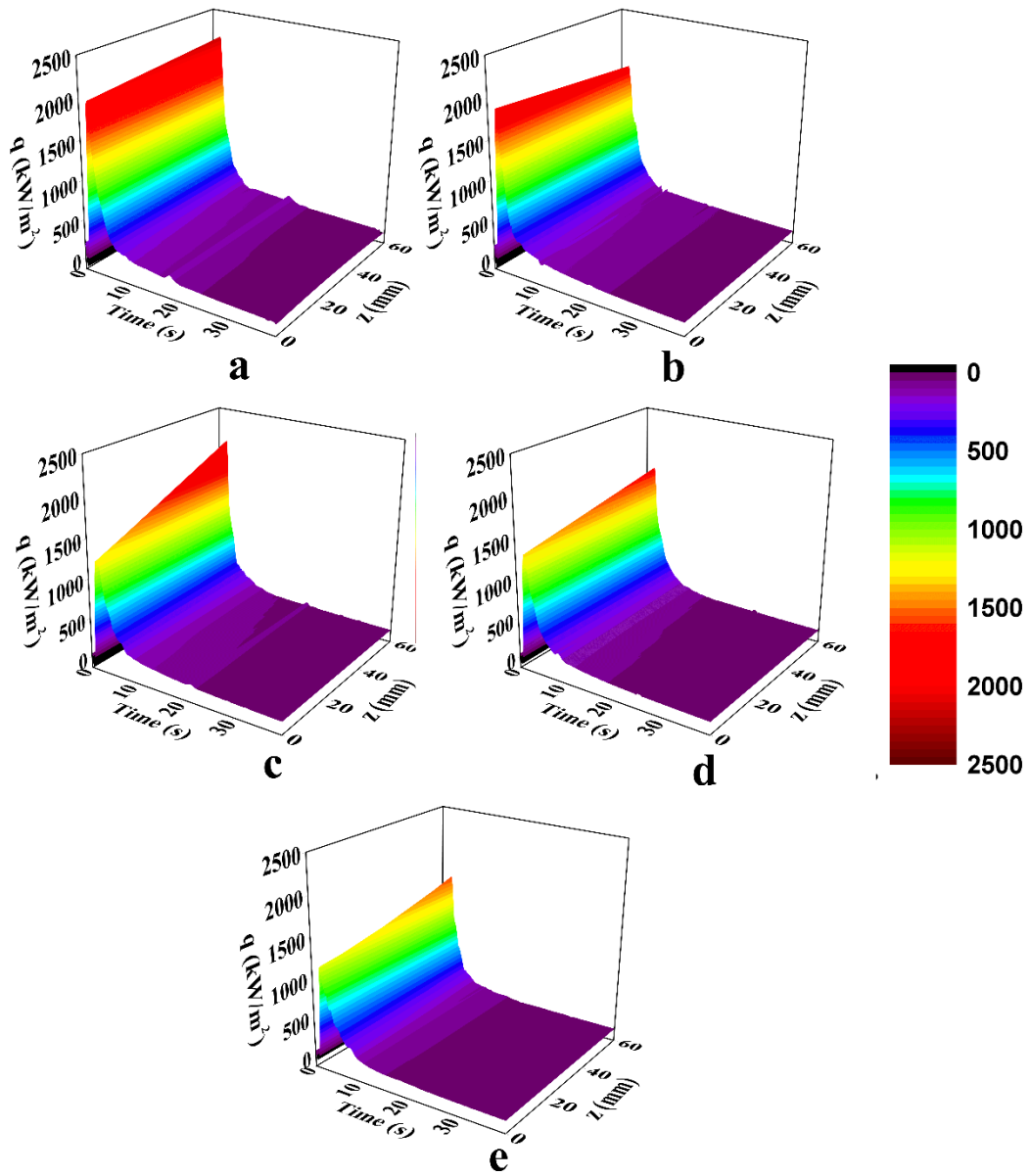


Figure B.2: Spatially dependent transient heat flux for inconel probe quenched in 75N salt mixture maintained at a)300°C b) 350°C c) 400°C d)450°C e) 500°C

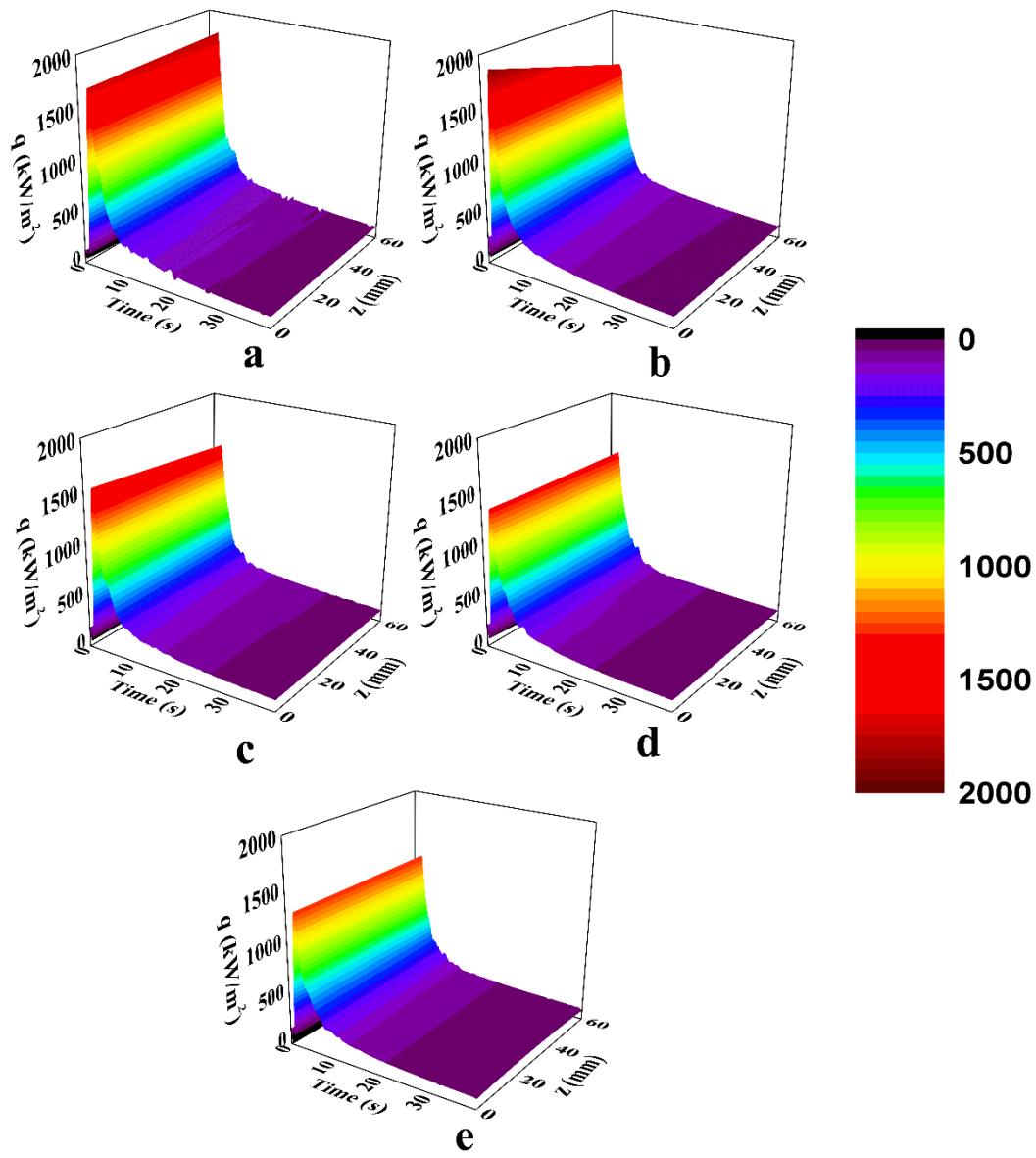


Figure B.3: Spatially dependent transient heat flux for inconel probe quenched in 55N salt mixture maintained at a)250°C b) 300°C c) 350°C d)400°C e)500°C

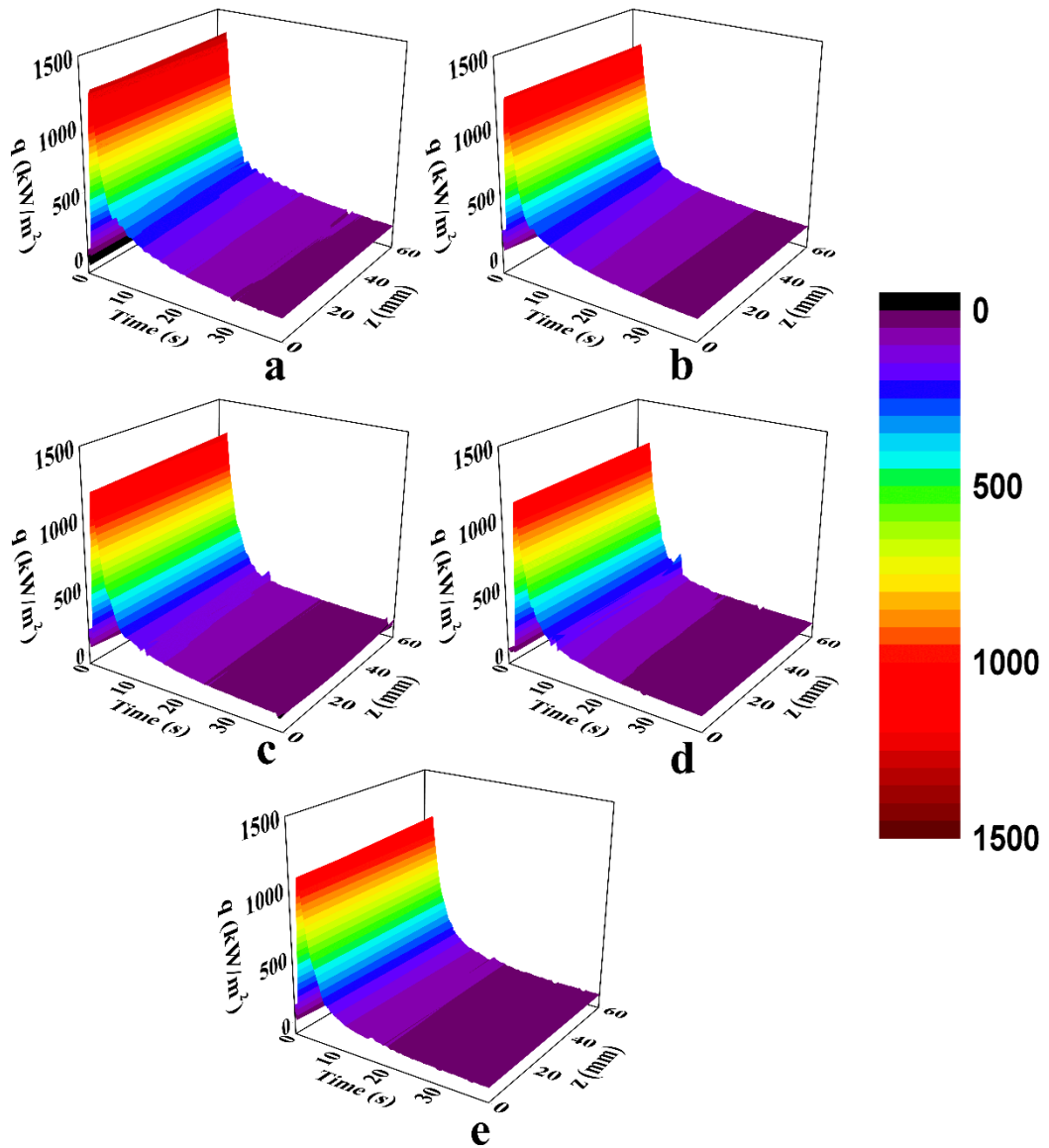


Figure B.4: Spatially dependent transient heat flux for inconel probe quenched in 25N salt mixture maintained at a)300°C b) 350°C c) 400°C d)450°C e)500°C

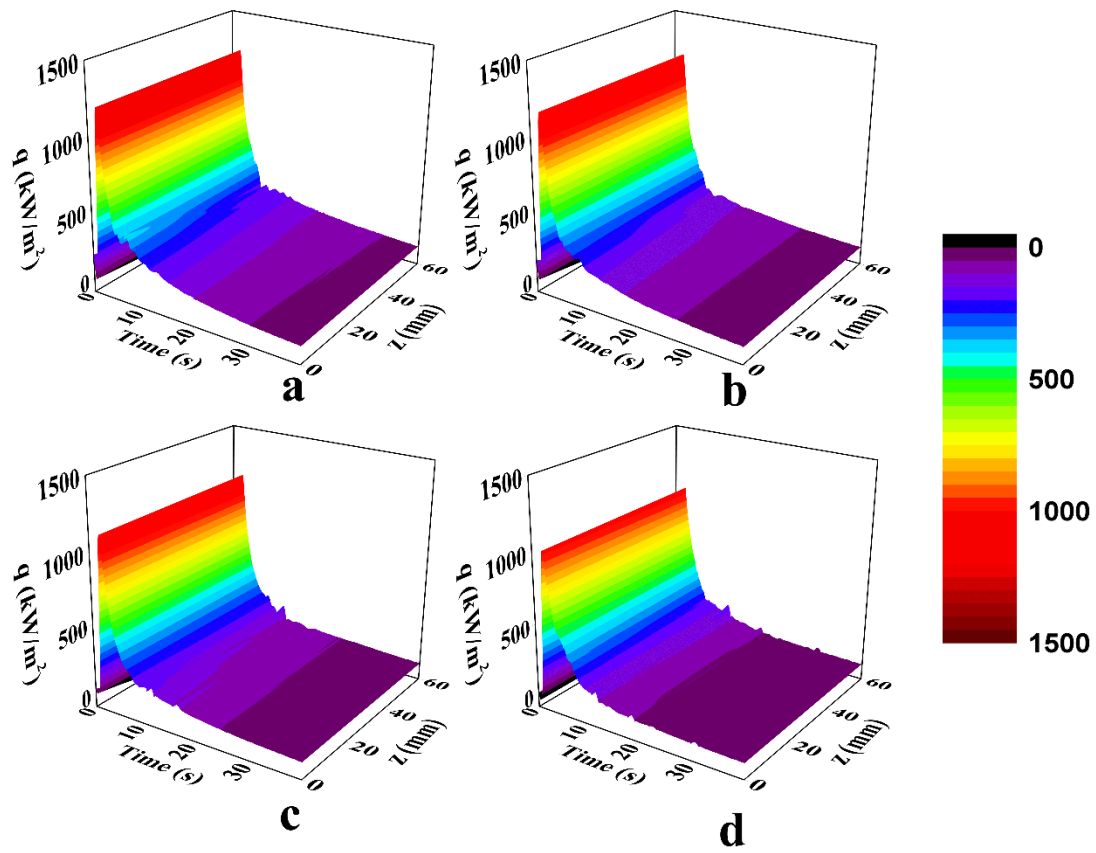


Figure B.5: Spatially dependent transient heat flux for inconel probe quenched in 0N salt mixture maintained at a)350°C b) 400°C c) 450°C d)500°C

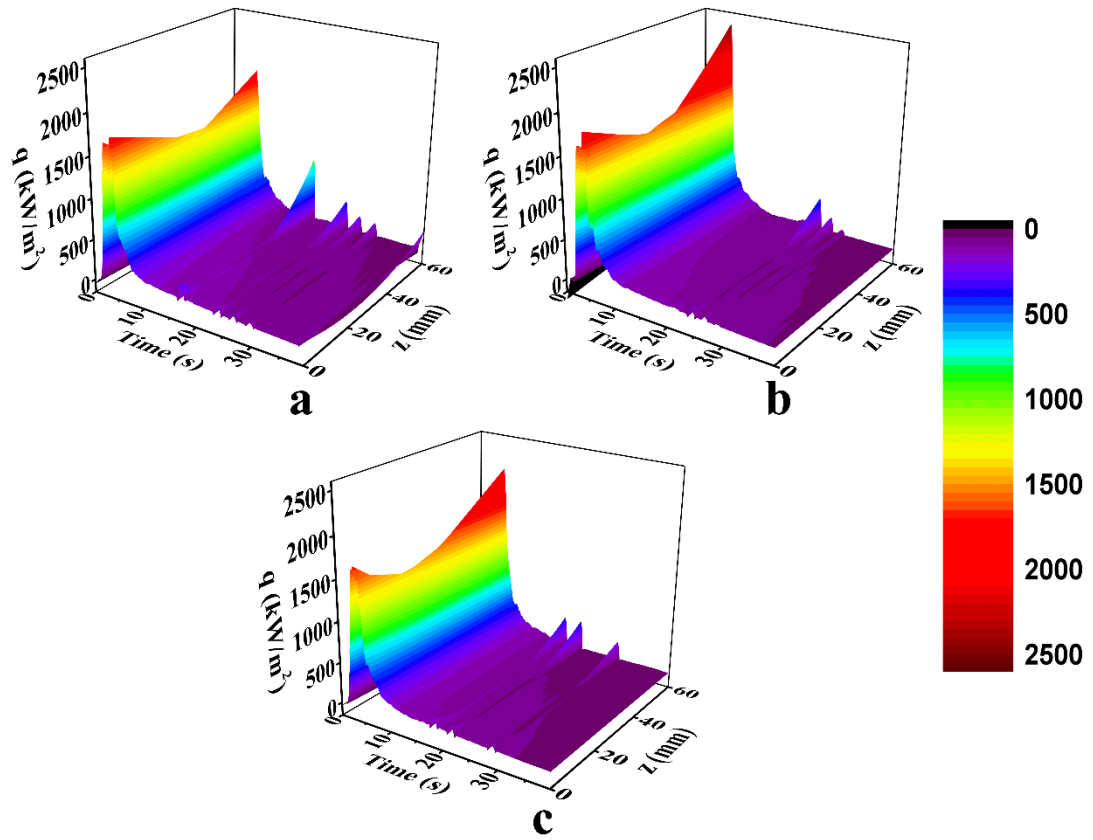


Figure B.6: Spatially dependent transient heat flux for inconel probe quenched in Hot oil maintained at a)100°C b) 150°C c) 200°C

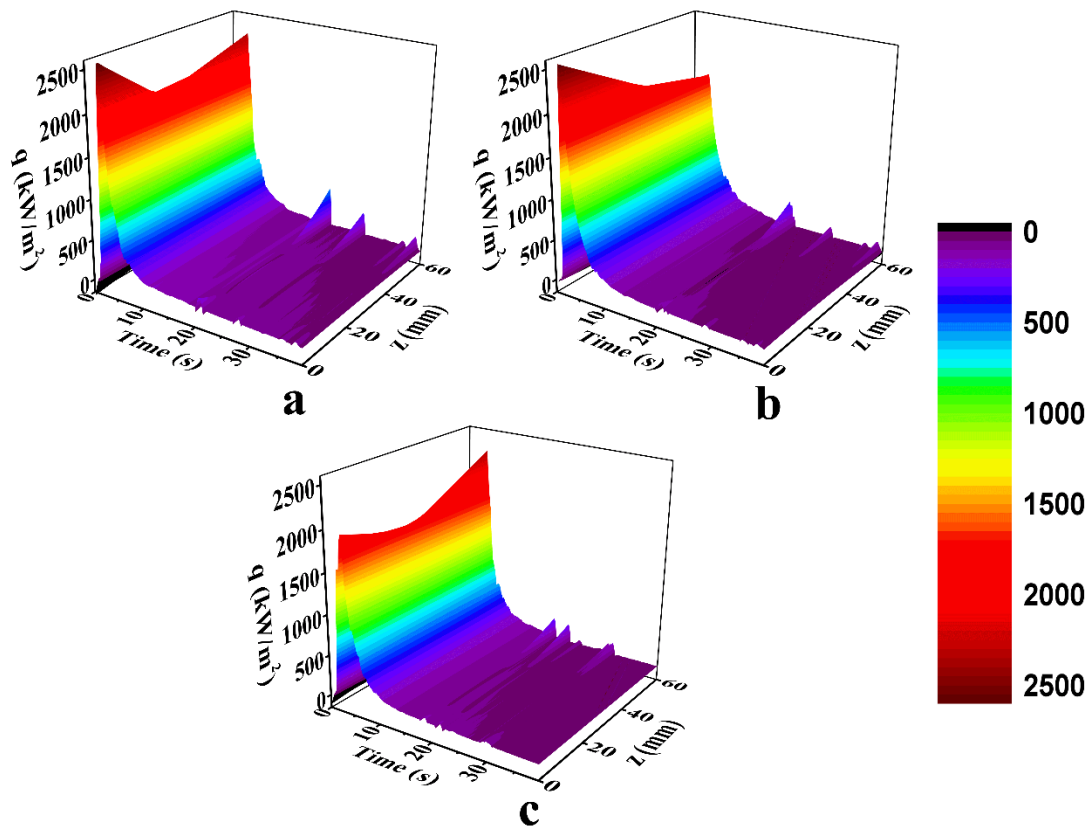


Figure B.7: Spatially dependent transient heat flux for inconel probe quenched in Neem oil maintained at a)100°C b) 150°C c) 200°C

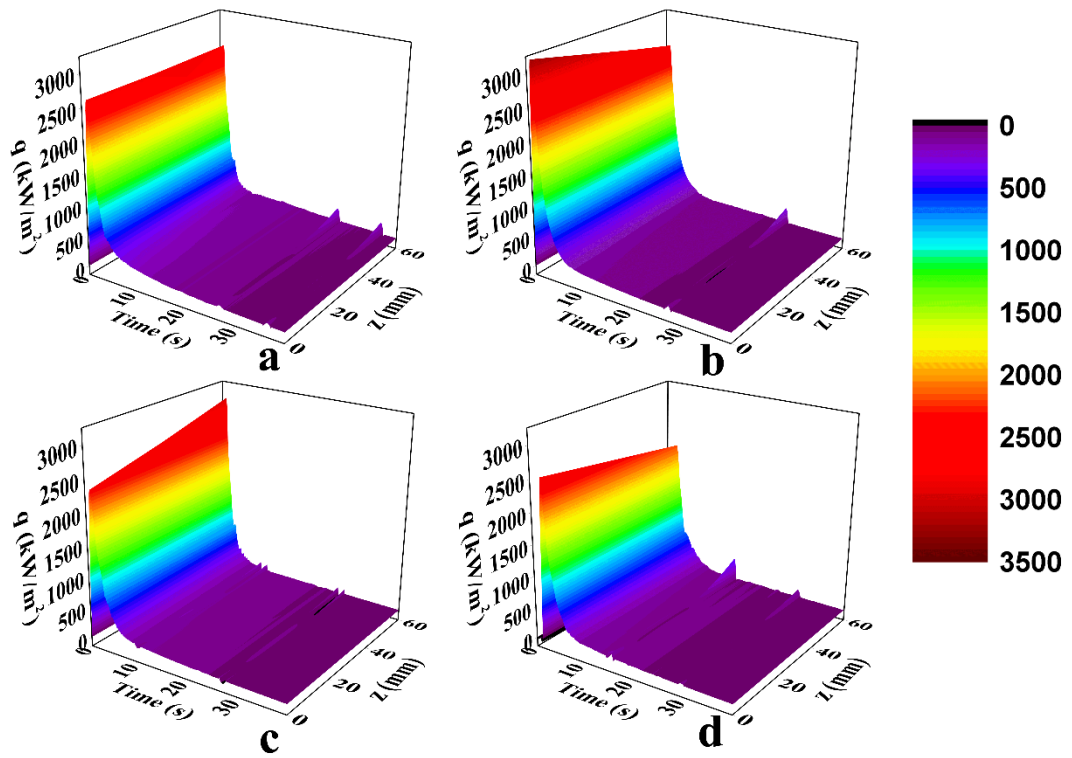


Figure B.8: Spatially dependent transient heat flux for inconel probe quenched in molten NaNO₂ eutectic salt mixture maintained at a)150°C b) 200°C c) 250°C d)300°C

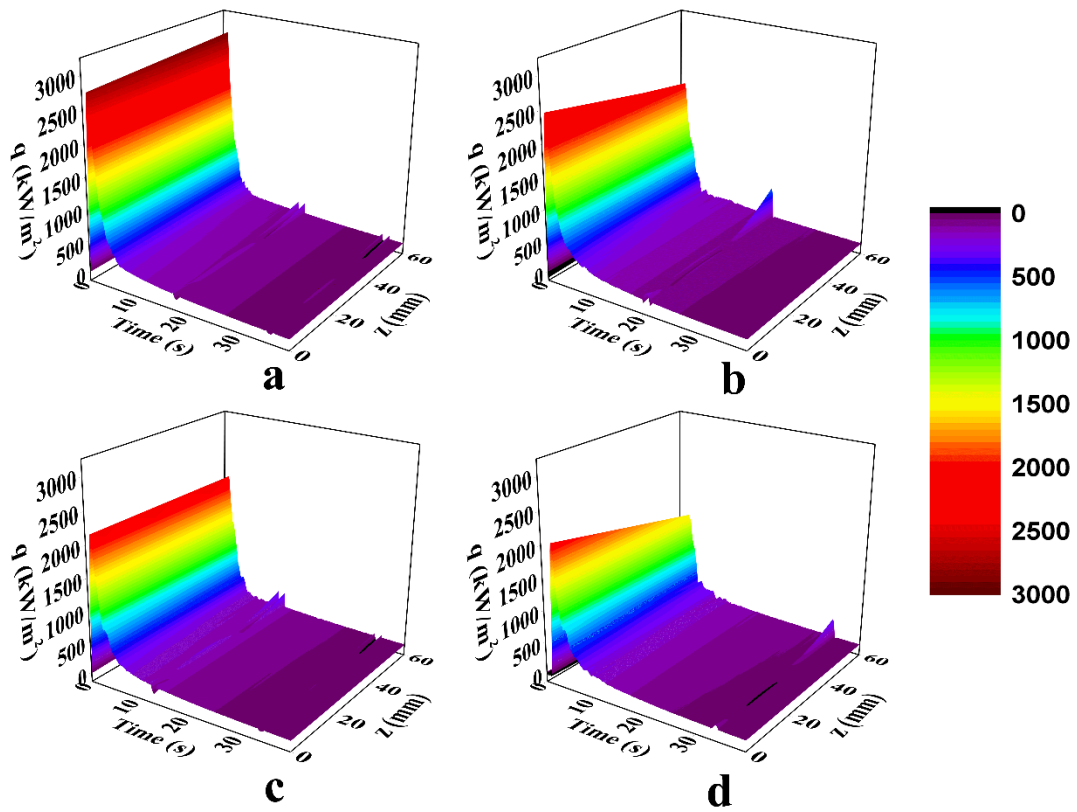


Figure B.9: Spatially dependent transient heat flux for inconel probe quenched in molten LiNO₃ eutectic salt mixture maintained at a)150°C b) 200°C c) 250°C d)300°C

APPENDIX C: EFFECT OF SECTION THICKNESS, HEAT TRANSFER COEFFICIENT, BATH TEMPERATURE AND RESIDENCE TIME ON HARDNESS OF AISI 4140 STEEL CYLINDER DURING MARTEMPERING

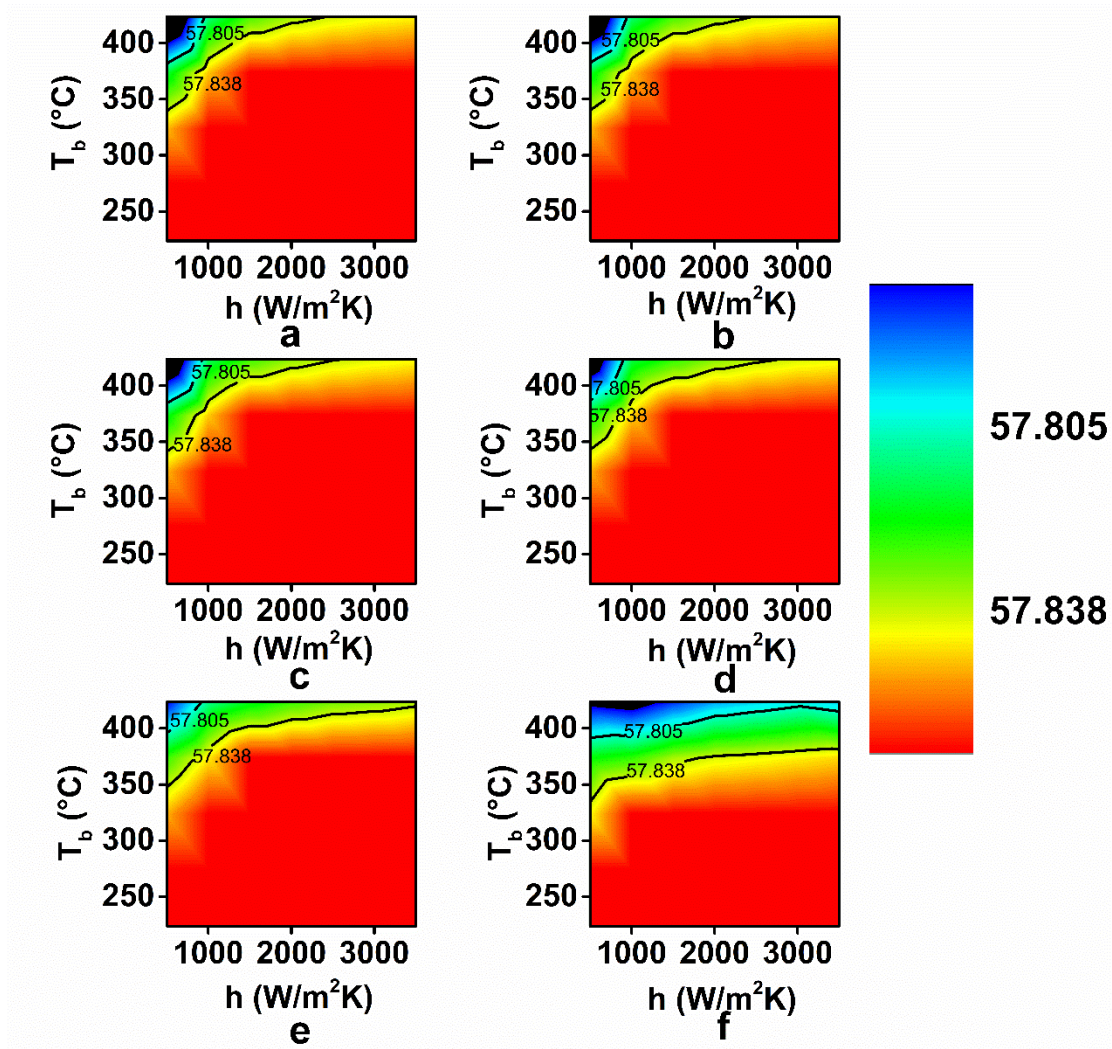


Figure C.1: Effect of heat transfer coefficient and bath temperature on the average hardness in AISI 4140 cylinder of 2mm diameter for residence time fraction of a) 1 b) 0.99 c) 0.95 d)0.9 e) 0.75 f) 0.5

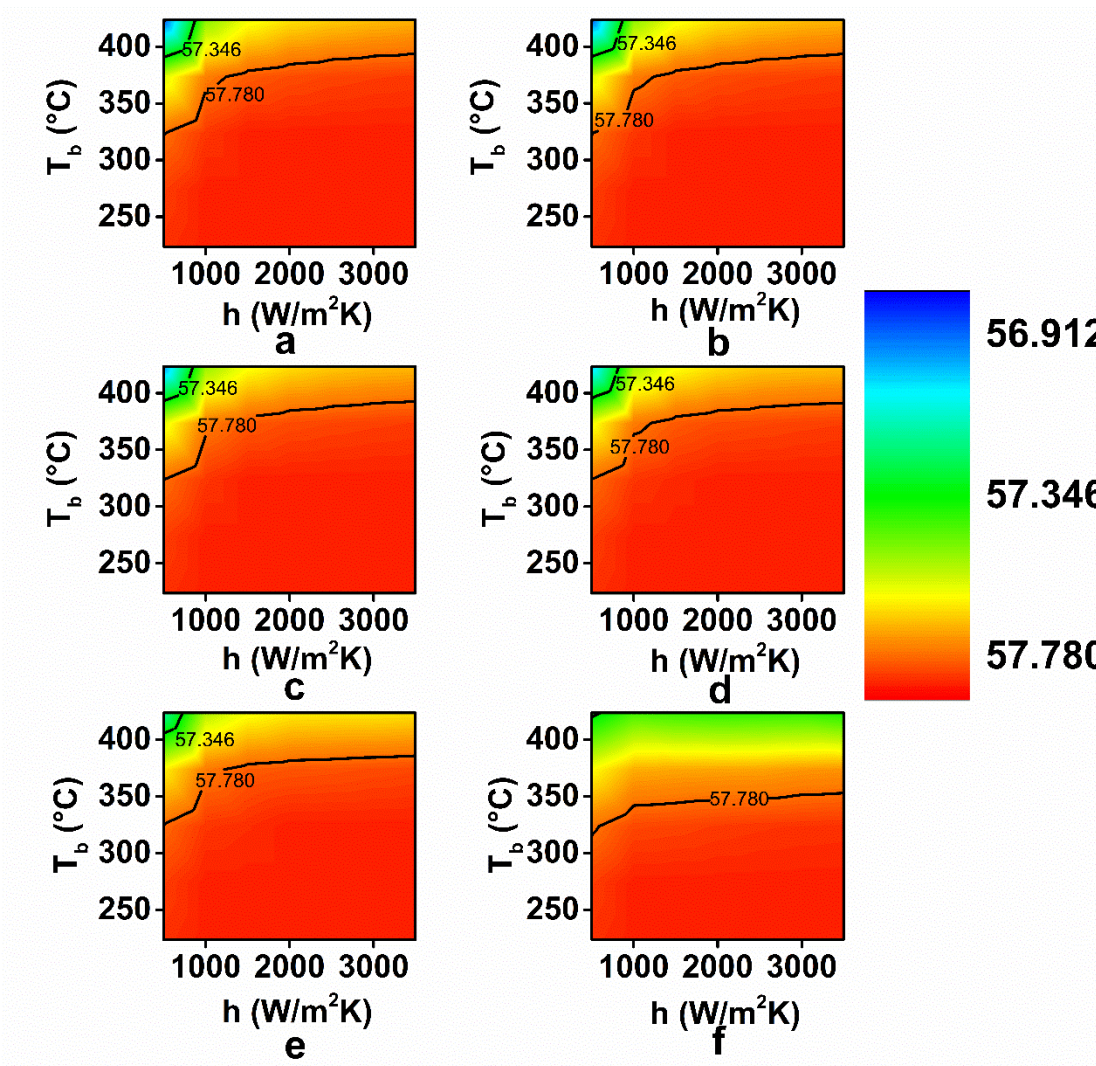


Figure C.2: Effect of heat transfer coefficient and bath temperature on the average hardness in AISI 4140 cylinder of 5 mm diameter for residence time fraction of a) 1 b) 0.99 c) 0.95 d)0.9 e) 0.75 f) 0.5

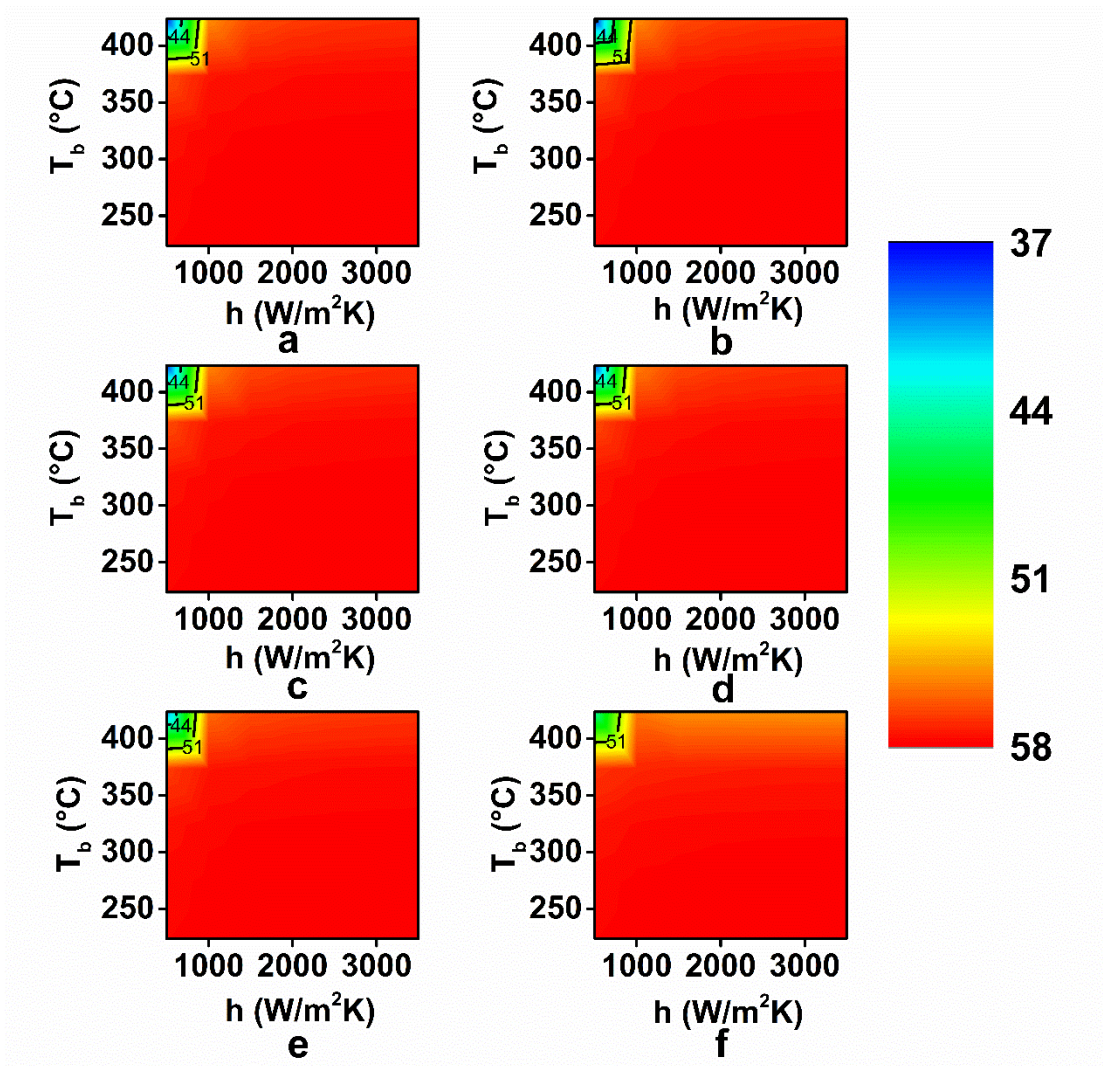


Figure C.3: Effect of heat transfer coefficient and bath temperature on the average hardness in AISI 4140 cylinder of 10mm diameter for residence time fraction of a) 1 b) 0.99 c) 0.95 d)0.9 e) 0.75 f) 0.5

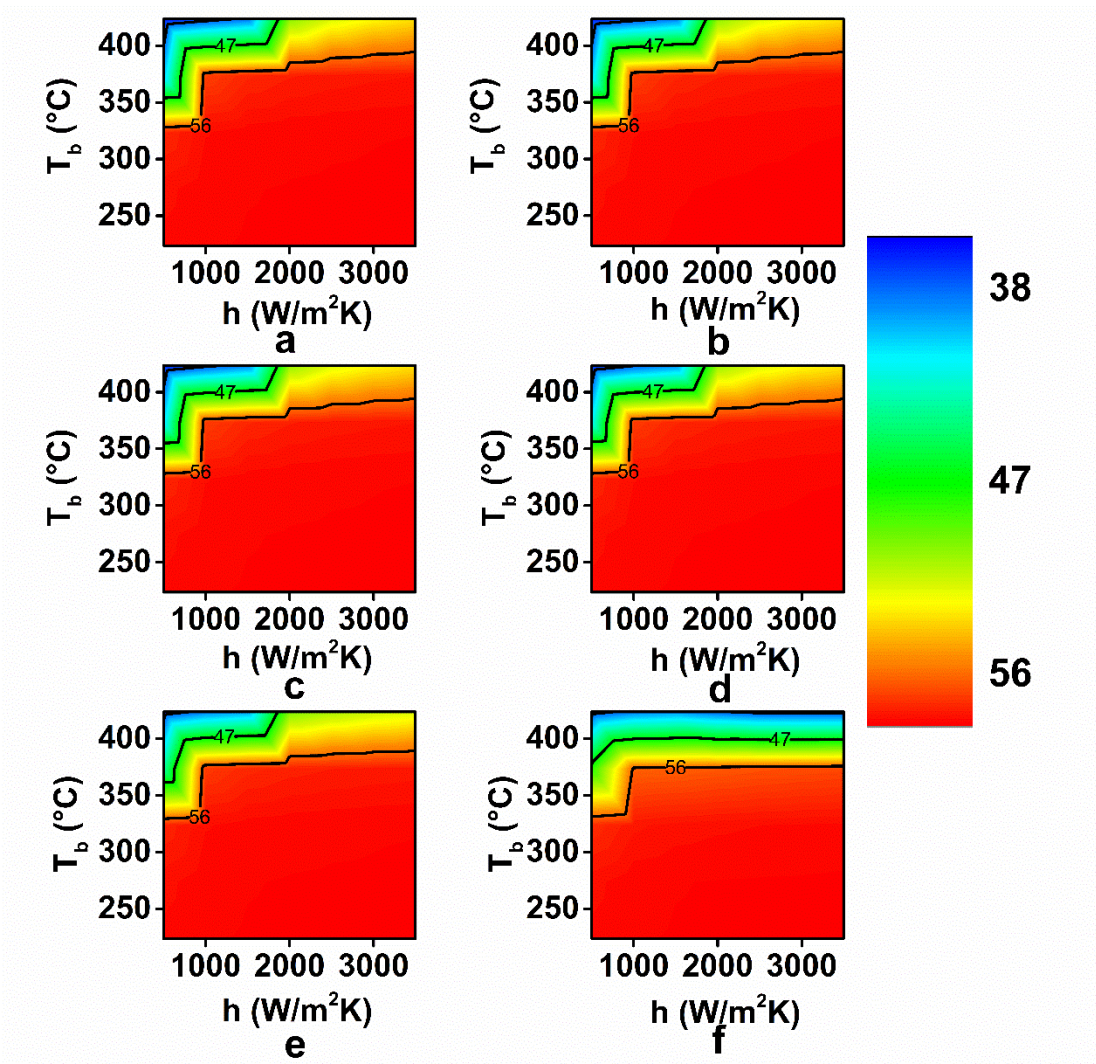


Figure C.4: Effect of heat transfer coefficient and bath temperature on the average hardness in AISI 4140 cylinder of 15mm diameter for residence time fraction of a) 1 b) 0.99 c) 0.95 d)0.9 e) 0.75 f) 0.5

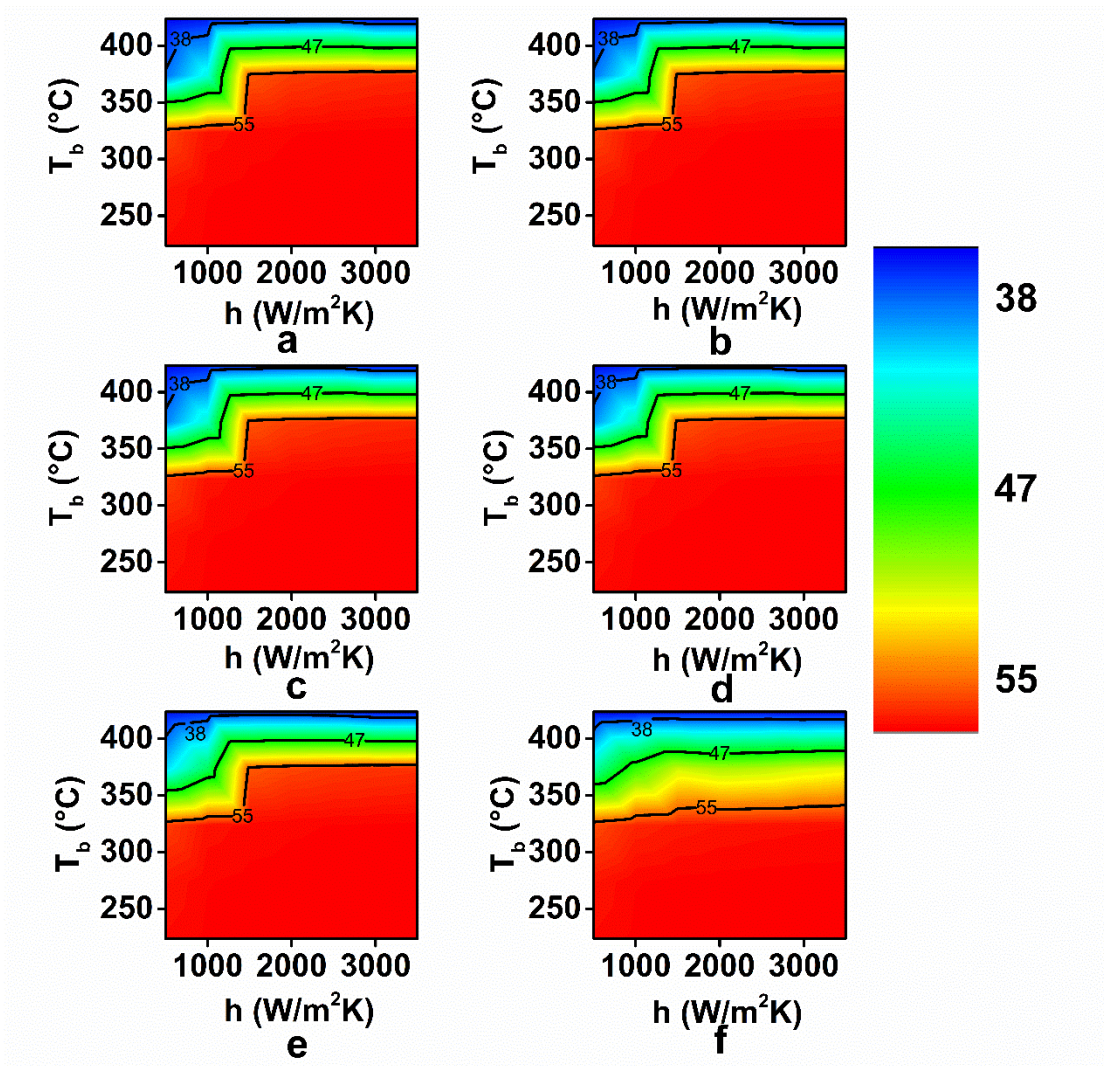


Figure C.5: Effect of heat transfer coefficient and bath temperature on the average hardness in AISI 4140 cylinder of 20mm diameter for residence time fraction of a) 1 b) 0.99 c) 0.95 d)0.9 e) 0.75 f) 0.5

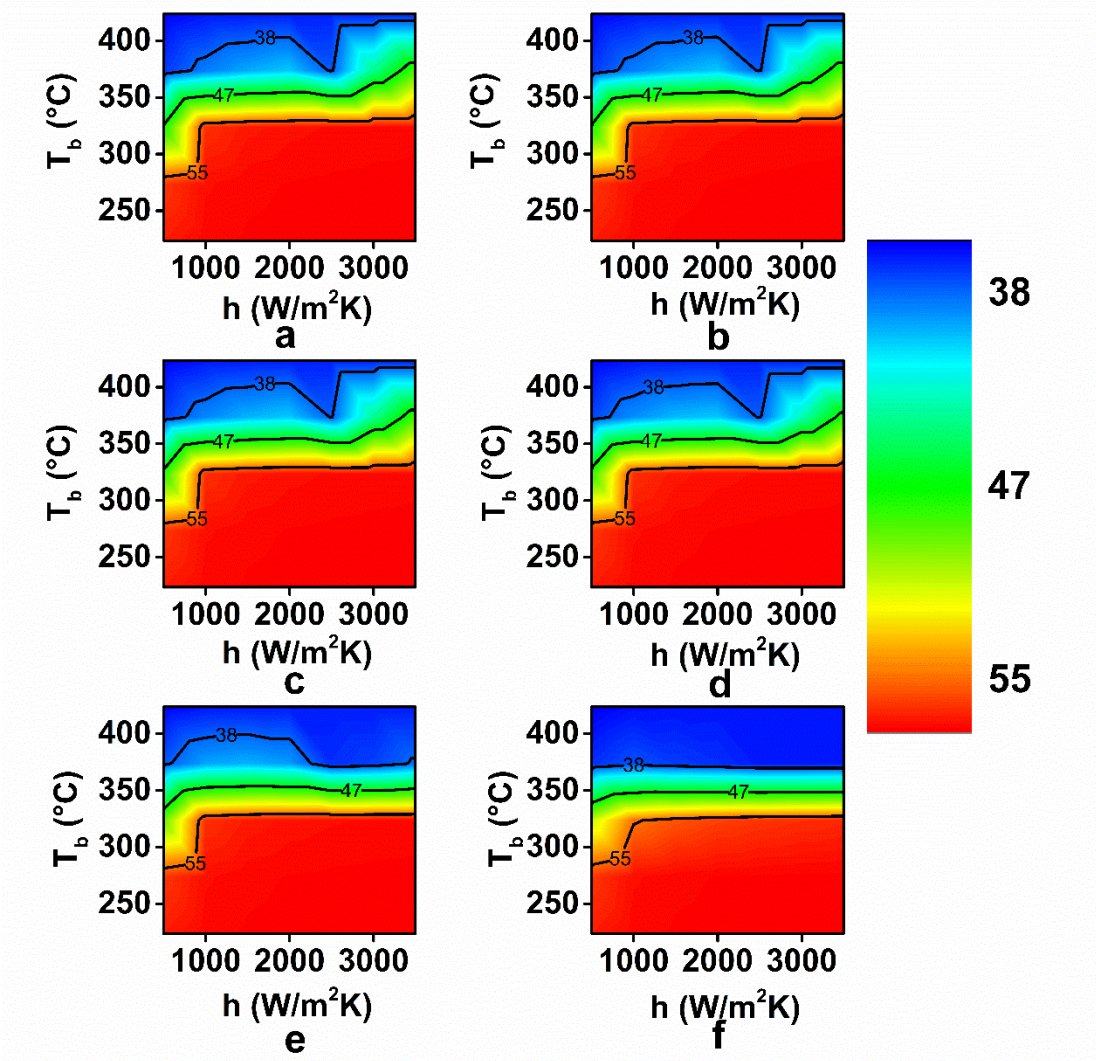


Figure C.6: Effect of heat transfer coefficient and bath temperature on the average hardness in AISI 4140 cylinder of 30mm diameter for residence time fraction of a) 1 b) 0.99 c) 0.95 d)0.9 e) 0.75 f) 0.5

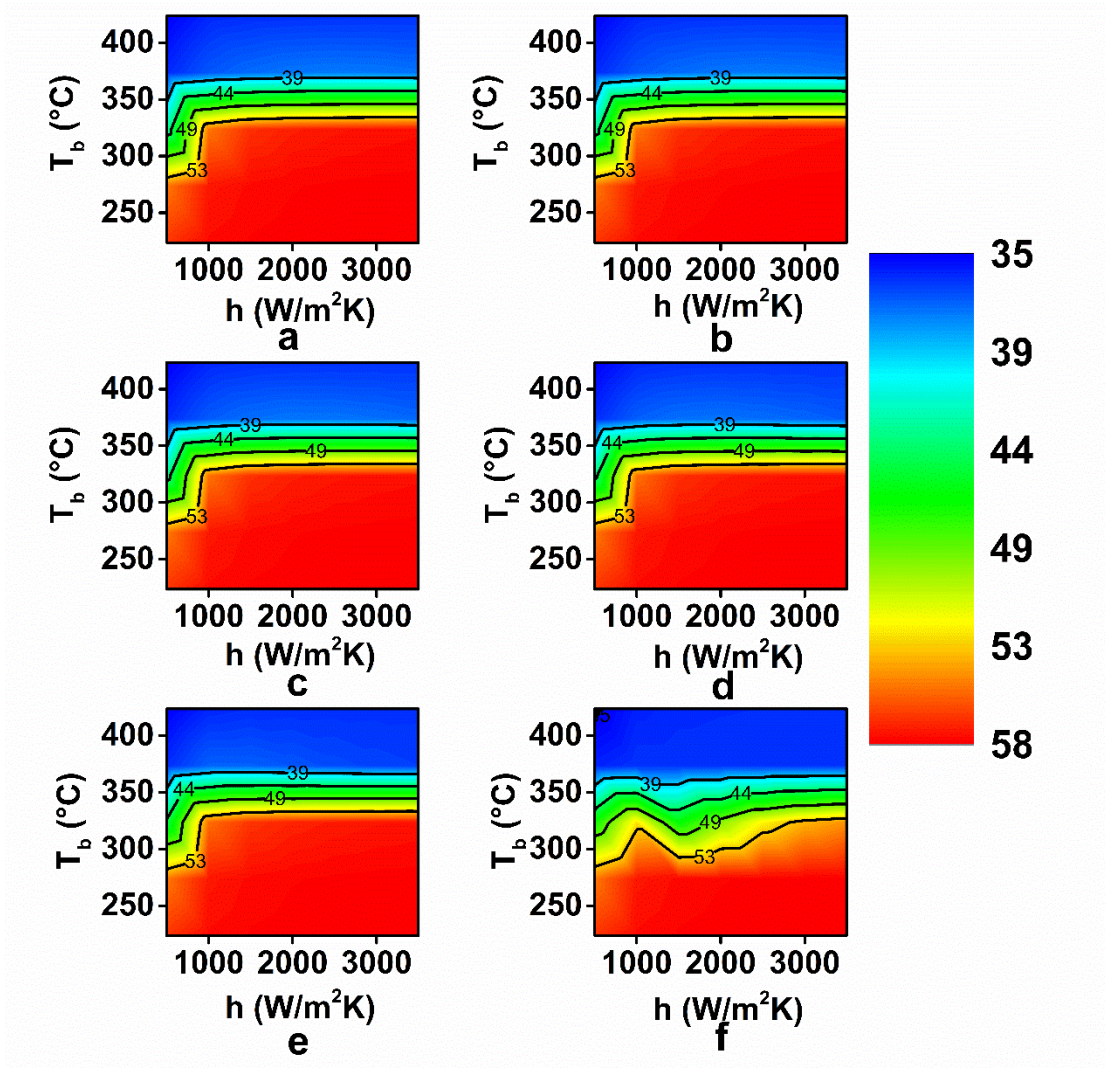


Figure C.7: Effect of heat transfer coefficient and bath temperature on the average hardness in AISI 4140 cylinder of 40mm diameter for residence time fraction of a) 1 b) 0.99 c) 0.95 d)0.9 e) 0.75 f) 0.5

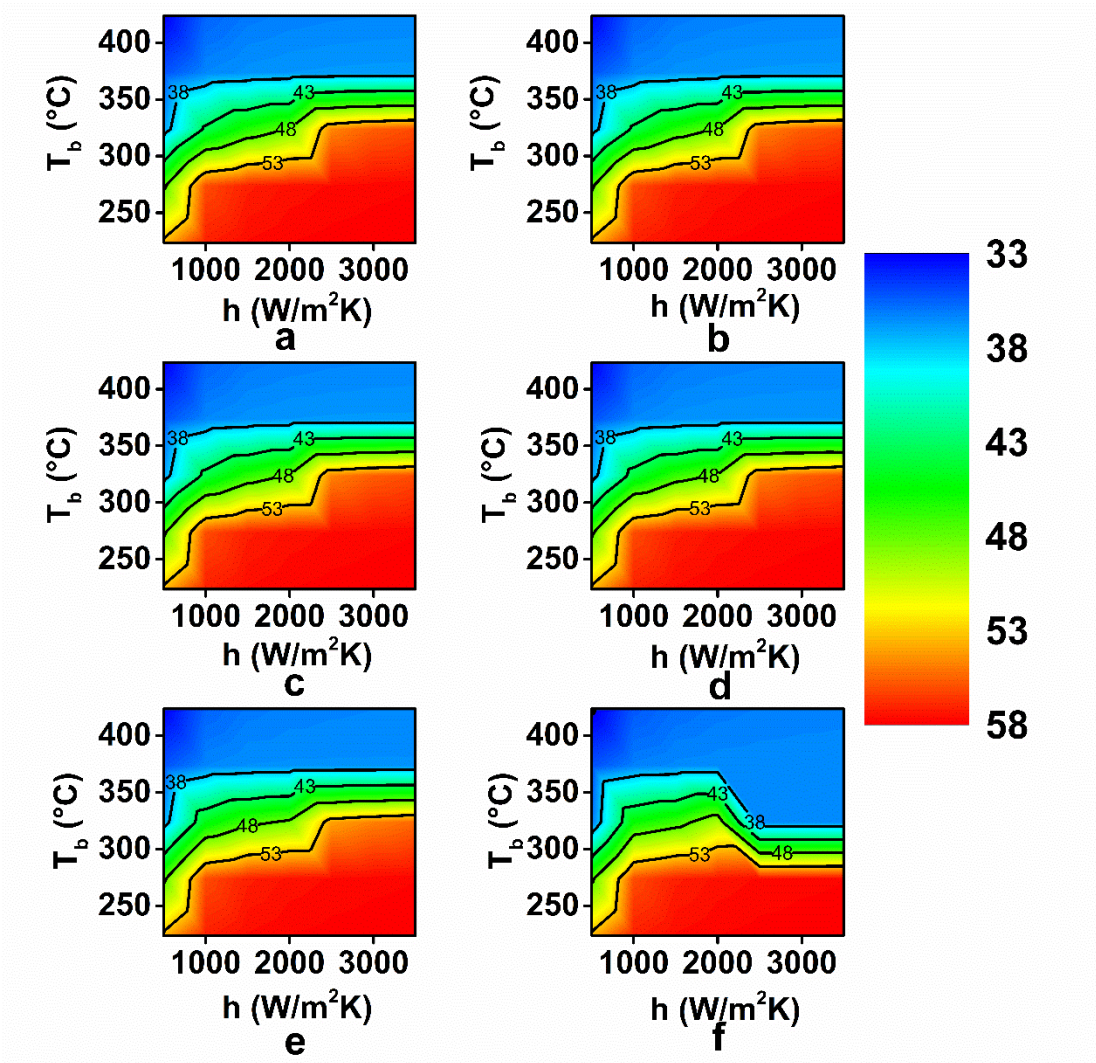


Figure C.8: Effect of heat transfer coefficient and bath temperature on the average hardness in AISI 4140 cylinder of 60mm diameter for residence time fraction of a) 1 b) 0.99 c) 0.95 d)0.9 e) 0.75 f) 0.5

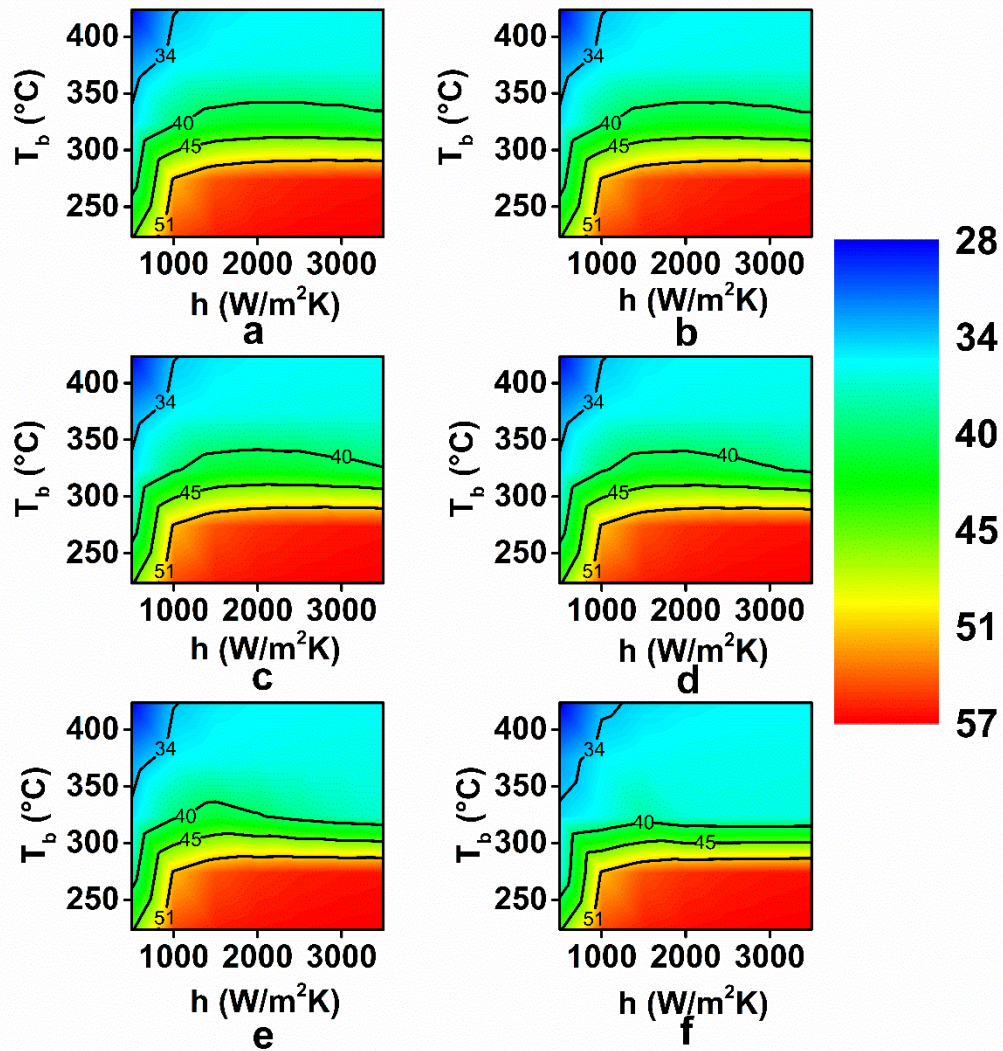


Figure C.9: Effect of heat transfer coefficient and bath temperature on the average hardness in AISI 4140 cylinder of 80mm diameter for residence time fraction of a) 1 b) 0.99 c) 0.95 d)0.9 e) 0.75 f) 0.5

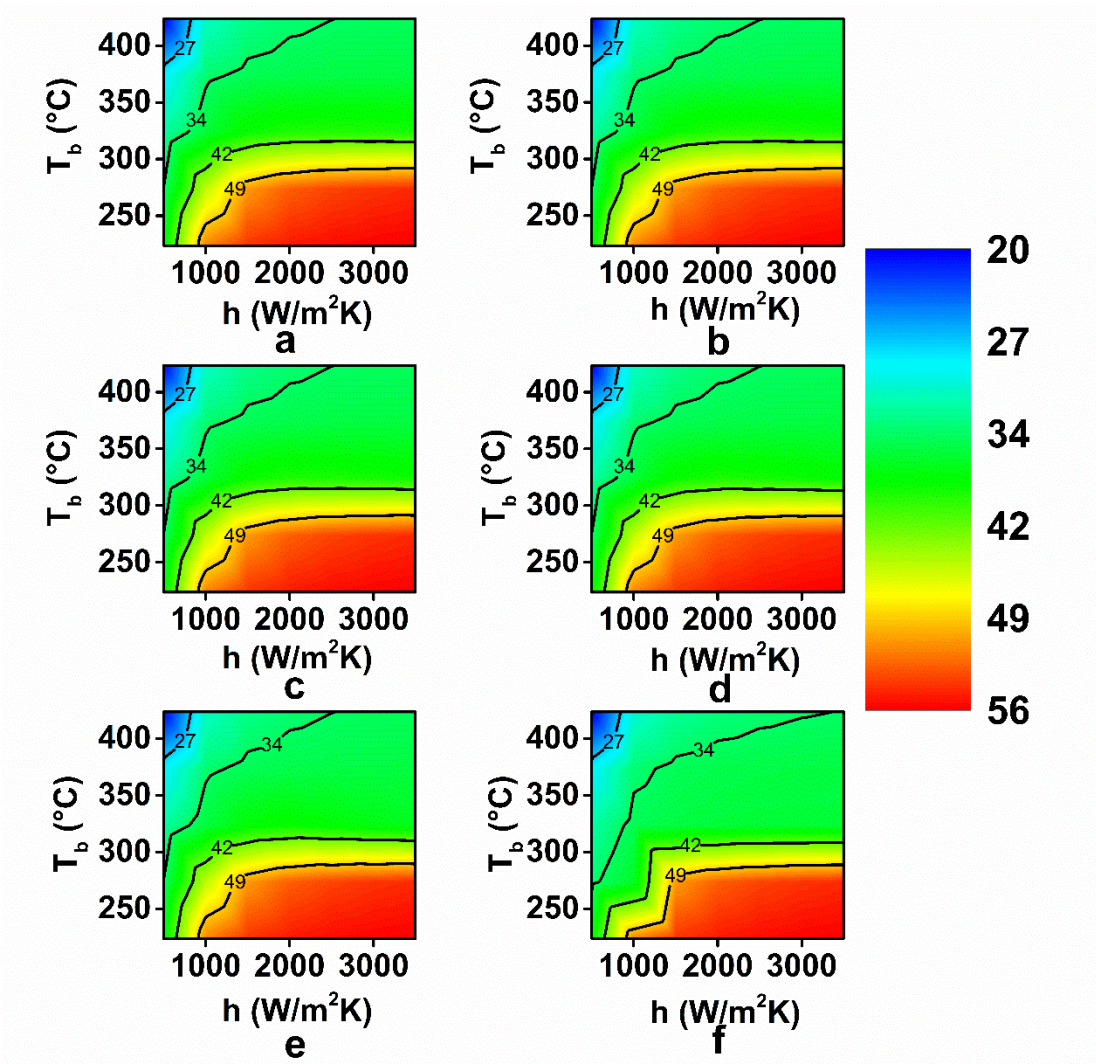


Figure C.10: Effect of heat transfer coefficient and bath temperature on the average hardness in AISI 4140 cylinder of 100mm diameter for residence time fraction of a) 1 b) 0.99 c) 0.95 d)0.9 e) 0.75 f) 0.5

APPENDIX D: WEIGHTS AND BIAS FOR ARTIFICIAL NEURAL NETWORK MODEL

j	W_{1,j}	W_{2,j}	W_{3,j}	W_{4,j}	W_{5,j}	W_{0,j}	b_j
1	4.492603	0.054934	-5.08655	0.783852	0.055709	-2.98211	-7.24139
2	-0.6905	0.094646	-1.47182	0.076989	0.013129	1.179655	1.091808
3	-0.37052	1.497062	-1.37877	-1.67004	0.005636	-0.01899	-2.35544
4	-1.18454	3.019145	0.074979	-0.93708	-0.06961	1.909715	3.46264
5	-9.54444	0.755572	-16.2657	1.561605	0.007497	-0.18663	6.408081
6	0.767698	0.023879	0.048547	0.487942	0.794669	6.055483	-3.87458
7	-2.84446	0.258235	-1.71212	-0.78966	0.005831	0.532277	0.934729
8	0.209203	1.394904	-1.64777	-1.54386	-0.01999	-0.16848	0.099309
9	2.887866	2.089068	10.65952	-2.74416	-0.10115	0.055021	-7.72186
10	2.291986	-0.39156	2.08661	0.787674	-0.01146	0.584253	-1.28031
11	1.198053	-2.83948	-0.05875	1.099371	0.088066	1.694199	-3.3097
12	-3.64561	-0.30463	-0.68556	-1.60414	-0.01428	-0.15509	-0.45347
13	-12.3348	0.136089	-9.98664	2.108396	0.068137	0.165096	3.164992
14	-0.7424	1.075641	-1.12914	-0.06884	0.00643	17.95364	0.731976
15	-5.61135	-0.05063	5.49732	-0.80394	-0.05941	-2.98014	8.385253
16	0.264735	-1.3608	-1.53398	-0.32562	0.062692	0.083633	-0.36446
17	6.24201	0.220558	3.928629	-0.7437	-0.03775	0.150824	0.107486
18	-13.2923	1.958165	-21.9448	-2.72919	0.08047	0.23651	1.651672
19	-14.0021	1.06473	-7.62084	-1.54792	-0.02622	4.120855	-3.41239
20	-14.9592	-0.09496	-29.7522	3.631593	0.040068	0.226373	10.39039
21	0.206447	-1.13724	-1.03732	0.502724	0.045574	-0.10534	0.804228
22	10.96785	-2.90453	12.91009	-50.5459	0.006387	0.302004	-51.9761
23	-14.0079	1.094948	-7.60315	-1.53471	-0.02759	-4.00721	-3.38446
24	-16.4834	1.615599	-3.33929	76.43355	-0.00401	14.75319	64.87251
25	-0.80544	1.232852	-1.11738	-0.09919	0.004065	-9.09161	0.702555
26	3.037347	-3.60937	2.423694	-0.12605	-0.79645	-0.36204	-9.17145
27	-16.4785	1.626744	-3.30308	77.16986	-0.00415	-14.6326	65.5622
28	11.81401	-0.94906	1.596262	-110.599	-0.00023	-16.5745	-103.054
29	-0.68184	0.854129	-1.15797	0.00016	0.009935	-9.46744	0.800716
30	3.069873	-1.78486	-5.64006	1.760682	0.005621	-0.38596	10.98341
b₀	1.7527						

LIST OF PUBLICATIONS

Journal publications

Pranesh Rao, K. M., and Narayan Prabhu, K. (2017). “Effect of Bath Temperature on Cooling Performance of Molten Eutectic $\text{NaNO}_3\text{-KNO}_3$ Quench Medium for Martempering of Steels.” *Metall. Mater. Trans. A*, 48(10), 4895–4904.

Pranesh Rao, K. M., and Prabhu, K N. (2017). “Estimation of Spatially Dependent Heat Flux Transients during Quenching of Inconel Probe in Molten Salt Bath.” *Mater. Perform. Charact.*, 6(5), 733-744.

Conference proceedings

Pranesh Rao, K. M., and Narayan Prabhu, K. (2016) “Simulation of the effect of heat transfer coefficient, bath temperature and section thickness on phase evolution during martempering of 4140 steel”. Heat treatment society- ASM Conference, Mumbai

Pranesh Rao, K. M., and Narayan Prabhu, K. (2016). “Estimation of Spatially Dependent Heat Flux Transients during quenching of Inconel Probe in Molten Salt Bath” Mediterranean conference on heat treatment and surface Engineering, Portoroz, Slovenia

BIO-DATA

Name	Pranesh Rao K M
Date of Birth	10-04-1990
Permanent address	Door # 1226/2A, Sri Saraswathi Sadhana, Kantaraj Urs road K M Puram Mysore- 570004
Email	praneshraokm@gmail.com

Academic qualification

Bachelor of Engineering (B.E.) :Mechanical Engineering; National Institute of Engineering; 2012.

Master of Technology (M.Tech.) :Process Metallurgy; National Institute of Technology Karnataka; 2014.